Technical Report
TR-16-04
August 2016

Buffer homogenisation

Status report 3

Ann Dueck
Reza Goudarzi
Lennart Börgesson

SVENSK KÄRNBRÄNSLEHANTERING AB

SWEDISH NUCLEAR FUEL
AND WASTE MANAGEMENT CO

Box 250, SE-101 24 Stockholm
Phone +46 8 459 84 00
skb.se

SVENSK KÄRNBRÄNSLEHANTERING

ISSN 1404-0344
SKB TR-16-04
ID 1533322

August 2016

Buffer homogenisation

Status report 3

Ann Dueck, Reza Goudarzi, Lennart Börgesson
Clay Technology AB

Keywords: Bentonite, Swelling, Swelling pressure, Homogenisation.

Abstract

The present status report is a compilation of laboratory test results from a project on homogenisation tests of bentonite. The main purpose of the status report is to account for results derived up to July 2014 and to provide results that can be used for modelling some well defined benchmark tests in order to improve the models or determine mechanical parameters for thermo-hydro-mechanical modelling of the behaviour of the bentonite buffer. Further analysis of the tests, test conditions, test results and limitations of the results will be made later in the project.

Results from several laboratory test series are presented in this status report. Swelling tests in two series with different scales are presented where the larger scale admits relatively high resolution in the distribution of base variables over the specimens to be measured. Results from tests on the friction between confined specimens at saturation and different types of surfaces are also shown. Buffer homogenisation has also been studied by two medium scale tests involving loss of bentonite and the results from one finished test are presented in this report.

Sammanfattning

Denna lägesrapport innehåller en sammanställning av laboratorieförsök som utförts för att studera homogeniseringsprocessen i bentonitlera. Huvudsyftet med rapporten är att presentera försöksresultat från försök som utförts fram till och med juli 2014 och att tillhandahålla resultat som kan användas för modellering, för att förbättra modeller eller för att bestämma mekaniska parametrar för den termo-hydro-mekaniska modelleringen av bentonitbuffertens uppförande. Analys av försöken, förutsättningar, försöksresultat och begränsningar i försöken kommer att göras senare i projektet.

Resultat från flera olika försöksserier presenteras i denna lägesrapport. Försökserier som inkluderar svällning har utförts i två olika skalor där resultaten från försöken i den större skalan (cylindriska prover med diametern 100 mm) medger relativt sett högre upplösning i de basvariabler som bestämts över proverna. I en annan försöksserie har friktionen mellan inspända vattenmättade prover och olika ytor studerats. Homogenisering av bentonitbuffert har också undersökts med två försök i medium skala (cylindriska prover med diametern 300 mm) där förlust av stora volymer bentonit har ingått. Resultaten från det av försöken som slutförts redovisas i denna rapport.

Contents

1 Introduction

1.1 Background

Swelling of the buffer blocks and buffer homogenisation are important functions to guarantee the requirements of the buffer in a deposition hole after full water saturation. It is important to understand and be able to predict the final condition of the buffer after the swelling and homogenisation, which occur both during the initial saturation and after possible loss of bentonite caused by for example erosion.

The project consists of four parts; theoretical studies, fundamental laboratory tests, laboratory study of the influence of friction and medium scale tests of the scenario involving loss of bentonite. The present status report describes results from fundamental laboratory swelling tests, from the study of influence of friction and from the medium scale tests of the scenario involving loss of bentonite.

The tests described were run from February 2012 and until July 2014. This is the third status report from the actual project and it is a continuation of the previous status reports with laboratory test results: TR-12-02 (Dueck et al. 2011) and TR-14-25 (Dueck et al. 2014). In addition, material models have been developed and verified with some of the laboratory test results from this project.

1.2 Objective

The objective of the described tests has been to further improve the knowledge of the process of swelling and buffer homogenisation. The main purpose of this status report is to account for results derived up to July 2014 and provide results that can be used for modelling some well-defined benchmark tests in order to improve the models or determine mechanical parameters for thermo-hydro-mechanical modelling of the behaviour of the buffer.

1.3 Content of the report

The determination of base variables is described in Chapter 2 and the material used for the tests are described in Chapter 3. The test techniques used for the tests of fundamental swelling in the basic series and the so called high resolution series are presented in Chapter 4. In this chapter also the test technique used for the tests to measure friction between bentonite specimens and other surfaces, e.g. steel and plastic, is described. The test results from these test types are presented in Chapter 5. In Chapter 6 test description, equipment and results from the medium scale tests of a scenario involving loss of bentonite are presented. The focus of this chapter is the completed test in this series which has been terminated and dismantled. Short comments about the test results are given directly after each section with presented results. Since the present report is a status report analyses and conclusions of the test results will be provided in the next report from this project. All tests mentioned in this report are tabulated in Appendix 7.

Some of the tests run in this project were used as tasks in the SKB project Task Force on Engineered Barriers (TFEBS). Results from the tests HR-A1, HR-Ro1, HR-Ri1 and HR-Iso (section 5.2) were used as well as results from the not yet finished medium scale test SH1 (section 6). In addition, the test results from the friction tests Fr1-1 to Fr1-9 (section 4.3) were presented as additional material properties.

2 Determination of basic variables

2.1 General

The basic variables water content and bulk density are measured in each test and from those variables the dry density and degree of saturation are calculated. The swelling pressure is represented by the measured radial and axial stresses in all the fundamental tests.

2.2 Water content and bulk density determination

The basic geotechnical variables water content w (%), void ratio e, degree of saturation S_r (%) and dry density ρ_d (kg/m^3) are determined according to Equations 2-1 to 2-4.

$$w = 100 \cdot \frac{m_{tot} - m_s}{m_s} \tag{2-1}$$

$$e = \frac{\rho_s}{\rho}(1 + w/100) - 1 \tag{2-2}$$

$$S_r = \frac{\rho_s \cdot w}{\rho_w \cdot e} \tag{2-3}$$

$$\rho_d = \frac{m_s}{V} \tag{2-4}$$

where

m_{tot} = total mass of the specimen (kg)

m_s = dry mass of the specimen (kg)

ρ_s = particle density (kg/m^3)

ρ_w = density of water (kg/m^3)

ρ = bulk density of the specimen (kg/m^3)

V = total volume of the specimen (m^3)

The dry mass of a specimen is obtained from drying a wet specimen at 105 °C for 24h. The bulk density is calculated from the total mass of a specimen and the volume determined by weighing the specimen above and submerged into paraffin oil.

3 Materials

Two bentonite materials have been used; the commercial Wyoming bentonite with brand name Volclay MX-80 from American Coll. Co. and the commercial bentonite Calcigel from Süd-Chemie AG. Descriptions of the materials and basic variables were presented by Svensson et al. (2011).

The bentonite powder is delivered with an approximate water content of 10 %. For tests where higher initial water content was used the powder was mixed with de-ionised water. Blocks were made by compacted powder either by compaction directly to the intended size or by sawing from larger compacted blocks.

For determination of void ratio and degree of saturation the particle densities ρ_s = 2 780 kg/m^3 and ρ_s = 2 695 kg/m^3 were used for MX-80 and Calcigel, respectively (Svensson et al. 2011) and the water density ρ_w = 1 000 kg/m^3.

The majority of the tests were supplied with de-ionised stagnant water if nothing else is specified. However, in many tests the filters were flushed in order to get rid of air bubbles.

4 Test technique

The test techniques described in this chapter were already reported in the previous status reports of this project; TR-12-02 and TR-14-25, but is here given to increase the readability of the new test results presented in Chapter 5.

4.1 Fundamental swelling tests – basic series

Swelling of water saturated bentonite specimens with access to water was studied in the following three test series, illustrated in Figure 4-1*:*

- Axial swelling in a device with constant radius and limited height. Variation of the height of the gap. (A0).
- Radial swelling of the outer surface in a device with constant height and limited radius. Variation of the radial gap. (R1).
- Radial swelling into a cylindrical cavity in a device with constant height and radius. Variation of the radius of the cavity. (R2).

The tests were mainly done with free swelling surfaces, i.e. no counteracting force until the swelling bentonite gel had reached the outer limited surface. In all tests the friction was minimised by use of a mineral-oil based lubricant on relevant surfaces.

Equipment

The three different types of test were carried out in devices with the design shown in Figure 4-2 to Figure 4-4. The equipment consists of a steel ring surrounding each specimen. In the device used for axial swelling a filter is placed above the specimen, which covers the cross section area. In case of the radial swelling a circular radial filter is placed between the circumference of the specimens and the steel ring. In all three types of test the top and bottom plates are bolted together with the steel ring in order to keep the volume constant. In each set-up the forces are measured by two load cells placed in the vertical and radial directions, respectively. The load cells are placed between a fixed plate and a movable piston where small deformation required by the load cells is admitted. The force was measured during the entire course of the tests. The transducers were calibrated prior to, and checked after, each test.

Preparation of specimens

Cylindrical specimens were prepared by compaction of powder to a certain density. The specimens used for the axial type of swelling had a diameter of 50 mm and a height of 20 mm. For the radial types of swelling specimens with diameter 47 mm and height 40 mm were used.

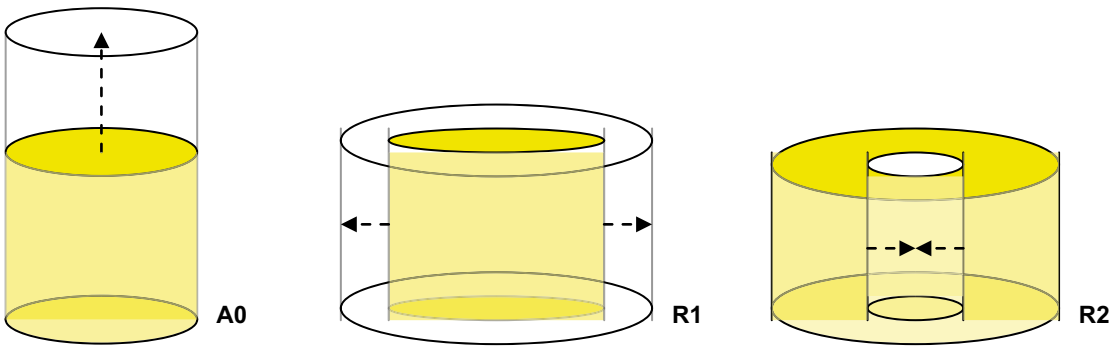

Figure 4-1. *Illustration of the geometry of the test types carried out.*

Test procedure

The tests consisted of two phases; the water saturation phase and the swelling phase. After mounting the specimen in one of the devices shown in Figure 4-2 to Figure 4-4, de-ionised water was applied to the filters after air evacuation of the filters and tubes. The specimens had free access to water during the water saturation. When only small changes in swelling pressure with time were noticed the water was evacuated from the filters and tubes and the second phase, i.e. the swelling and homogenisation, started. Depending on the type of swelling the following measures were taken;

- For the axial swelling (A0) the upper piston was moved upwards and fixed with spacers admitting a certain volume for the swelling. After evacuation of air, water was applied to the upper part of the specimen.
- For the radial swelling of the outer surface (R1) the water-saturated specimen was taken out and the diameter decreased by trimming the circumference of the specimen leaving a certain volume for swelling after re-mounting in the same device. After evacuation of air the filter was filled with water.
- For the radial swelling of an inner cavity (R2) the lower lid was opened and a hole was drilled in the center of the specimen. The cavity was filled with water, the lid was fixed and the outer filter was filled with water after evacuation of air.

After completed swelling and homogenisation, i.e. when no or negligibly small changes were noticed in the swelling pressure with time, the specimens were dismantled and cut in slices for determination of water content and density distribution in the direction of swelling.

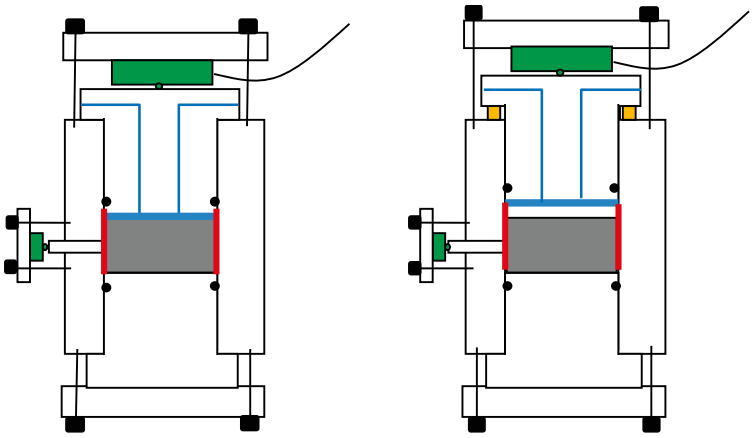

Figure 4-2. *Set-up used for the axial swelling tests (A). The red lines represent the lubricated surfaces and the blue lines represent filters and water supply.*

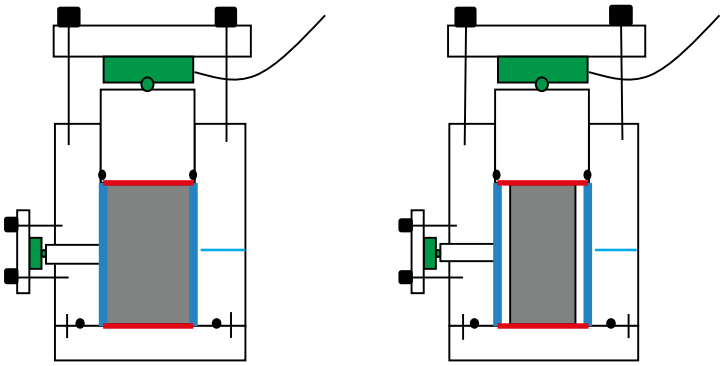

Figure 4-3. *Set-up used for the radial outward swelling tests (R1). The red lines represent the lubricated surfaces and the blue lines represent filters and water supply.*

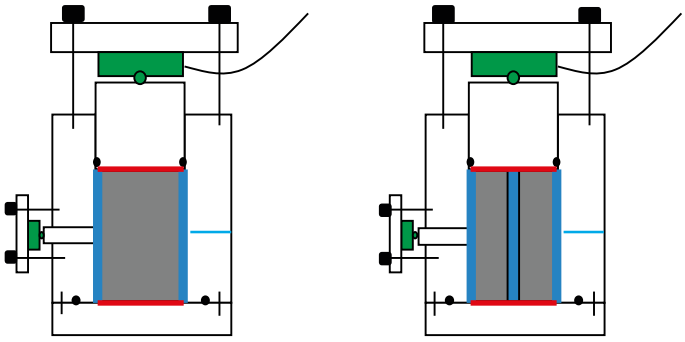

Figure 4-4. *Set-up used for the inward radial swelling tests (R2). The red lines represent the lubricated surfaces and the blue lines represent filters and water supply.*

Test results

The test results are presented with w, ρ_d and S_r as a function of the specimen height (series A0) or radius (series R1 and R2), i.e. as distribution in the direction of swelling. The measured stresses are also shown and compared with a model of swelling pressure of MX-80 presented by Börgesson et al. (1995). For all types of tests the swelling was calculated according to Equation 4-1 where V_i, V_f, ρ_{di} and ρ_{df} are the initial volume, final volume, initial dry density and final dry density, respectively.

$$s = \frac{\Delta V}{V_i} = \frac{V_f}{V_i} - 1 = \frac{\rho_{di}}{\rho_{df}} - 1 \qquad (4\text{-}1)$$

Test series

The tests run within the basic test series are shown in Table 4.1.

Table 4-1. Tests run in the basic series.

Axial swelling	Radial outward swelling	Radial inward swelling	Material
A01-14 to A01-16			MX-80
A04-1, A01-2			Calcigel
	R11-22 to R11-24		MX-80
	R14-1, A14-2		Calcigel
		R21-13, R21-14	MX-80
		R24-1, R24-2	Calcigel

4.2 Fundamental swelling tests – high resolution series

In the High Resolution (HR) series the same type of tests as in the basic series were run. The main difference between the two series was the size of the specimens where the larger specimens in the HR-series admitted higher resolution in the distribution of base variables over the specimens.

As in the basic series, swelling was studied in three series; axial swelling (HR-A), radial outward swelling (HR-Ro) and radial inward swelling (HR-Ri), illustrated in Figure 4-1. As in the basic series the tests were mainly done with free swelling surfaces, i.e. no counteracting force until the swelling bentonite gel had reached the outer limited surface. In all tests the friction was minimised by use of a mineral-oil based lubricant on relevant surfaces.

Equipment

The three different types of test were carried out in devices with the design shown in Figure 4-5 to Figure 4-7. The devices consist of a steel ring surrounding the specimen. A movable piston is placed vertically, in the axial direction above the specimen. Radial pistons are placed in holes through the steel ring for measurement of radial forces.

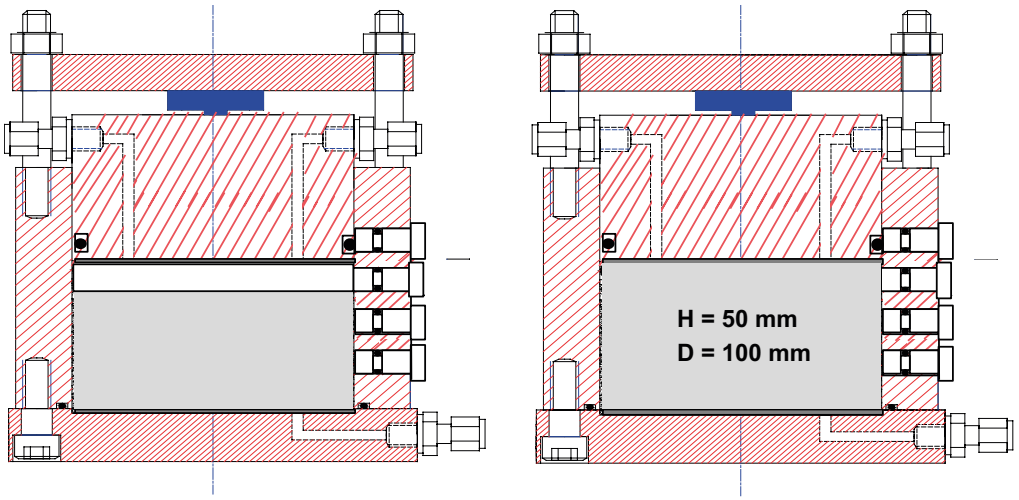

Figure 4-5. *Set-up used for the axial swelling tests (HR-A). Water was only supplied from a filter placed above the specimen.*

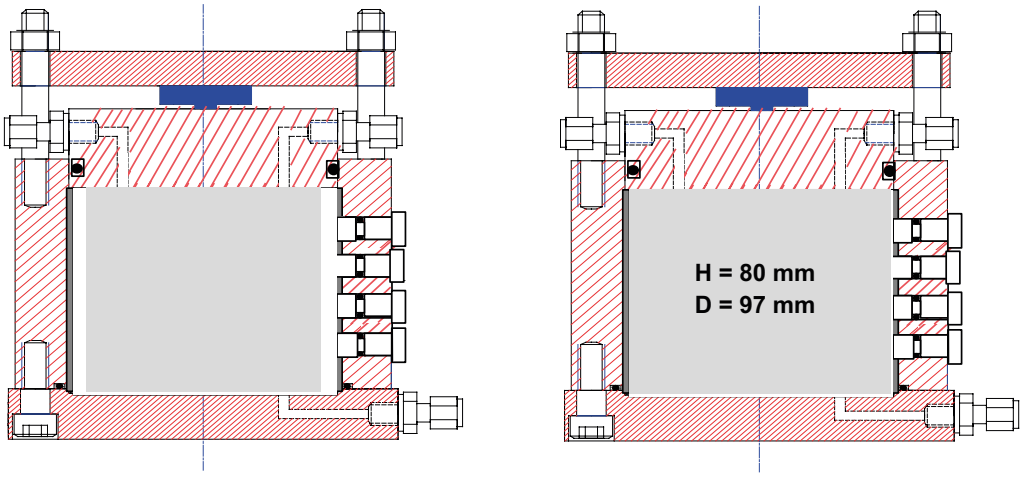

Figure 4-6. *Set-up used for the radial outward swelling tests (HR-Ro). Water was supplied from a radial filter between the surrounding steel ring and the specimen. The radial stress was generally only measured at one level.*

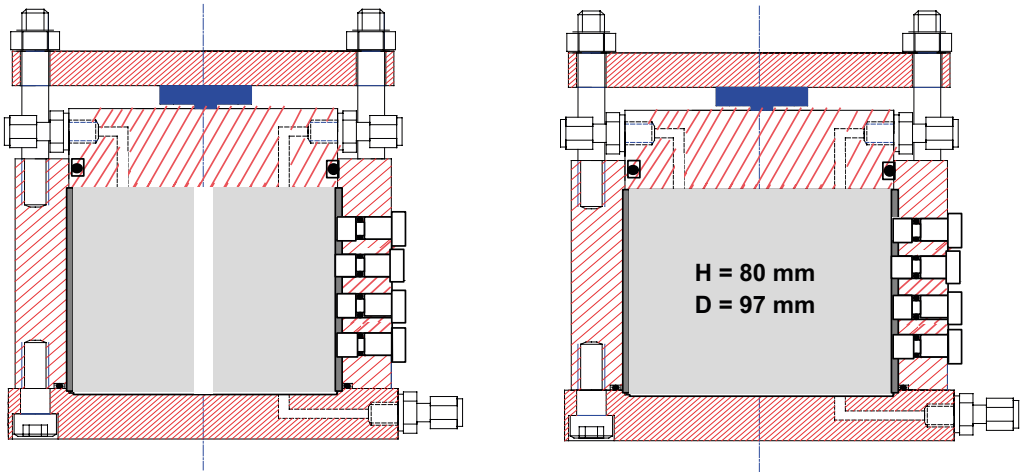

Figure 4-7. *Set-up used for the inward radial swelling tests (HR-Ri). Water was initially filled into the cavity and then only supplied from a radial filter between the surrounding steel ring and the specimen. The radial stress was generally only measured at one level.*

In the device used for the axial swelling a steel filter is placed on the upper side of the sample while in case of radial swelling a radial plastic filter is placed between the surrounding steel ring and the specimen.

In the devices the bottom and top plates and the steel ring are bolted together to keep the volume constant. Load cells are placed in the vertical and radial directions. The load cells are placed between a fixed plate and the movable piston where the small deformation required by the load cell is admitted. During the entire course of the tests the forces were measured by the load cells which were calibrated prior to, and checked after, each test.

Preparation of specimens

The specimens were sawn and trimmed from larger blocks with the initial water content between 21 % and 24 % which corresponded to a degree of saturation between 97 % and 100 % for all specimens except a special one having a degree of saturation of 56 % in the HR-A series. The initial height and diameter of the specimens swelling axially were 40–50 mm and 100 mm, respectively. The specimens swelling radially had the initial height and outer diameter 80 mm and 80–97 mm, respectively.

Test procedure

In the HR-series the initial degree of saturation was high and for that reason the swelling phase started directly, i.e. no saturation took place in the test devices before the swelling phase. After preparation the specimens were mounted into one of the devices shown in Figure 4-5 to Figure 4-7 and de-ionised water was applied to the filters after air evacuation of the filters and tubes. In accordance with the fundamental tests in the basic series water was only applied to the upper part of the specimen at axial swelling, only applied to the radial filter at radial outward swelling and at the radial inward swelling applied to the radial filter and also filled into the cavity.

After completed swelling and homogenisation, i.e. when no or negligibly small changes were noticed in the measured swelling pressure, the specimens were dismantled and cut in slices for determination of water content and density distribution in the direction of swelling.

Test results

The test results are presented with w, ρ_d and S_r as a function of the specimen height (series HR-A) or radius (series HR-Ro and HR-Ri), i.e. as distribution in the direction of swelling. The measured stresses are shown and compared with models of swelling pressure of MX-80 presented by Börgesson et al. (1995) and by Åkesson et al. (2010) where the latter model was based on results presented by Karnland et al. (2006). The swelling was calculated according to Equation 4-1.

Test series

The tests run within the high resolution test series are shown in Table 4.2. In addition to the axial and radial types of swelling a test with swelling in all directions was run; HR-Iso.

Table 4-2. Tests run in the high resolution series.

Axial swelling	Radial outward swelling	Radial inward swelling	Isotropic swelling	Material
HR-A2 to HR-A4				MX-80
HR-A6				Calcigel
	HR-Ro2			Calcigel
		HR-Ri1		MX-80
			HR-Iso	MX-80

4.3 Measurements of friction between bentonite and different surfaces

Friction between confined specimens at saturation and different types of surfaces has been studied with the test set-up described below.

Equipment

The tests were carried out in the device shown in Figure 4-8. The swelling pressure device consists of a steel ring surrounding the specimen having filters on both sides. The inner surface of the ring can be prepared in different ways for example with or without lubrication. Two pistons are placed vertically, in the axial direction, above and below the specimen. A radial piston is placed in a hole through the steel ring for measurement of the radial stress.

The bottom and top plates are bolted together to keep the volume constant. Three load cells are used for the measurements of swelling pressure, two in the vertical direction and one in the radial direction. Each load cell is placed between a fixed plate and a movable piston where the small deformation required by the load cell is admitted. At shearing a forth load cell and a deformation transducer are installed for measuring the force applied for moving the ring relative the specimen and the deformation in the axial direction. The transducer and load cells were calibrated prior to, and checked after, each test.

Preparation of specimen

Cylindrical specimens were prepared by compaction of powder to a prescribed density. The specimens had a diameter of 50 mm and a height of 20 mm.

Test procedure

The tests consisted of two phases; the water saturation and the shearing phase. The entire test was done at constant volume conditions. The saturation started by mounting the specimen into the swelling pressure device (Figure 4-8, left) and applying de-ionised water to the filters after air evacuation of the filters and tubes. When the measured swelling pressure had come to equilibrium the friction phase started.

During the shearing phase the swelling pressure device was placed in a load frame (Figure 4-8, right) where the ring was fixed while the specimen was moved upwards with a constant rate, i.e. the specimen was pushed upwards through the ring. The set-up is also shown in Figure 4-9. During the shearing phase the required force to keep the ring in place as well as the deformation and swelling pressure were measured. The specimen had free access to water during both the saturation and the subsequent friction phase. After moving the specimen a distance similar to the height of the specimen the test was finished and the bentonite specimen was dismantled. The distributions of water content and density over the specimen height were then determined.

Test results

The friction angle was evaluated from Equation 4-2 where F is the measured force from the upper load cell, A_s is the radial surface area of the specimen, P_r is the radial stress perpendicular to the ring, and δ is the friction angle between the ring and the bentonite specimen. The swelling pressure and friction angle are presented with average values of w, ρ_d and S_r over the specimens.

$$F = A_s \cdot P_r \cdot \tan(\delta) \qquad (4\text{-}2)$$

Test series

The specimens were saturated with a minimum of swelling and after saturation the friction tests were run where the ring, surrounding the bentonite, had different inner surface; steel surface with or without grooves, plastic surface or acrylic plastic surface. In the eleven tests run MX-80 was used in ten of them and Calcigel in one.

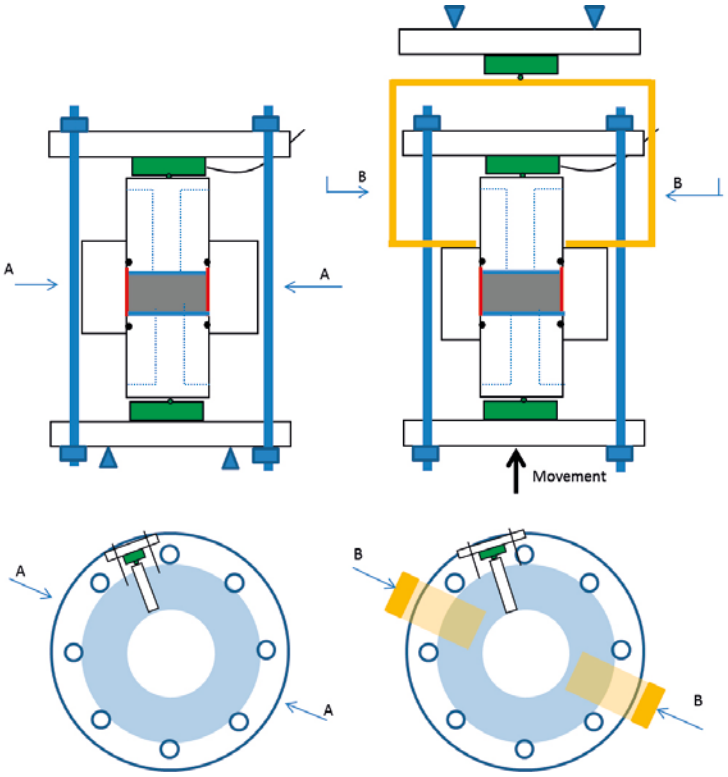

Figure 4-8. *Set-up used for the study of friction between the bentonite and different surfaces. The set-up used during saturation (left) and during shearing (right).*

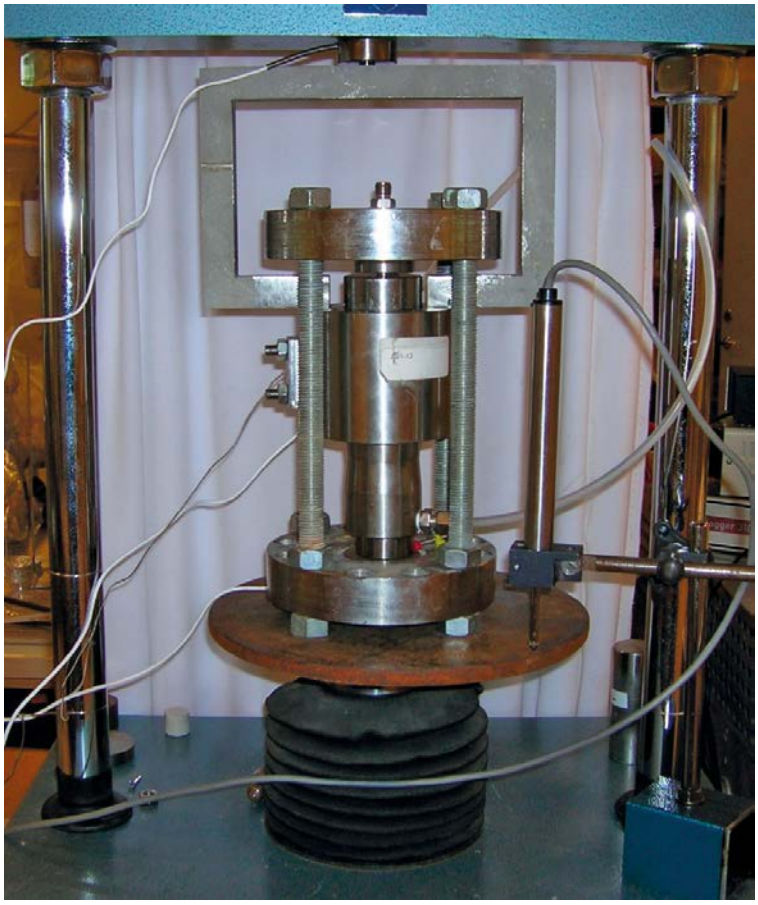

Figure 4-9. *Photo of the set-up during the shearing phase of the test.*

5 Results

In this chapter results from the fundamental swelling tests from the basic series and from the so called high resolution series are presented as well as the test results from the tests of friction between bentonite and different surfaces.

The term swelling pressure is in this project determined as an axial stress P_{axial} or a radial stress P_{radial} exerted as loads on a piston with a certain area. In some tests when a water pressure, P_w, is applied the results are given as an effective stress calculated as the total measured stress minus the water pressure; $P_{axial} - P_w$ or $P_{radial} - P_w$.

In some results the stresses are given as an average stress which is then calculated according to Equation 5-1.

$$\boldsymbol{P_{average} = (P_{axial} + 2 \cdot P_{radial})/3} \qquad (5\text{-}1)$$

5.1 Fundamental swelling tests – basic series

The completed tests in the basic series are presented in this section, see section 4.1 for a test description. Table 5-1, Table 5-2 and Table 5-3 show basic data for the three test types. For each type of swelling the test results are presented in diagrams with the measured distribution of water content w, dry density ρ_d and degree of saturation S_r in the swelling direction and in diagrams with the average stresses $P_{average}$ as a function of the dry density.

In this section and in the diagrams mentioned above the colours (blue, green, red) denote the type of swelling (axial, radial outward, radial inward) resulting from tests on specimens of MX-80 and the colours (brown, light brown, yellow) denote the type of swelling (axial, radial outward, radial inward) resulting from specimens of Calcigel.

For each type of swelling the measured axial and radial stresses are shown as a function of the dry density. In these diagrams the colours (blue, red) denote the direction (axial, radial) in tests with MX-80 and the colours (yellow, brown) denote the direction (axial, radial) in tests with Calcigel.

Additional test results are given in Appendix 1 to 3 where the evolution of the axial and the radial stresses with time is shown in Appendix 1.

Axial swelling

The completed tests with axial swelling are presented in Table 5-1. In Figure 5-1 to Figure 5-3 the distributions of water content w, dry density ρ_d and degree of saturation S_r, measured after the completed tests, are shown. In Figure 5-4 the average stresses, calculated according to Equation 5-1, are plotted as a function of the dry density. In Figure 5-5 both the axial and radial stresses are given as a function of the dry density of each specimen and the stresses are plotted both with a linear vertical axis (to the left) and with a logarithmic vertical axis (to the right). Stresses higher than 6 300 kPa in Figure 5-4 and Figure 5-5 represent the measured initial stresses at saturation. The test on specimen A01-16 included water pressure which is denoted with *Pw* in the label used in some of the diagrams. The use of water pressure is further commented below.

Table 5-1. Specimens used in the series with axial swelling A0. The swelling (%) was calculated from Equation 4-1.

Specimen ID	Material	Initial water content %	Start dry density kg/m^3	Constant radius mm	Start height (target) mm	Final height mm	Swelling %
A01-14	MX-80	24	1618	25	20	27.5	36
A01-15	MX-80	13	1656	25	20	25	27
A01-16	MX-80	12	1658	25	20	21	8
A04-1	Calcigel	19	1661	25	20	25	28
A04-2	Calcigel	19	1661	25	20	27.5	35

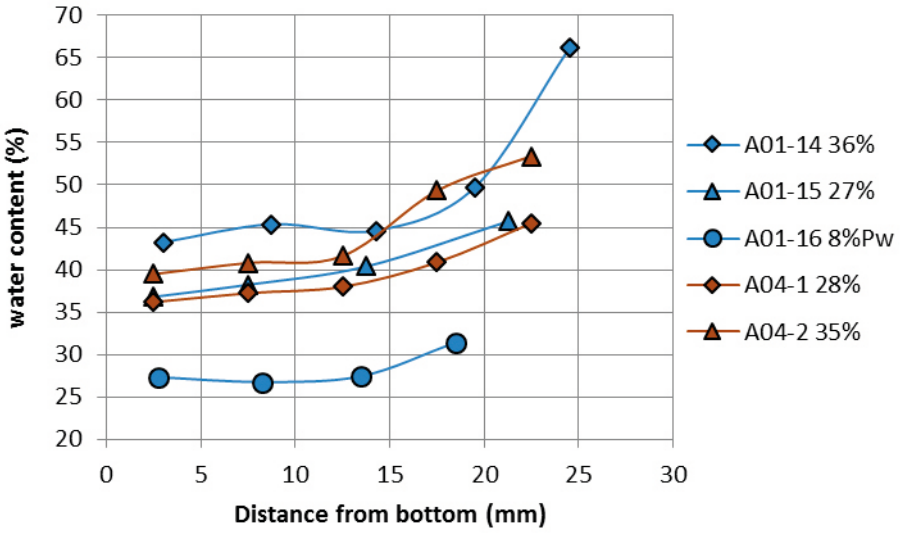

Figure 5-1. *Distribution of water content over the specimen height from series A0. The labels denote the specimen ID and the last figure denotes the swelling. The suffix Pw denotes the use of water pressure. The colours (blue, brown) denote the materials (MX-80, Calcigel).*

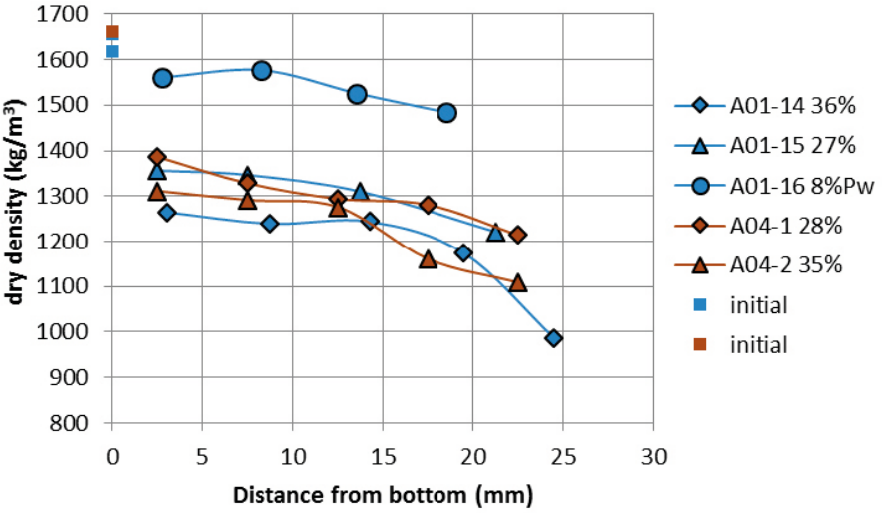

Figure 5-2. *Distribution of dry density over the specimen height from series A0. The same labels and colours as in Figure 5-1 were used. Initial conditions are marked at the distance 0 mm.*

Radial outward swelling

The completed tests with radial outward swelling are presented in Table 5-2. In Figure 5-6 to Figure 5-8 the distributions of water content w, dry density ρ_d and degree of saturation S_r measured after completed tests are shown. In Figure 5-9 the average stresses, calculated according to Equation 5-1, are plotted as a function of the dry density. In Figure 5-10 both the axial and radial stresses are given as a function of the dry density of each specimen and the stresses are plotted both with a linear vertical axis (to the left) and with a logarithmic vertical axis (to the right). The suffix *rad* and *Pw* used in some of the diagrams denote that the actual specimen was either radially sampled from a larger block (R11-22) or that the test included water pressure (R11-24). Both the sampling and the use of water pressure will be further discussed below. Stresses higher than 6 300 kPa in Figure 5-9 and Figure 5-10 represent the measured initial stresses at saturation.

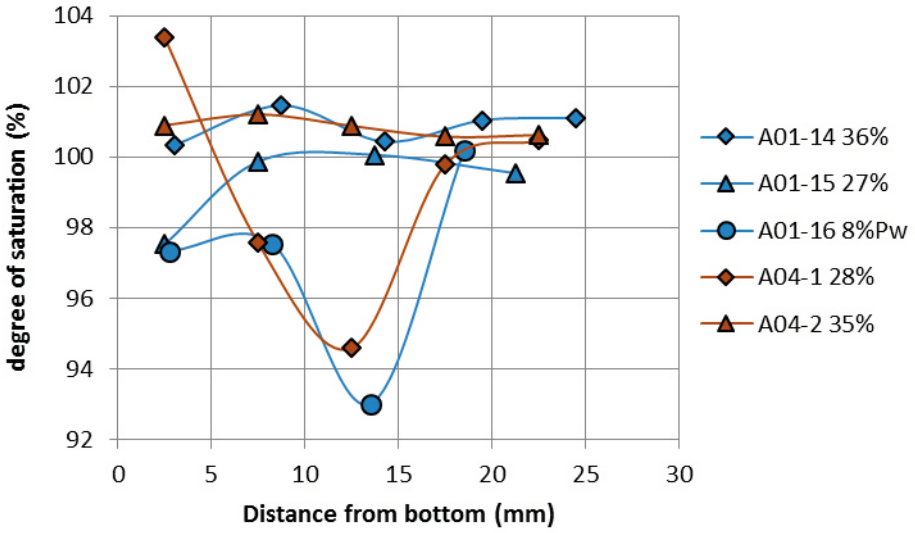

Figure 5-3. *Distribution of degree of saturation over the specimen height from series A0. The same labels and colours as in Figure 5-1 were used.*

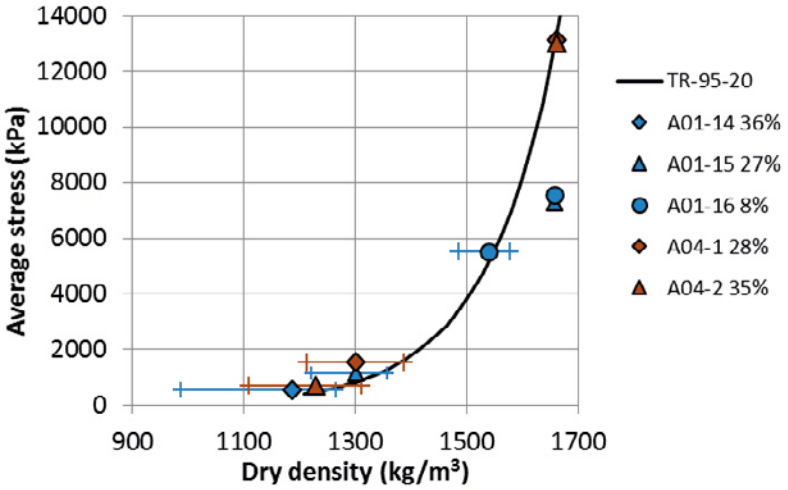

Figure 5-4. *Average stresses as a function of the dry density resulting from series A0. The labels denote the specimen ID and the last figure denotes the swelling in the axial direction. The colours (blue, brown) denote the materials (MX-80, Calcigel).The bars show the minimum and maximum dry density of each specimen. A model of MX-80 presented by Börgesson et al. (1995) is also shown.*

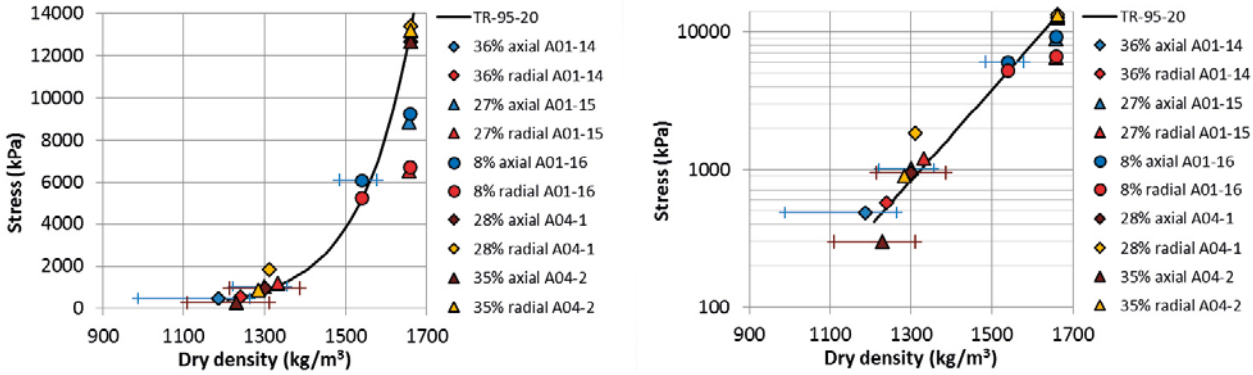

Figure 5-5. *Measured radial and axial stresses as a function of the dry density resulting from series A0. The labels denote the swelling in the axial direction (%), the direction of the measured stress and the specimen ID. The bars show the minimum and maximum dry density of each specimen. The stresses are shown with a linear vertical axis (to the left) and a logarithmic vertical axis (to the right). A model of MX-80 presented by Börgesson et al. (1995) is also shown.*

Table 5-2. Specimens used in the series with radial outward swelling R1. The swelling (%) was calculated from Equation 4-1.

Specimen ID	Material	Initial water content %	Start dry density kg/m^3	Constant height mm	Initial diameter (target) mm	Final diameter mm	Swelling %
R11-22	MX-80	11.6	1599	40	40.8	46.8	34
R11-23	MX-80	12.7	1655	40	40.8	46.8	24
R11-24	MX-80	10.6	1648	40	40.8	46.8	37
R14-1	Calcigel	19.8	1649	40	40.8	46.8	34
R14-2	Calcigel	17.9	1650	40	43.8	46.8	16

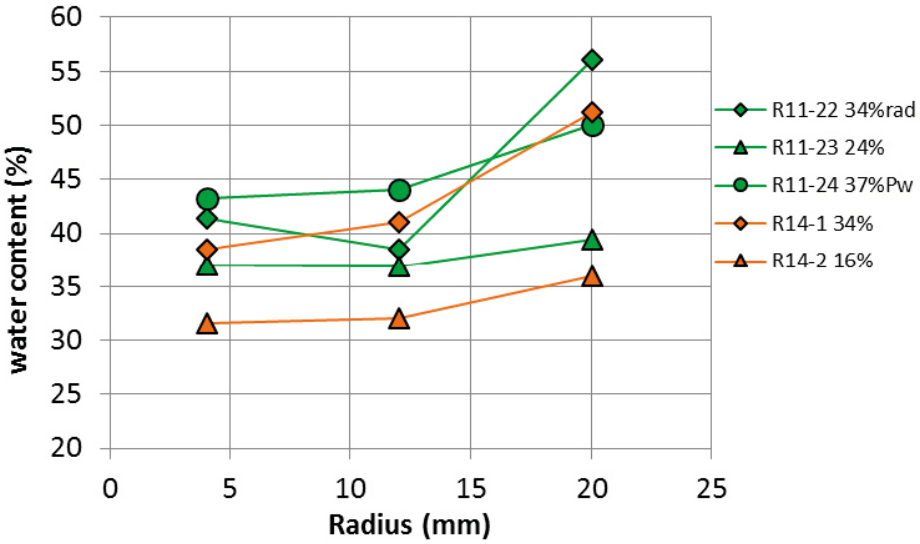

Figure 5-6. Distribution of water content over the radius of the specimens in series R1. The labels denote the specimen ID and the last figure denotes the swelling. The suffixes rad and Pw indicate a special type of sampling and the use of water pressure, respectively. The colours (green, light brown) denote the materials (MX-80, Calcigel).

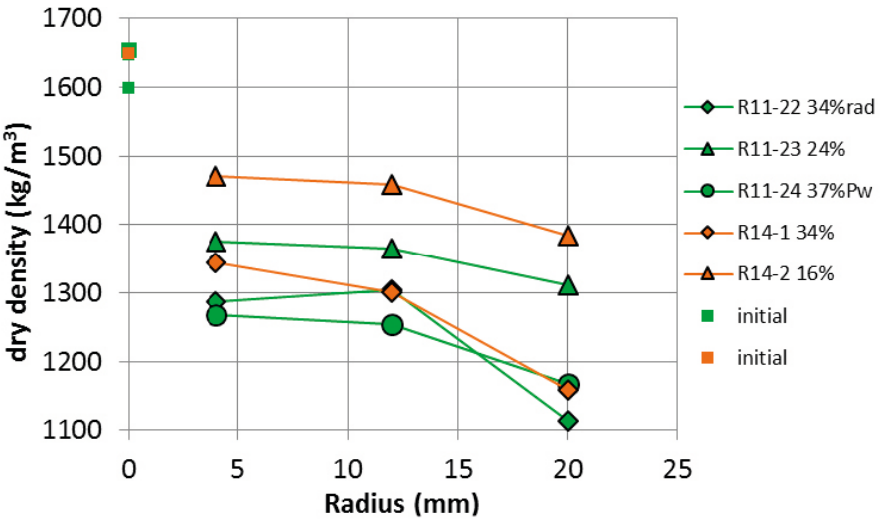

Figure 5-7. Distribution of dry density over the radius of the specimens in series R1. The same labels and colours as in Figure 5-6 were used. Initial conditions are marked at the radius 0 mm.

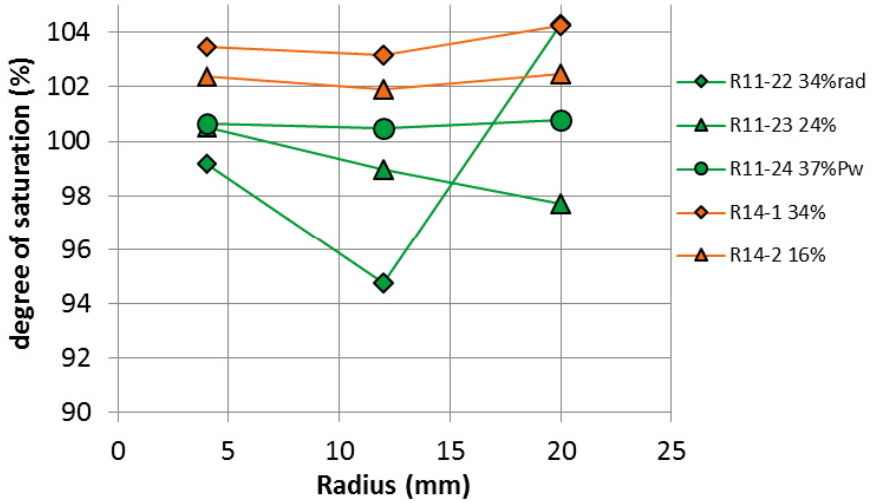

Figure 5-8. *Distribution of degree of saturation over the radius of the specimens in series R1. The same labels and colours as in Figure 5-6 were used.*

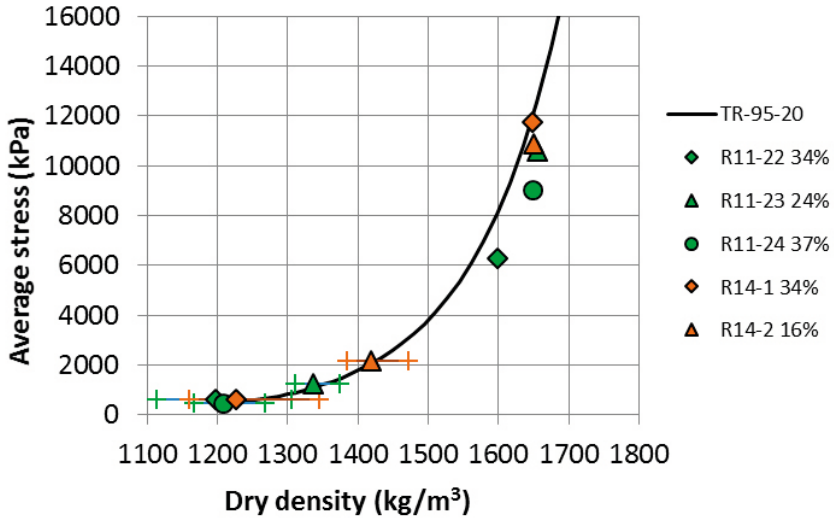

Figure 5-9. *Average stresses as a function of the dry density resulting from series R1. The labels denote the specimen ID and the last figure denotes the swelling in the radial direction. The colours (green, light brown) denote the materials (MX-80, Calcigel).The bars show the minimum and maximum dry density of each specimen. A model of MX-80 presented by Börgesson et al. (1995) is also shown.*

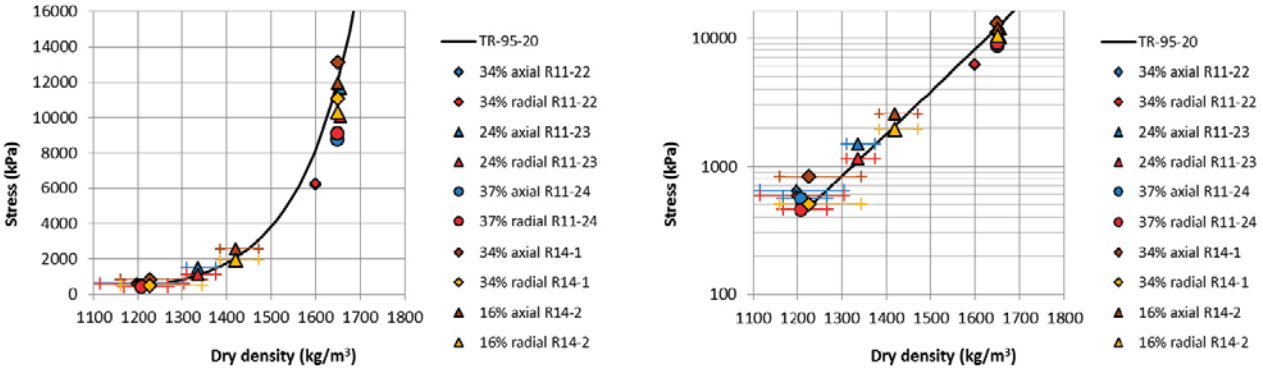

Figure 5-10. *Measured radial and axial stresses as a function of the dry density resulting from series R1. The labels denote the swelling in the radial direction (%), the direction of the measured stress and the specimen ID. The bars show the minimum and maximum dry density of each specimen. The stresses are shown with a linear vertical axis (to the left) and a logarithmic vertical axis (to the right). A model of MX-80 presented by Börgesson et al. (1995) is also shown.*

Radial inward swelling

The completed tests with radial inward swelling are presented in Table 5-3. In Figure 5-11 to Figure 5-13 the distributions of water content w, dry density ρ_d and degree of saturation S_r measured after completed tests are shown. In Figure 5-14 the average stresses, calculated according to Equation 5-1, are plotted as a function of the dry density. In Figure 5-15 both the axial and radial stresses are given as a function of the dry density of each specimen and the stresses are plotted both with a linear vertical axis (to the left) and with a logarithmic vertical axis (to the right). Stresses higher than 6 300 kPa in Figure 5-14 and Figure 5-15 represent the measured initial stresses at saturation.

Some problem was found with the force transducer used for the measurement of the radial stress of R24-1. An inexplicable increase during the last part of the test was seen and the sensor was considered defect. Although the first part of the actual measurement can be considered as likely but uncertain.

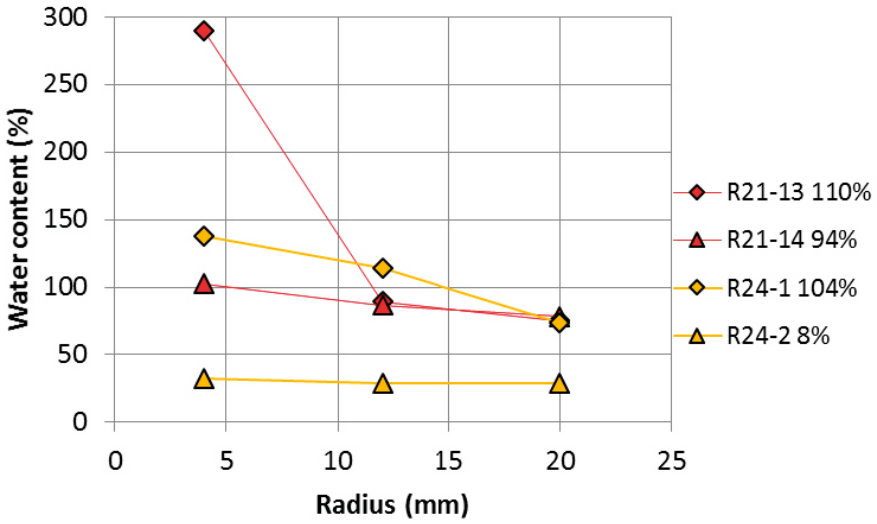

Figure 5-11. *Distribution of water content over the radius of the specimens in series R2. The labels denote the specimen ID and the last figure denotes the swelling. The colours (red, yellow) denote the materials (MX-80, Calcigel).*

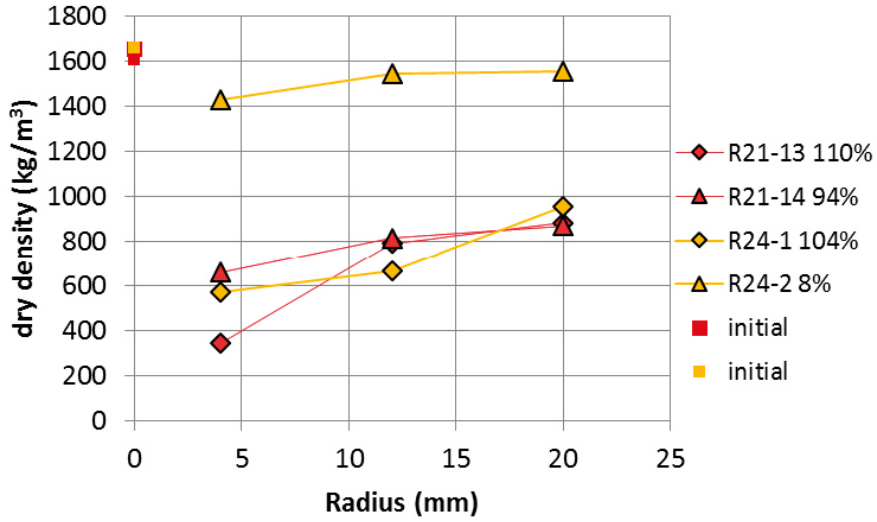

Figure 5-12. *Distribution of dry density over the radius of the specimens in series R2. The same labels and colours as in Figure 5-11 were used. Initial conditions are marked at the radius 0 mm.*

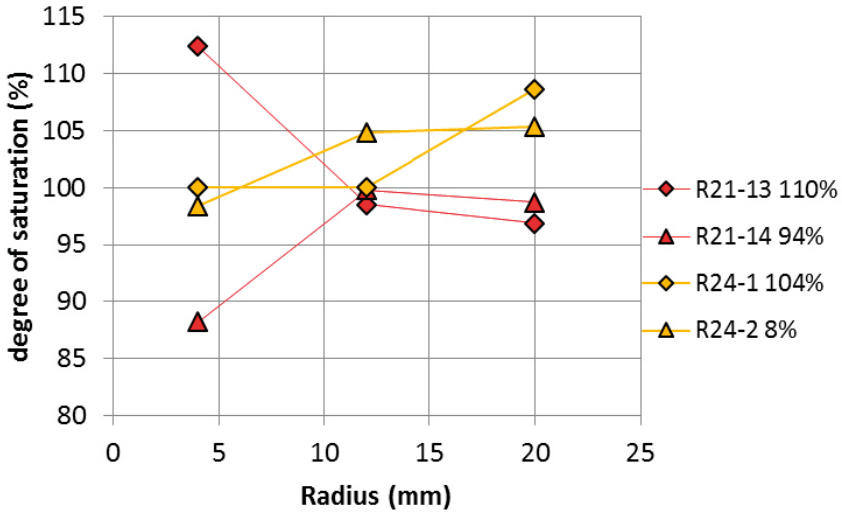

Figure 5-13. *Distribution of degree of saturation over the radius of the specimens in series R2. The same labels and colours as in Figure 5-11 were used.*

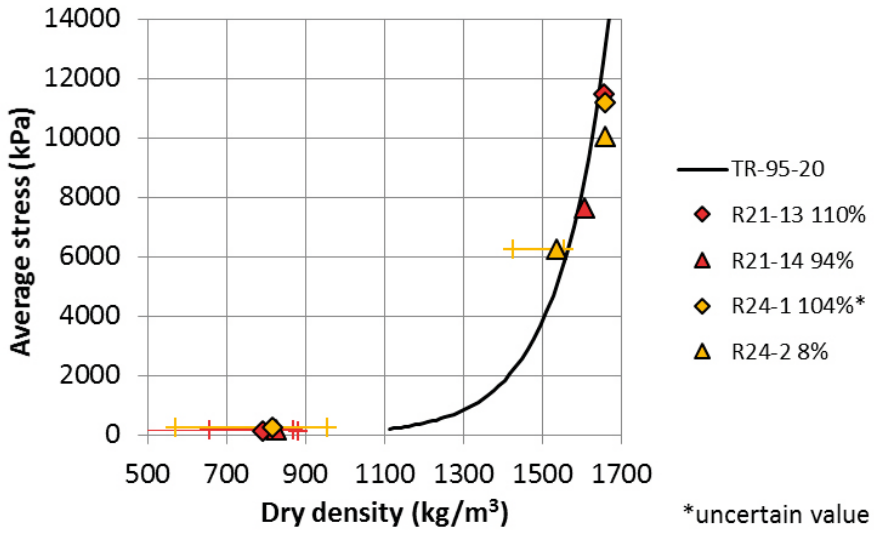

Figure 5-14. *Average stresses as a function of the dry density resulting from series R2. The labels denote the specimen ID and the last figure denotes the swelling in the radial direction. The colours (red, yellow) denote the materials (MX-80, Calcigel). The bars show the minimum and maximum dry density of each specimen. A model of MX-80 presented by Börgesson et al. (1995) is also shown.*

Table 5-3. Specimens used in the series with radial inward swelling R2. The swelling (%) was calculated from Equation 4-1.

Specimen ID	Material	Initial water content	Start dry density	Constant height	Constant outer diameter	Cavity diameter (target)	Swelling
		%	kg/m³		mm	mm	%
R21-13	MX-80	12.6	1656	40	46.8	33	110
R21-14	MX-80	12.5	1606	40	46.8	33	94
R24-1	Calcigel	18	1658	40	46.8	33	104
R24-2	Calcigel	18	1658	40	46.8	10.5	8

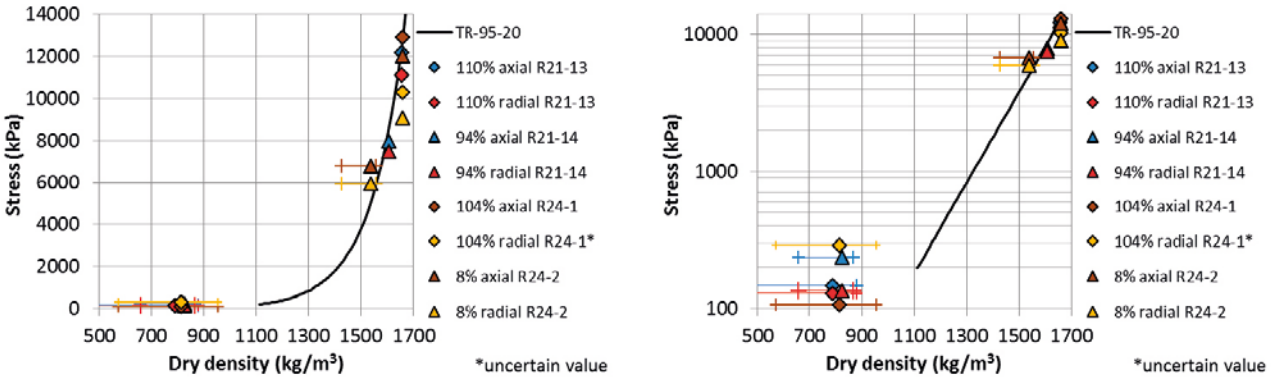

Figure 5-15. *Measured radial and axial stresses as a function of the dry density resulting from series R2. The labels denote the swelling in the radial direction (%), the direction of the measured stress and the specimen ID. The bars show the minimum and maximum dry density of each specimen. The stresses are shown with a linear vertical axis (to the left) and a logarithmic vertical axis (to the right). A model of MX-80 presented by Börgesson et al. (1995) is also shown.*

Comments

In the following analysis the stresses after swelling are compared in diagrams slightly different from above. In addition, some comments regarding influence of water pressure, time and sampling are given. In the following diagrams the new results presented above are shown together with results from previous reports of this project (TR-14-25 or TR-12-02). The results from the previous reports are shown with open symbols. Regarding the high degrees of saturation, above 100 %, observed after dismantling some of the specimens, this is further commented in section 5.2.

In Figure 5-16 to Figure 5-18 test results of MX-80 specimens from the basic test series are presented. Average stresses are plotted as a function of the dry density and the ratio of the dry density and the average dry density is shown as a function of the height or the radius of each specimen. Each type of swelling is shown in separate diagrams.

The diagrams show that at a certain density the average stresses measured in the tests are equal to or slightly higher than the values shown by the model presented by Börgesson et al. (1995) (label TR-95-20). Deviations from this are mainly seen in the results from R11-19 and R11-21.

Average stresses from all tests on Calcigel are presented in similar diagrams in Figure 5-19 to Figure 5-21 where the lines represent results of MX-80. The behaviour of the Calcigel specimens resembles that of the MX-80 specimens.

A pressure was applied to the water supply during the final part of two tests with MX-80, i.e. A01-16 and R11-24. In Figure 5-22 and Figure 5-23 the evolution of the measured axial stress, radial stress and applied water pressure are shown to the left and the stresses minus the water pressure, i.e. the so called effective stresses, are shown to the right. In the diagrams to the left the stresses during both the saturation and the homogenisation phases are shown while the stresses in the diagrams to the right only show the second homogenisation phase.

In general, the effective stress decreases with increased applied water pressure but an increase is seen, compared to the initially measured, when the water pressure is adjusted back to zero. However, during the first two steps of increased water pressure of R11-24, the effective stress increased and never returned to its initial value when the water pressure was adjusted back to zero. The cause of this is not clear but must be regarded as an uncertainty in this measurement. It may be an indication that a small water pressure is useful in order to yield full water saturation and full swelling pressure.

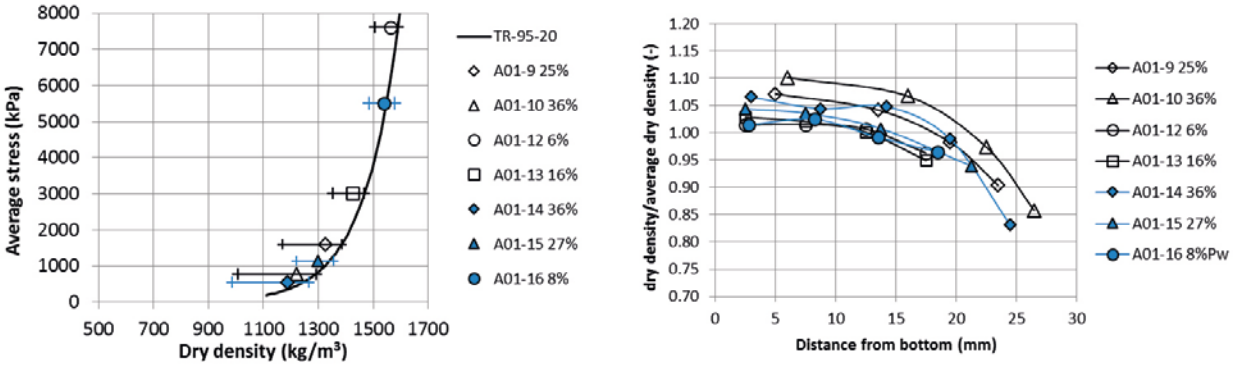

Figure 5-16. *Test results from axial swelling of MX-80 specimens (series A01). Average stress after homogenisation as a function of the dry density with maximum and minimum dry density marked (to the left) and corresponding ratios of dry density to the average dry density as a function of distance (to the right). The labels denote the specimen ID and the last figure denotes the swelling in the axial direction.*

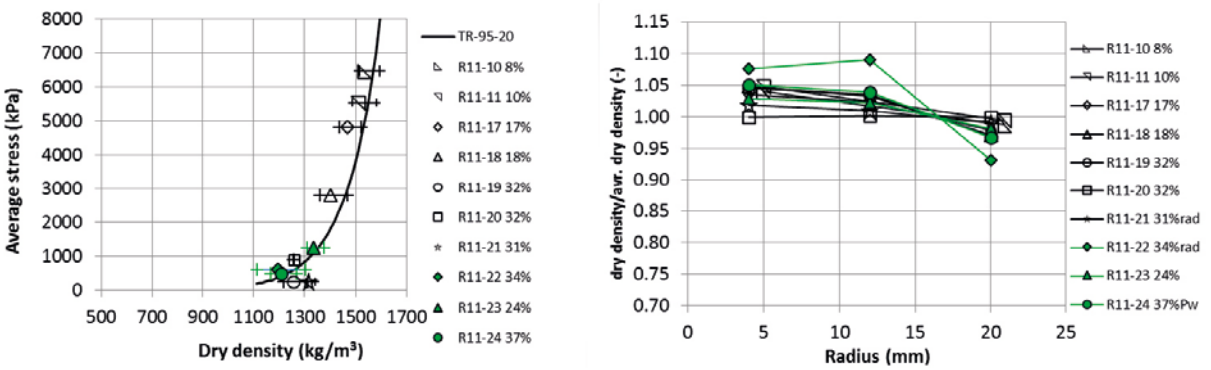

Figure 5-17. *Test results from radial outward swelling of MX-80 specimens (series R11). Average stress after homogenisation as a function of the dry density with maximum and minimum dry density marked (to the left) and corresponding ratios of dry density to the average dry density as a function of distance (to the right). The labels denote the specimen ID and the last figure denotes the swelling in the radial direction.*

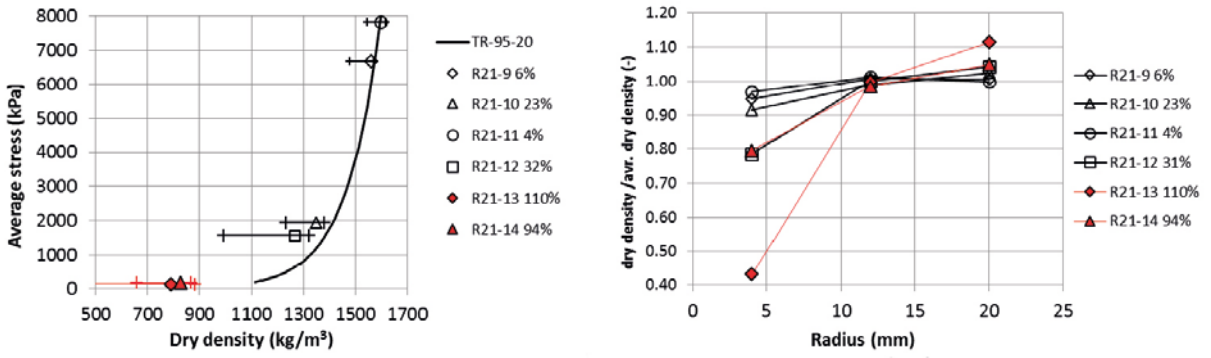

Figure 5-18. *Test results from radial inward swelling of MX-80 specimens (series R21). Average stress after homogenisation as a function of the dry density with maximum and minimum dry density marked (to the left) and corresponding ratios of dry density to the average dry density as a function of distance (to the right).The labels denote the specimen ID and the last figure denotes the swelling in the radial direction.*

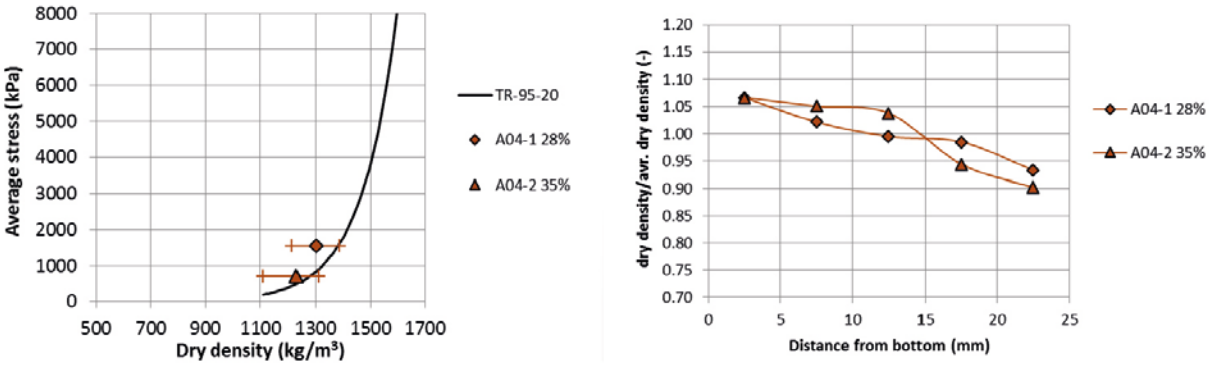

Figure 5-19. *Test results from axial swelling of Calcigel specimens (series A04). Average stress after homogenisation as a function of the dry density with maximum and minimum dry density marked (to the left) and corresponding ratios of dry density to the average dry density as a function of distance (to the right).The labels denote the specimen ID and the last figure denotes the swelling in the axial direction. A model of MX-80 presented by Börgesson et al. (1995) is also shown.*

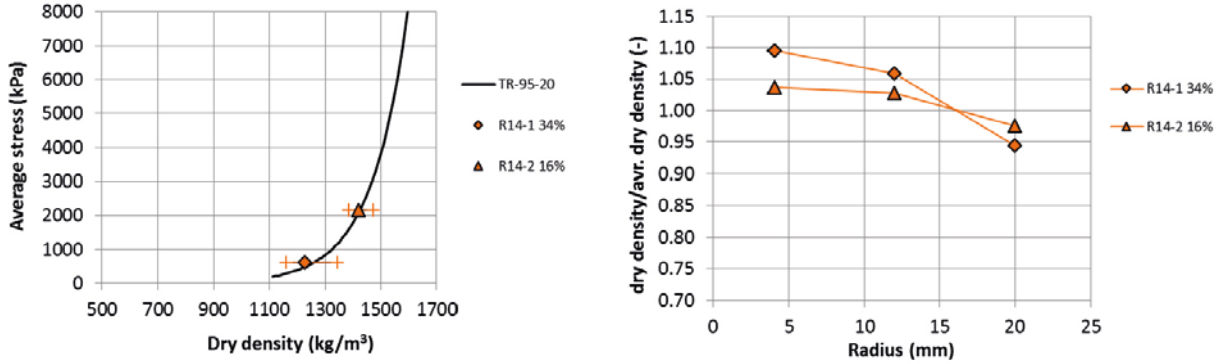

Figure 5-20. *Test results from radial outward swelling of Calcigel specimens (series R14). Average stress after homogenisation as a function of the dry density with maximum and minimum dry density marked (to the left) and corresponding ratios of dry density to the average dry density as a function of distance (to the right).The labels denote the specimen ID and the last figure denotes the swelling in the radial direction. A model of MX-80 presented by Börgesson et al. (1995) is also shown.*

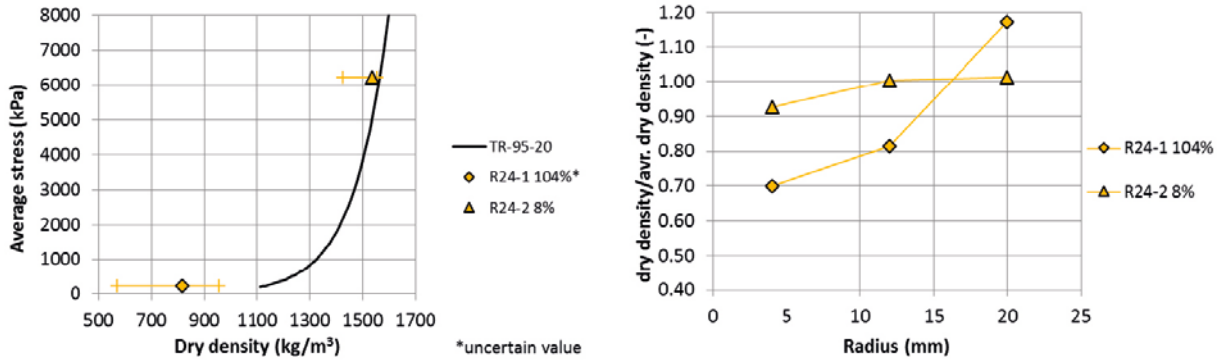

Figure 5-21. *Test results from radial inward swelling of Calcigel specimens (series R24). Average stress after homogenisation as a function of the dry density with maximum and minimum dry density marked (to the left) and corresponding ratios of dry density to the average dry density as a function of distance (to the right).The labels denote the specimen ID and the last figure denotes the swelling in the radial direction. A model of MX-80 presented by Börgesson et al. (1995) is also shown.*

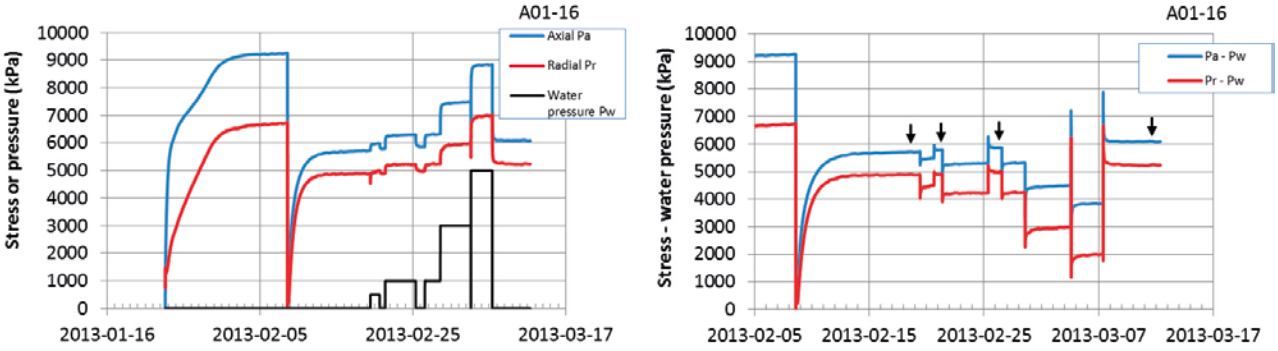

Figure 5-22. *Test results from axial swelling of MX-80 with water pressure applied. Evolution of measured total stress to the left and evolution of effective stress, calculated as total stress minus water pressure, after homogenisation (to the right). The arrows mark the stresses measured at zero water pressure.*

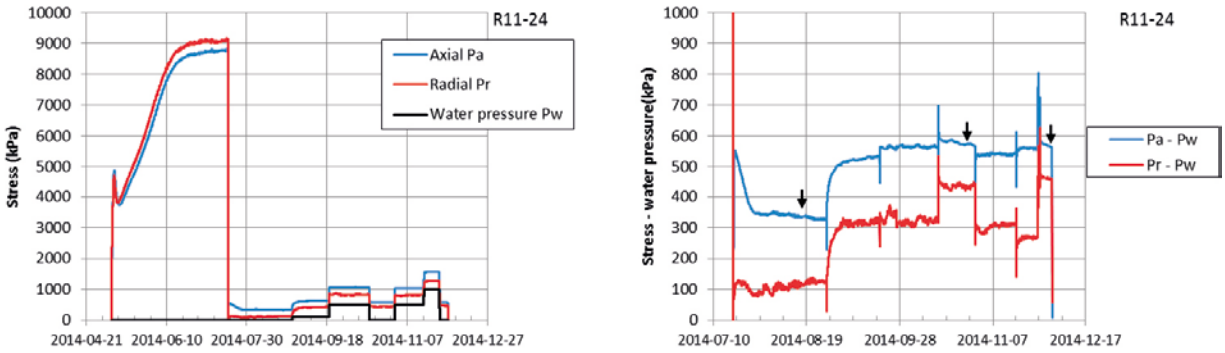

Figure 5-23. *Test results from radial outward swelling of MX-80 with water pressure applied. Evolution of measured total stress to the left and evolution of effective stress, calculated as total stress minus water pressure, after homogenisation (to the right). The arrows mark the stresses measured at zero water pressure.*

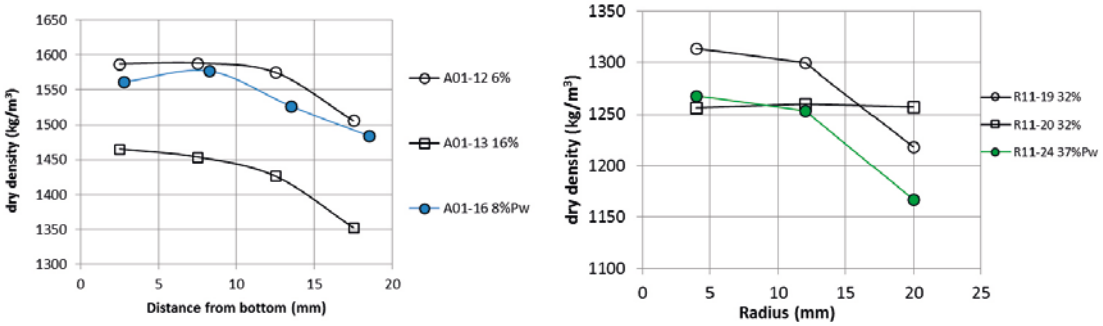

Figure 5-24. *Distribution of dry density for specimens with water pressure applied during the homogenisation, A01-16 and R11-24, shown with comparable tests results.*

In Figure 5-24 the distributions of dry density after tests A01-16 and R11-24 are plotted with comparable test results from the same type of swelling but without water pressure. No obvious influence of the water pressure can be seen in the diagrams.

One of the specimens, R11-22, was sampled radially from a larger block of MX-80 that was compacted in axial direction. The test results are compared with results of a similar test, R11-21, also sampled radially from the same block and presented in the previous report TR-14-25. In Figure 5-25 the results from the two tests are shown with stresses plotted as a function of the dry density (to the left) and the distribution of dry density plotted as a function of the radius (to the right). The large deviation between the initial stress measured after saturation of R11-21 and the expected stress from the model (label TR-95-20) was not seen after the saturation of specimen R11-22.

Since it is not possible to measure the density of the specimens at saturation, i.e. before the swelling, it is possible that the density of R11-21 at saturation was actually lower than the estimated value based on the measured initial density and the volume of the specimen, and the inner volume of the device.

There are additional unclear results in these two tests. Not only the stress after saturation but also the stress after homogenisation of specimen R11-21 deviates from the model. In addition the density distributions differ largely between the two specimens despite the use of approximately 20 days for the homogenisation of both specimens.

In Figure 5-26 the influence of the initial water content and thereby the degree of saturation can be studied by comparing the results from the two similar tests A01-10 and A01-14 having different initial water contents; 10 % and 24 %, respectively. No obvious difference is seen between these test results.

In Figure 5-26 the influence of time for the homogenisation can also be studied by comparison of the tests A01-9 and A01-15 since the main difference between these two tests was the time used for the homogenisation, 11 days and 28 days, respectively. Less density difference was logically seen in the specimen A01-15 having the longest time for homogenisation which indicates that 11days may be too short time for this type of test. Specimen A01-15 also showed less stress change, 5 kPa per 24h, just before termination compared to the stress change seen before the termination of A01-09, 30 kPa per 24h (this can be seen in Appendix 1 and in the report TR-12-02, respectively).

The influence of time can also be studied in the series with radial outward swelling (Figure 5-27) by comparison of R11-19 and R11-23, which were left to homogenise during 16 days and 51 days, respectively. The specimen homogenised for the longest time had marked less density difference in the direction of swelling. The change in stress with time was for both specimens 1 kPa per 24h (seen in TR-14-25 and Appendix 1, respectively).

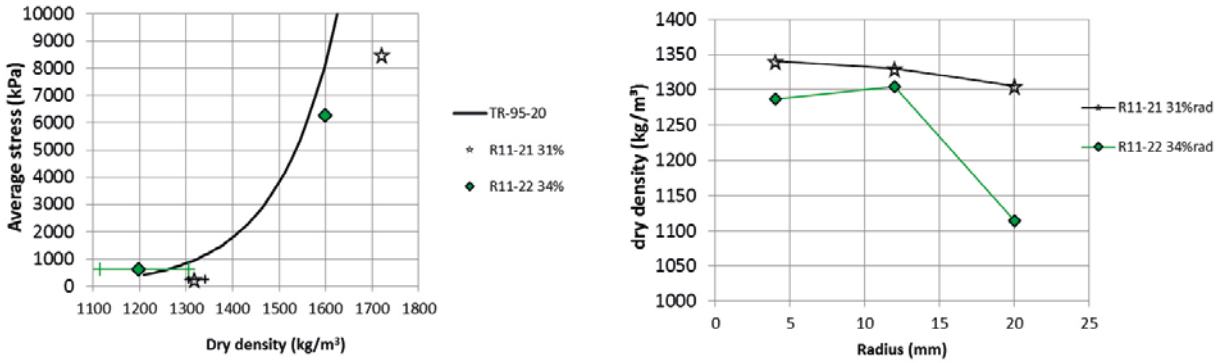

Figure 5-25. *Test results from R11-21 and R11-22.*

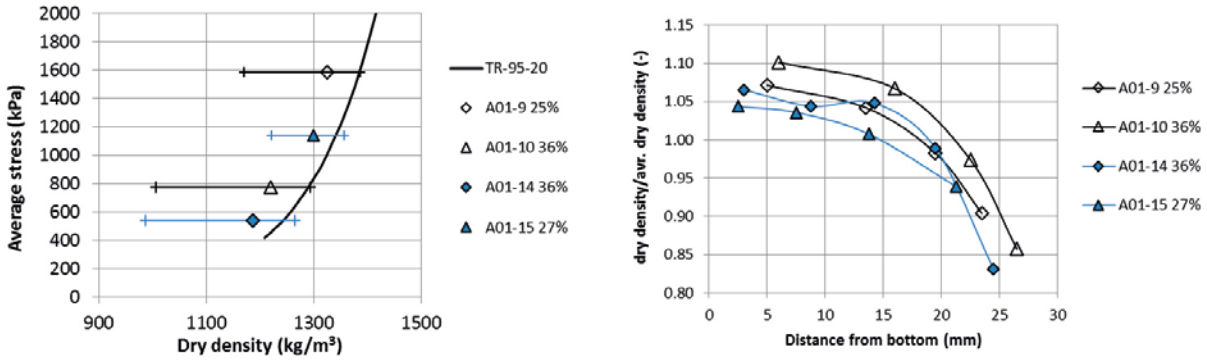

Figure 5-26. *Part of results shown in Figure 5-16.*

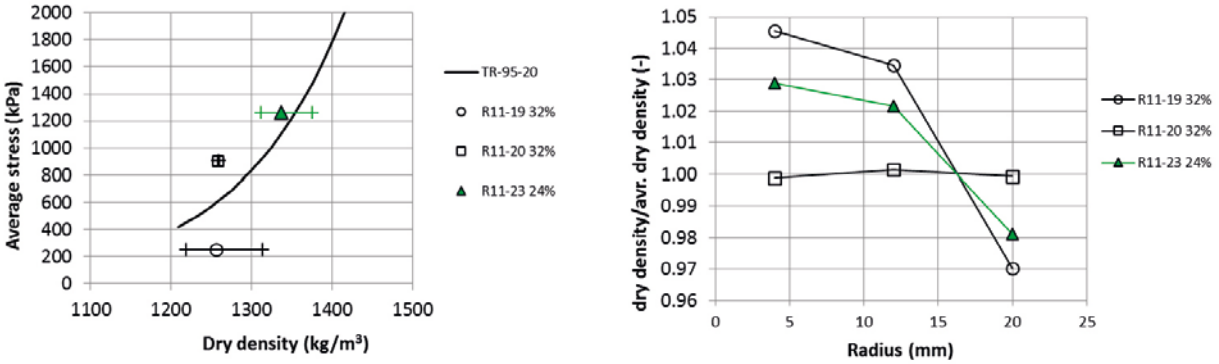

Figure 5-27. *Part of results shown in Figure 5-17.*

Regarding the required time to reach fully homogenised condition only 14 days was needed for test R11-20 until both constant stress with time was reached and also a minimum of density gradient was seen, Figure 5-27. The specimen in this test was otherwise similar to the specimen in test R11-19 except that it was compacted in two pieces, to make the specimen initially as homogeneous as possible in the axial direction. It should be noted that the use of an initially homogeneous specimen, i.e. specimen compacted in two pieces, was also used in test R11-23, however in spite of more than the doubled time for the homogenisation a relatively large density difference in the direction of swelling was seen. An additional test starting with two compacted specimens was R21-13.

The influence of resting time after large swelling could also be studied when comparing the inward swelling in test R21-13 and R21-14 where 14 days and 35 days, respectively, were used for the homogenisation. In both tests the stress change 1 kPa per 24h was registered during the last day but the longer testing time gave less density gradient in the direction of swelling, i.e. in the radial direction.

The observations mentioned above can be summarised by the following bullets (some of the points are based on very few samples and should be further verified):

- The average stresses after swelling and homogenisation show expected values corresponding to the actual average density.
- Resting time seems to influence the density gradient but still after long time density gradients are observed. Small or no stress change with time is no indication of fully homogenised specimen. However, a remaining high stress change with time indicates too short time used for the homogenisation.
- No clear effect on the final density gradient was seen from difference in the initial water content (degree of saturation) or from difference in the preparation of samples.
- No obvious influence on the density gradient could be observed when water pressure was applied during the homogenisation.
- Water pressure influenced the stresses in the sense that the effective stress decreased with increasing water pressure while the swelling pressure increased after removal of the cycles of water pressure.
- The swelling pressures at saturation, before swelling, have been plotted with estimated values of the corresponding dry densities and since these densities could not be measured they may in several cases have been overestimated.

5.2 Fundamental swelling tests – high resolution

The completed swelling tests made in the so called high resolution series are presented in this section. In this series larger specimens, compared to the specimens used in the basic series, are used which admit higher resolution both in radial stress measurements and measured density distribution. See section 4.2 for a test description.

For each type of swelling the tested specimens are listed in Table 5-4 to Table 5-7. The test results are presented in diagrams with the distributions of water content w, dry density ρ_d and degree of saturation S_r and in diagrams with the evolution of swelling pressure. The results are also presented in diagrams with the measured stress and the average stress $P_{average}$ as a function of the dry density. Additional results are given in Appendix 4.

The labels in the diagrams give information about the specimen ID, which includes the type of swelling; HR-A, HR-Ro or HR-Ri (axial swelling, radial outward swelling or radial inward swelling). In most of the labels the swelling, calculated according to Equation 4-1, is given in % and in some of the labels of stress measurements the position of the measurement is given as distance in mm from the bottom of the specimen.

For the tests involving radial swelling the water content and density distribution after completed swelling was measured by dividing the central part of the specimen in 5 mm pieces as shown in Figure 5-28 (to the left). It is desired to have the sampling done so that the density distribution could be plotted as a function of the radius but since this would give too small samples close to the centre, the sampling had to be done as shown in the figure. The results from each sample are therefore presented as a function of a radius r_c, calculated according to Equation 5-2, instead of as a function of the radius r_a measured along the x-axis, see Figure 5-28 (to the right). This is done to take into account that the x-axis is a symmetry plane.

$$r_c = (r_a^2 + (L/4)^2)^{0.5} \quad (5\text{-}2)$$

Axial swelling

The completed tests of axial swelling are presented in Table 5-4. In Figure 5-29 to Figure 5-41 the distributions of water content w, dry density ρ_d and degree of saturation S_r measured after completed tests are shown together with the evolution of the stresses measured during the tests. The axially and radially measured stresses are plotted in Figure 5-42 to Figure 5-44 and in Figure 5-45 the average stresses, calculated according to Equation 5-1, are plotted as a function of the dry density.

Table 5-4. Specimens used in the series with axial swelling, HR-A. Results from specimen HR-A1 (TR-14-25) are given as a complement. The swelling (%) was calculated from Equation 4-1.

Test ID	Material	Initial water content %	Initial dry density kg/m³	Initial degree of saturation	Constant diameter mm	Initial height mm	Final height mm	Final swelling %
HR-A1	MX-80	23.7	1666[2]	99	100	40	50	32
HR-A2	MX-80	24.4	1235[1]	56	100	50	50	0
HR-A3	MX-80	23.7	1666[2]	99	100	40	48	22
HR-A4	MX-80	22.5	1693[2]	97	100	50	70	41
HR-A6	Calcigel	20.9	1730[2]	100	100	50	70	46

[1] Compacted in two pieces with different dry density; 1450 and 1020 kg/m³. The given value is the average.

[2] Sampled from lager block with the given density and trimmed to fit the device.

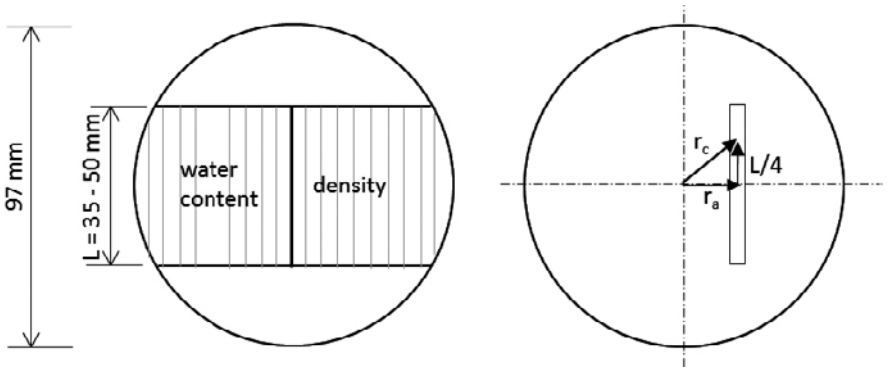

Figure 5-28. *Sampling scheme for the HR-R tests (left). Calculation of the corrected radius r_c of the sampling (right). The distance L is equal to 50 mm and 35 mm in the tests HR-Ro and HR-Ri, respectively.*

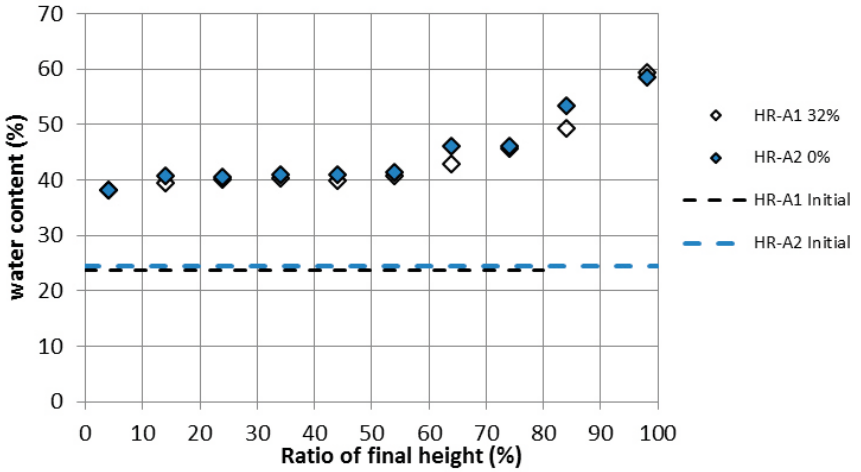

Figure 5-29. *Distribution of water content over the specimen height, HR-A2. Results from HR-A1 are given with open symbols.*

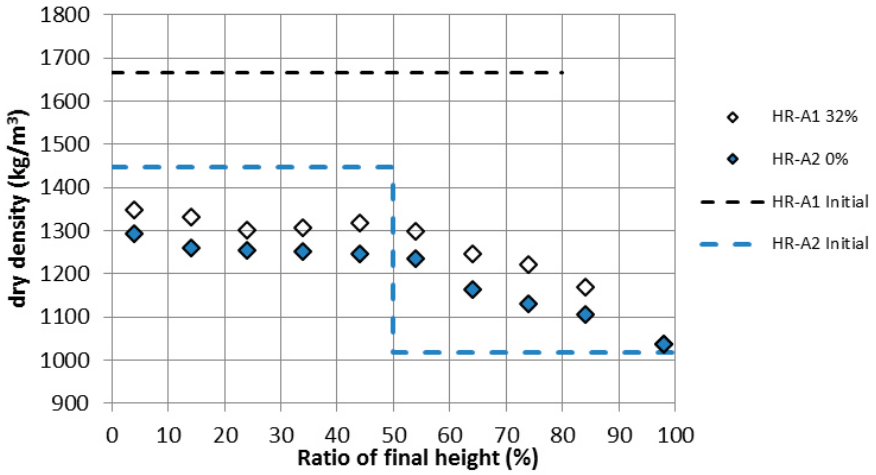

Figure 5-30. *Distribution of dry density over the specimen height, HR-A2. Results from HR-A1 are given with open symbols.*

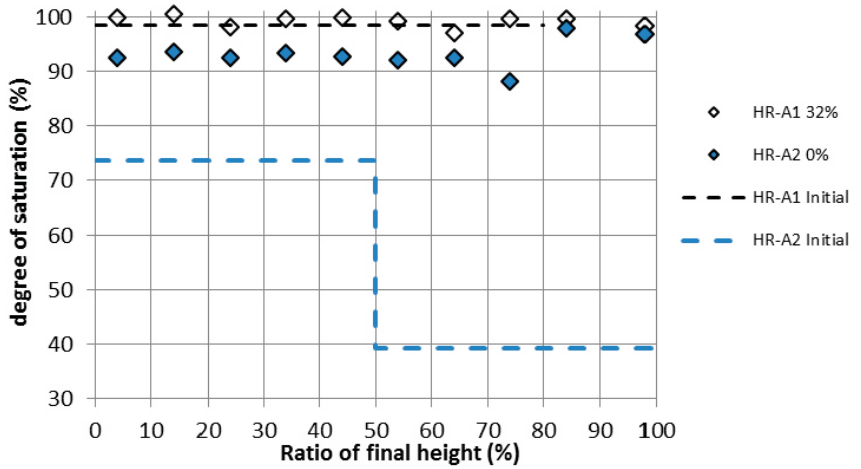

Figure 5-31. *Distribution of degree of saturation over the specimen height, HR-A2. Results from HR-A1 are given with open symbols.*

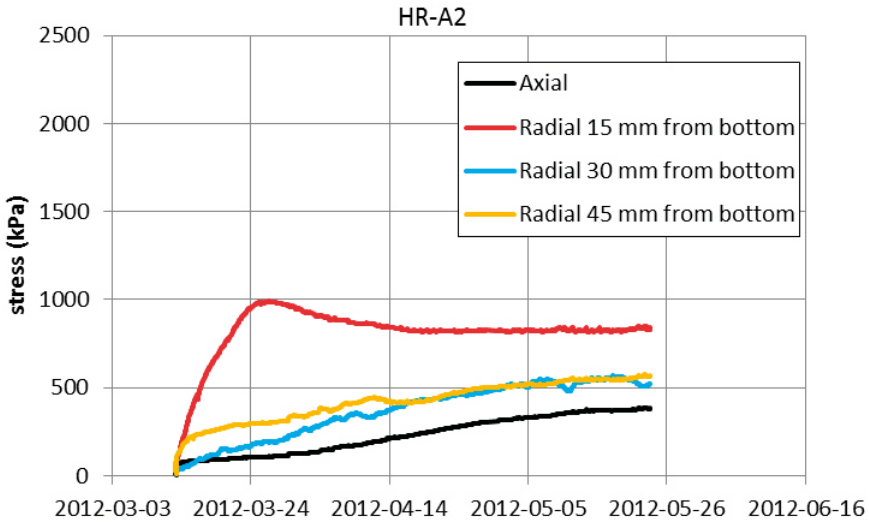

Figure 5-32. *Evolution of swelling pressure over time, HR-A2.*

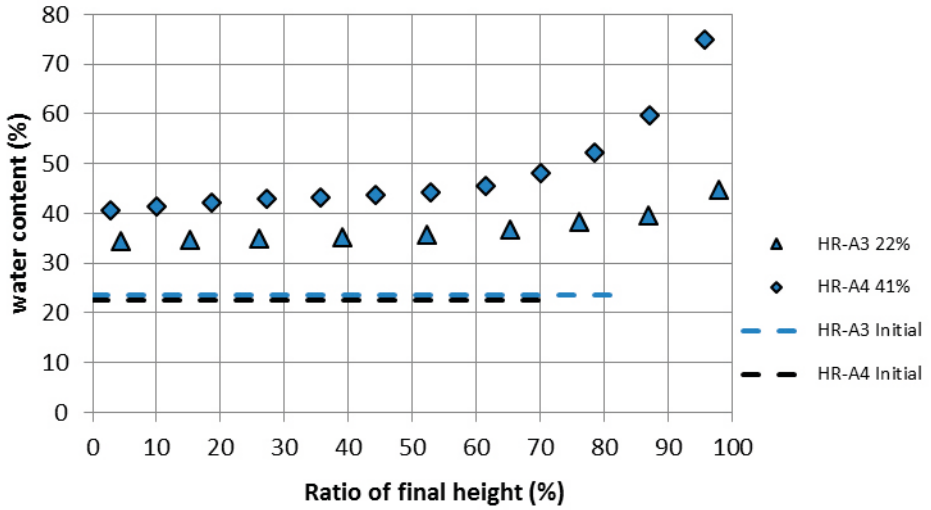

Figure 5-33. *Distribution of water content over the specimen height, HR-A3 and HR-A4.*

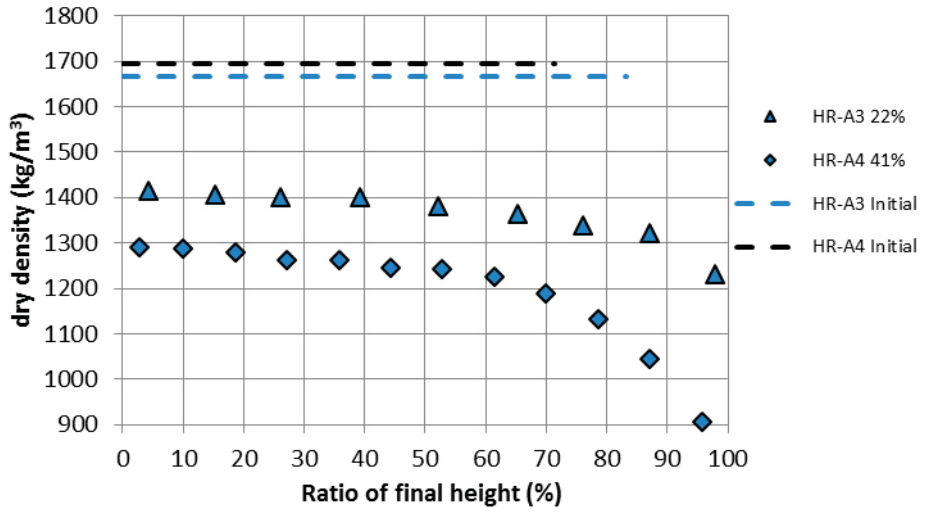

Figure 5-34. *Distribution of dry density over the specimen height, HR-A3 and HR-A4.*

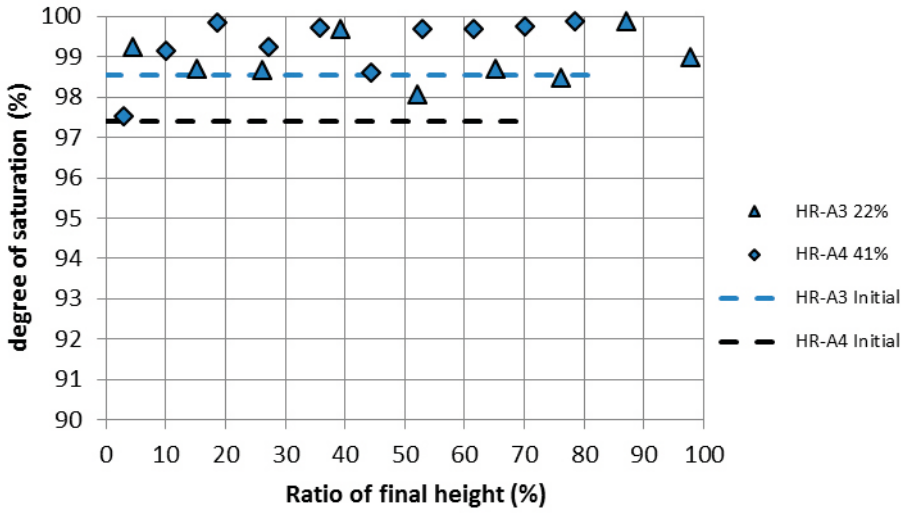

Figure 5-35. *Distribution of degree of saturation over the specimen height, HR-A3 and HR-A4.*

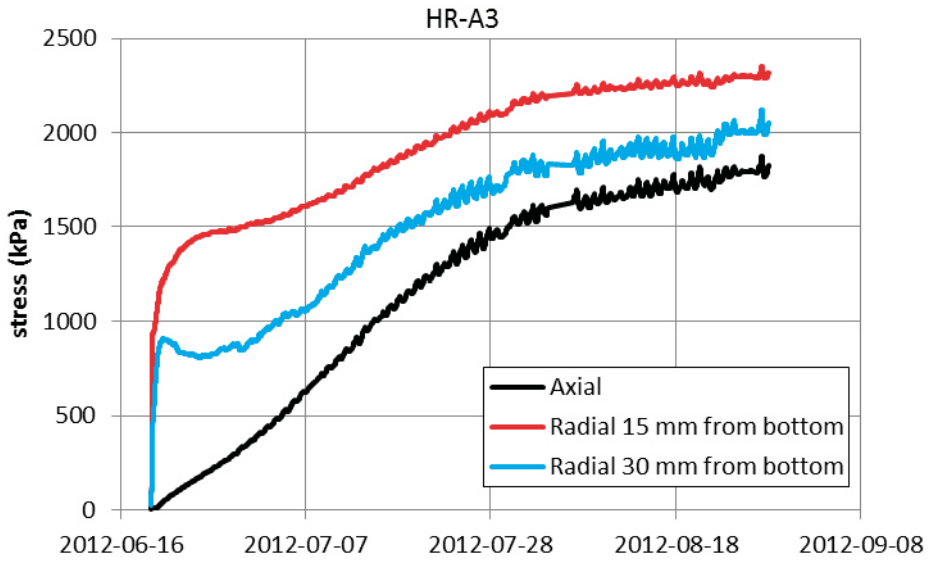

Figure 5-36. *Evolution of swelling pressure over time, HR-A3.*

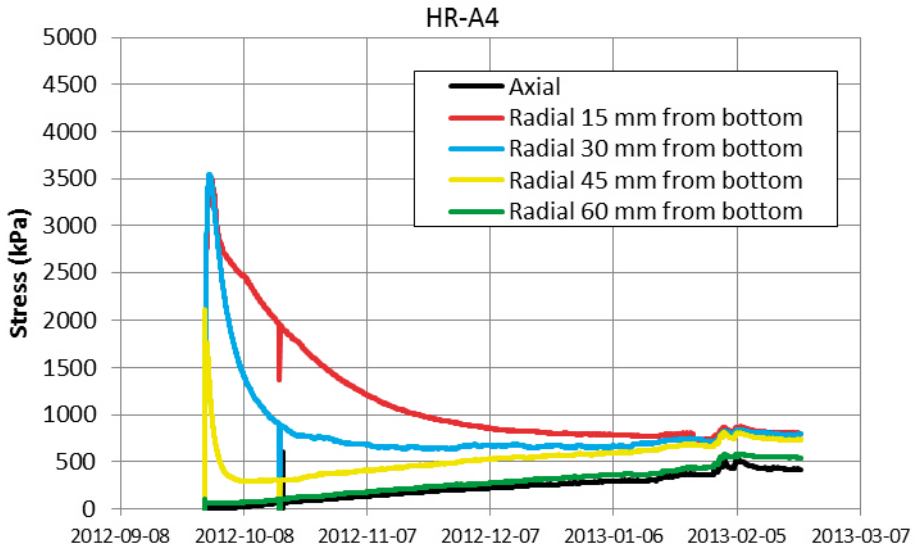

Figure 5-37. *Evolution of swelling pressure over time, HR-A4.*

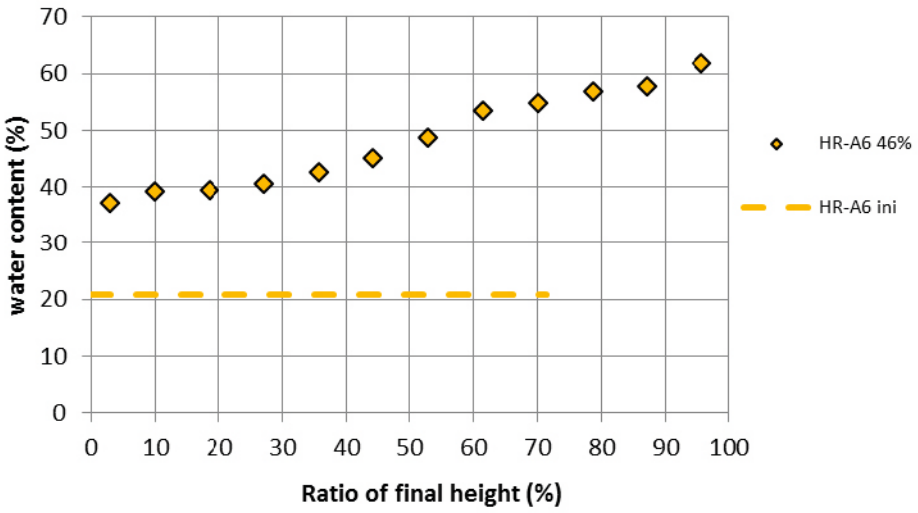

Figure 5-38. *Distribution of water content over the specimen height, HR-A6.*

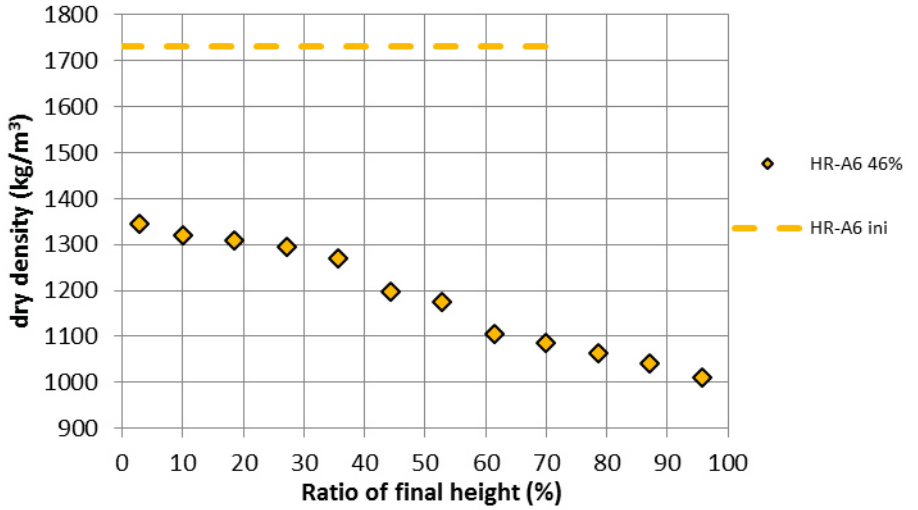

Figure 5-39. *Distribution of dry density over the specimen height, HR-A6.*

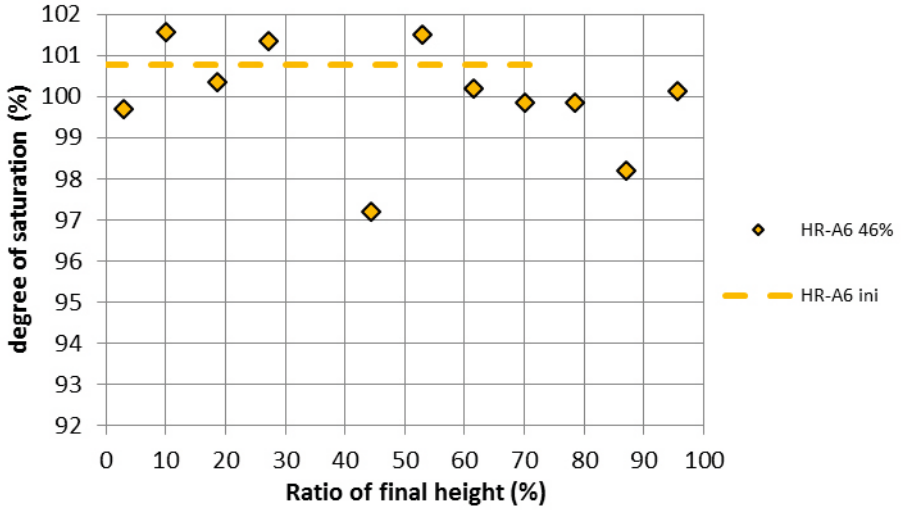

Figure 5-40. *Distribution of degree of saturation over the specimen height, HR-A6.*

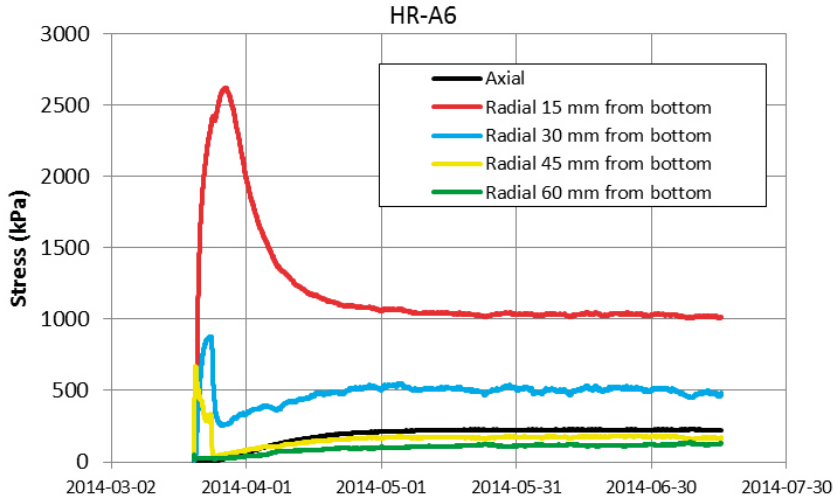

Figure 5-41. *Evolution of swelling pressure over time, HR-A6.*

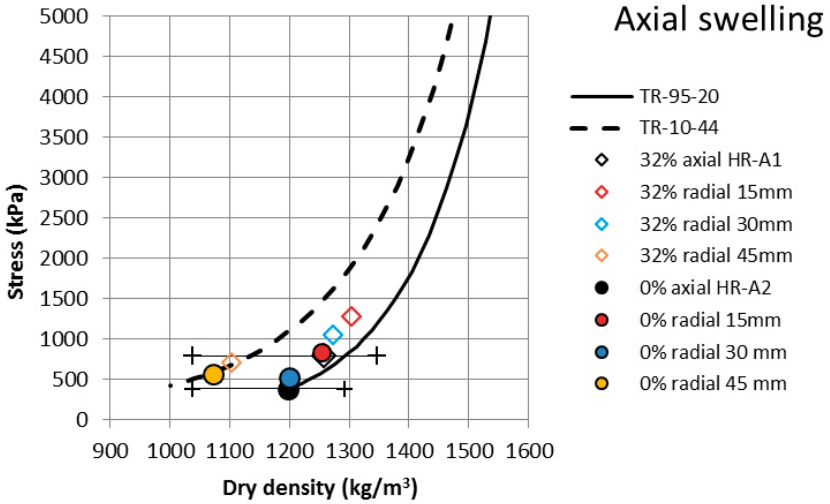

Figure 5-42. *Stresses as a function of the dry density from HR-A2. Results from HR-A1 (TR-14-25) are shown with open symbols together with models presented by Börgesson et al. (1995) and Åkesson et al. (2010). The bars show the maximum and minimum dry density of the specimens.*

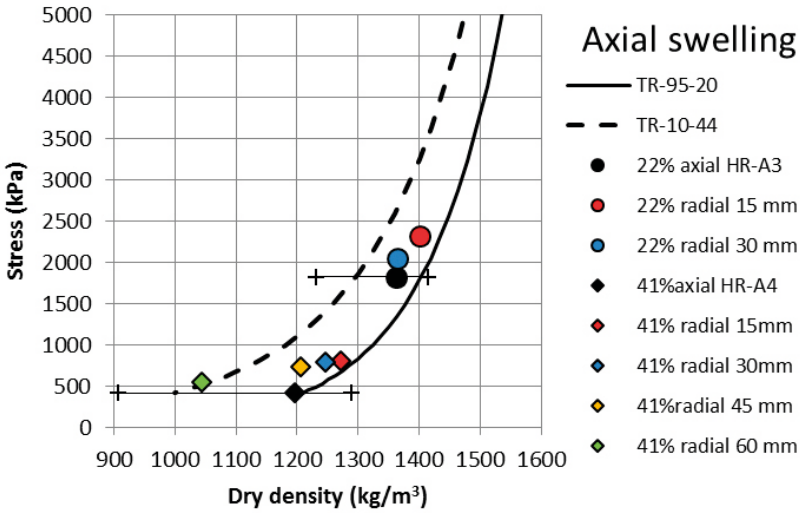

Figure 5-43. *Stresses as a function of the dry density from HR-A3 and HR-A4. Models presented by Börgesson et al. (1995) and Åkesson et al. (2010) are also shown. The bars show the maximum and minimum dry densities of the specimens.*

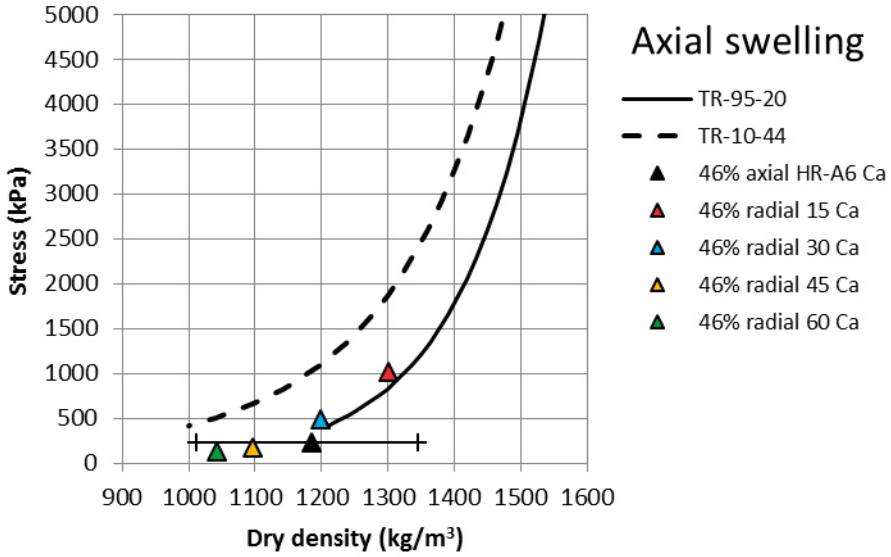

Figure 5-44. *Stresses as a function of the dry density from HR-A6. Models of MX-80 presented by Börgesson et al. (1995) and Åkesson et al. (2010) are also shown. The bars show the maximum and minimum dry density of the specimen.*

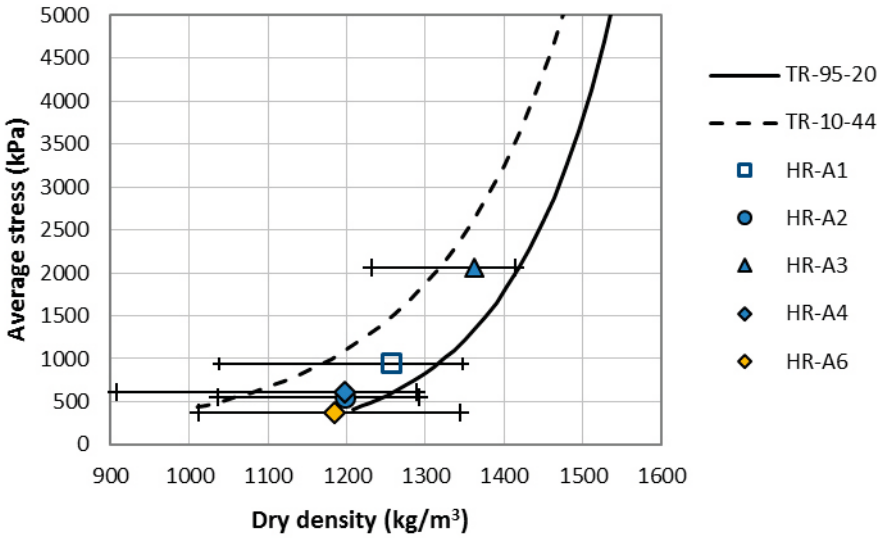

Figure 5-45. *Average stresses as a function of the dry density from HR-A2 to HR-A6. Results from HR-A1 (TR-14-25) are shown with an open symbol. In addition, models of MX-80 presented by Börgesson et al. (1995) and Åkesson et al. (2010) are shown. The bars show the maximum and minimum dry densities of the specimens.*

Radial outward swelling

The only completed test with radial outward swelling is HR-Ro2, which is presented in Table 5-5. The sampling was done according to Figure 5-28. However, the specimen was surprisingly brittle and it was only possible to determine density at three positions located at the innermost part. From these three densities and the water contents at the same positions the degree of saturation was calculated to be between 98 and 101 %. In Figure 5-46 and Figure 5-47 the distributions of the water content w and dry density ρ_d over the radius are shown. In Figure 5-47 the three measured dry densities are marked with larger symbols while the smaller symbols represent calculated values. The evolution of the stresses with time is shown in Figure 5-48. In Figure 5-49 the stresses are plotted as a function of the dry density. In Figure 5-50 the average stress, calculated according to Equation 5-1, is plotted as a function of the dry density together with comparable results from tests on Calcigel and MX-80.

Table 5-5. Specimens used in the series with radial outward swelling, HR-Ro. The swelling (%) was calculated from Equation 4-1.

Test ID	Material	Initial water content	Initial dry density	Initial degree of saturation	Constant height	Initial diameter	Final diameter	Swelling
		%	kg/m^3	%	mm	mm	mm	%
HR-Ro2	Calcigel	20.9	1716[1]	99	80	82.5	96.8	37

[1] Sampled from lager block with the given density.

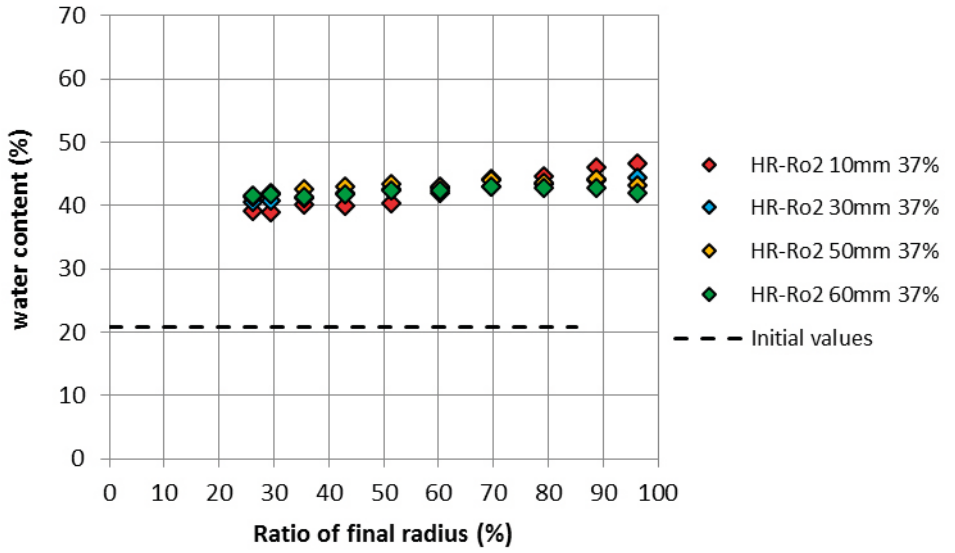

Figure 5-46. *Distribution of water content over the radius in test HR-Ro2.*

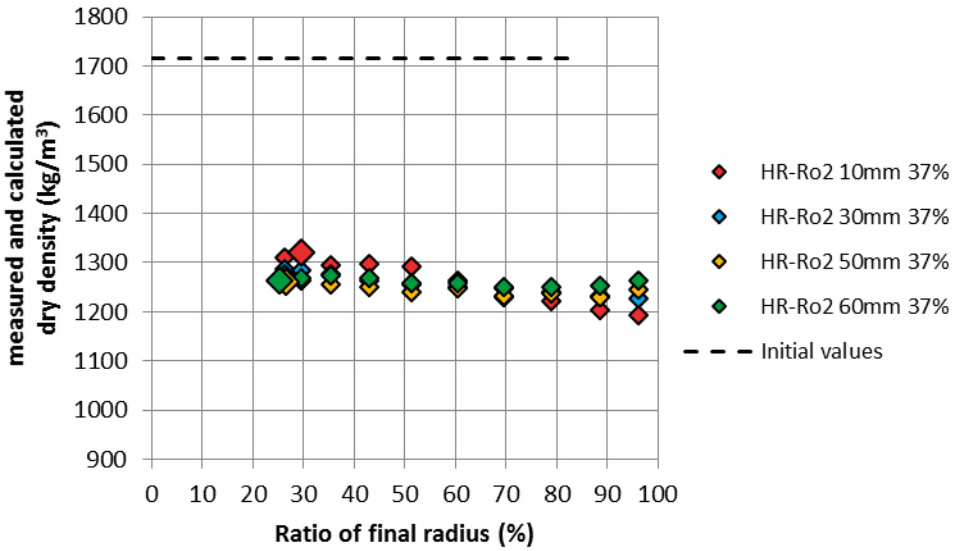

Figure 5-47. *Distribution of dry density over the radius in test HR-Ro2. The calculated dry densities are based on 100 % saturation. The dry density was only measured in three positions, in the innermost part, marked with larger symbols.*

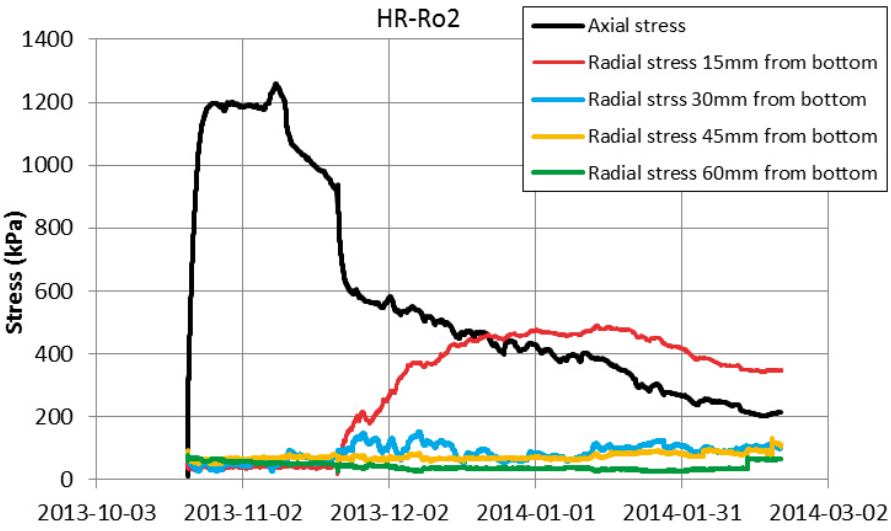

Figure 5-48. *Evolution of swelling pressure with time from test HR-Ro2.*

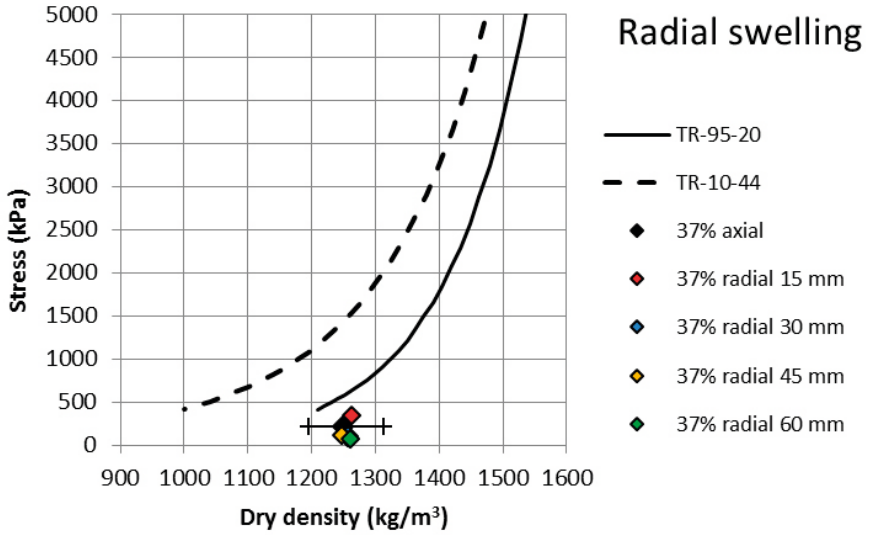

Figure 5-49. *Stresses as a function of dry density from test HR-Ro2. Models of MX-80 presented by Börgesson et al. (1995) and Åkesson et al. (2010) are also shown. The bars show the maximum and minimum dry densities of the specimen.*

Radial inward swelling

The completed test of radial inward swelling is presented in Table 5-6. In Figure 5-51 to Figure 5-53 the distributions of water content w, dry density ρ_d and degree of saturation S_r measured after completed tests are shown. The evolution of the stresses with time is shown in Figure 5-54. The stresses are plotted as a function of the dry density in Figure 5-55 and in Figure 5-56 the average stress, calculated according to Equation 5-1, is plotted as a function of the dry density together with previous comparable results.

Table 5-6. Specimen used in the series with radial inward swelling, HR-Ri. The swelling (%) was calculated from Equation 4-1.

Test ID	Material	Initial water content %	Initial dry density kg/m³	Initial degree of saturation %	Constant height mm	Outer radius mm	Cavity diameter mm	Swelling %
HR-Ri1	MX-80	23.7	1666[1]	99	80	96.8	49	43

[1] Sampled from larger block with the given density and trimmed to fit the device.

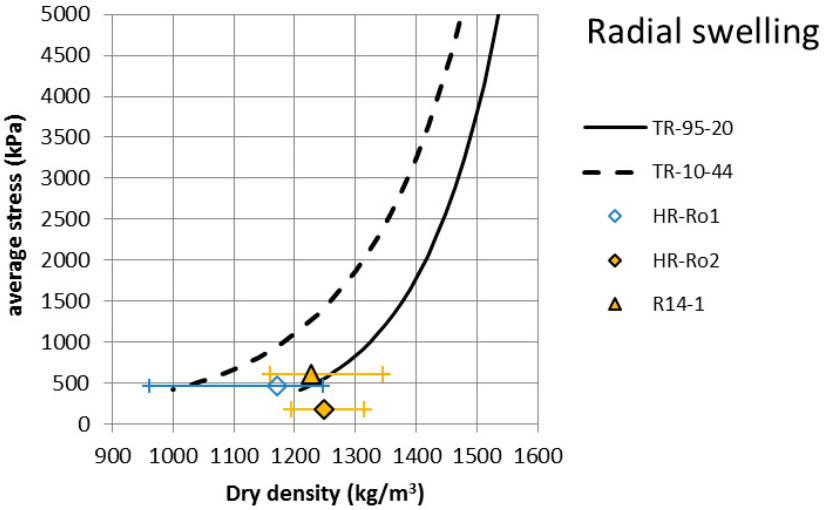

Figure 5-50. *Average stresses as a function of dry density from test HR-Ro2 plotted with results from R14-1 (cf. Figure 5-9). Corresponding result of MX-80 from HR-Ro1 (TR-14-25) is shown with an open symbol. Models of MX-80 presented by Börgesson et al. (1995) and Åkesson et al. (2010) are also shown. The bars show the maximum and minimum dry densities of the specimens.*

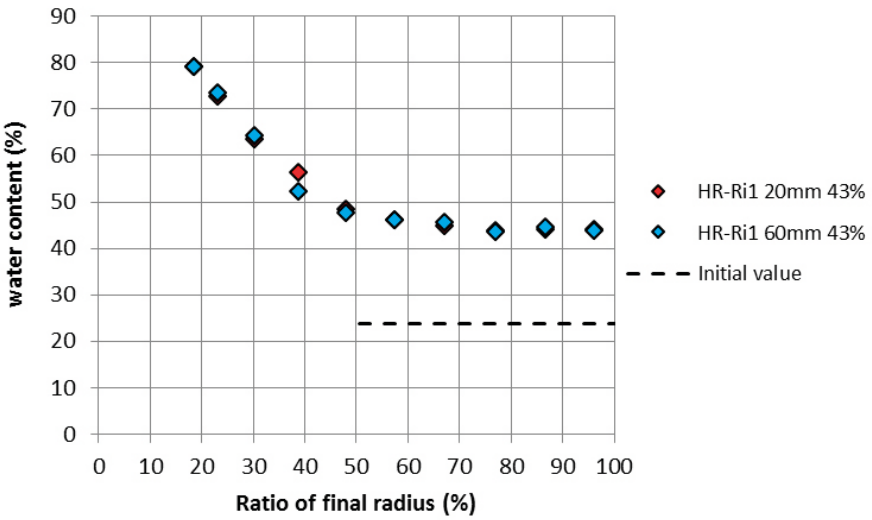

Figure 5-51. *Distribution of water content over the radius in test HR-Ri1.*

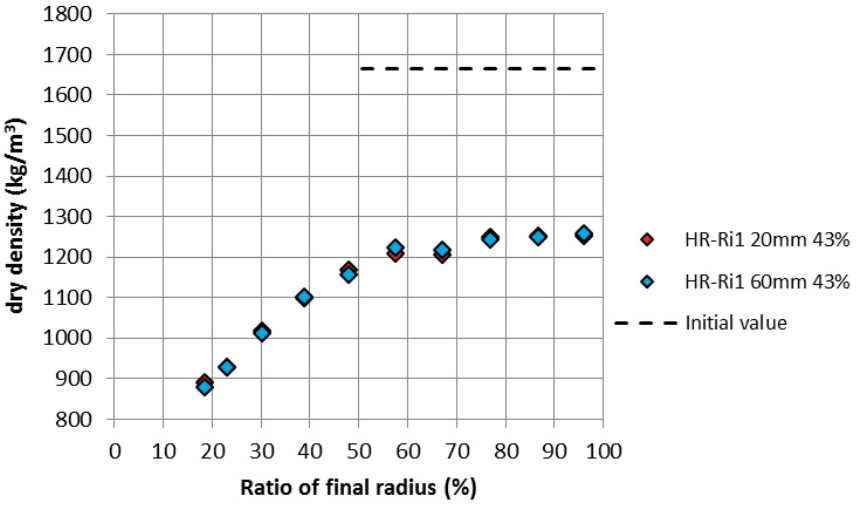

Figure 5-52. *Distribution of dry density over the radius in test HR-Ri1.*

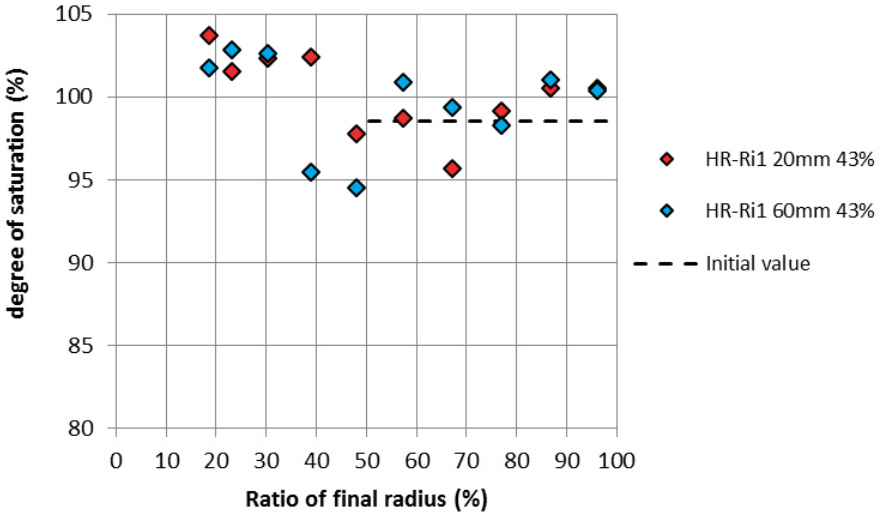

Figure 5-53. *Distribution of the degree of saturation over the radius in test HR-Ri1.*

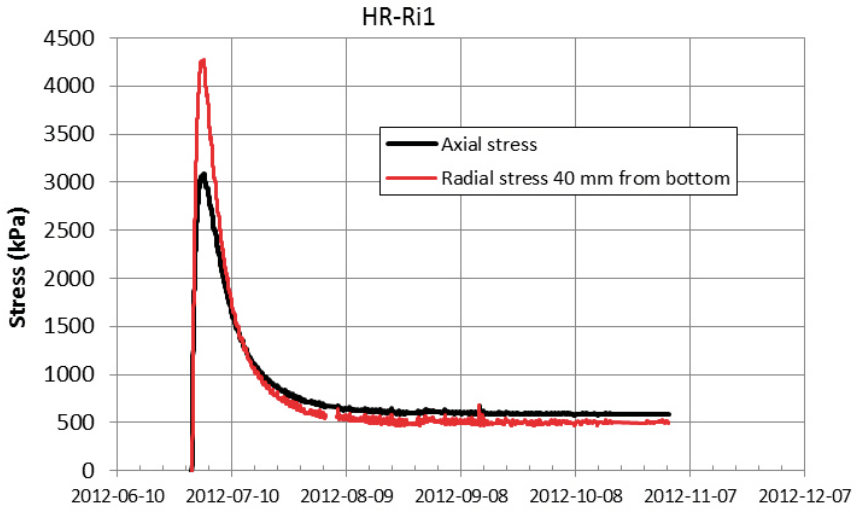

Figure 5-54. *Evolution of the swelling pressure with time from test HR-Ri1.*

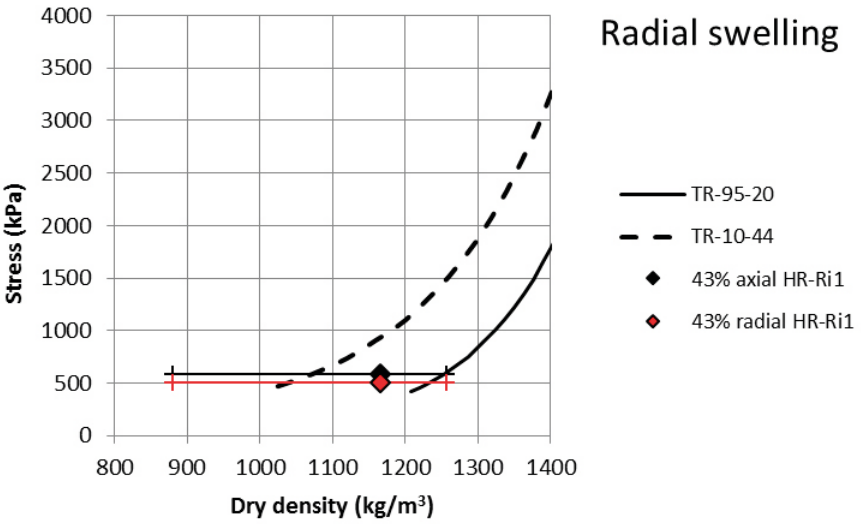

Figure 5-55. *Stresses as a function of dry density from test HR-Ri1. Models presented by Börgesson et al. (1995) and Åkesson et al. (2010) are also shown. The bars show the maximum and minimum dry densities of the specimen.*

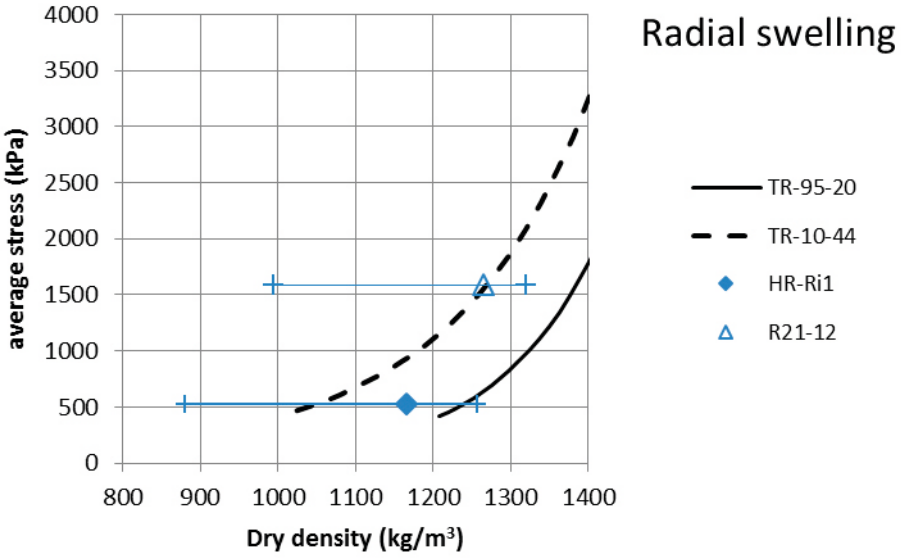

Figure 5-56. *Average stresses as a function of dry density from test HR-Ri1 and from R21-12 (TR-14-25) with an open symbol. Models presented by Börgesson et al. (1995) and Åkesson et al. (2010) are also shown. The bars show the maximum and minimum dry densities of the specimens.*

Special test – swelling in all directions

All swelling and homogenisation tests in different geometries have had swelling either in the radial direction or in the axial direction. However, in the present test the objective was to study the density profile and swelling pressure evolution after isotropic swelling i.e. swelling in all directions at the same time. The test was assumed to have a stress path with decreasing average stress without deviator stresses in order to study the effect of purely reversible swelling.

The test was run in the device shown in Figure 5-57 where the specimen was placed centric. A filter, fixed to the bottom side of the vertical piston, was used to distribute the water from above and over the cross section of the specimen. Flushing of water was made at regular intervals. A photo of the specimen before the installation is shown in Figure 5-58.

The initial and final average conditions of the specimen are shown in Table 5-7. The final dry density was calculated from the initial dry mass and the final volume. The distributions of water content w and dry density ρ_d are given in Figure 5-59 to Figure 5-61 where the dry densities are calculated values based on the measured water contents and an assumed degree of saturation of 100 %. The degree of saturation was checked on some samples taken from the inner part of the specimen and it was determined to be between 99.5 % and 100.2 %. In Figure 5-59 the water contents are shown as an average of two specimens, sampled at the same radius but in opposite directions. In Figure 5-61 all measured values are shown. The time evolution of the swelling pressure is shown in Figure 5-62. In Figure 5-63 the stresses are plotted as a function of dry density.

Table 5-7. Specimen used for the HR-Iso test. The specimen was sawn and trimmed from a larger block of bentonite. The swelling (%) was calculated from Equation 4-1.

Test ID	Material	Initial w %	Initial ρ_d kg/m³	Initial S_r %	Initial diameter mm	Initial height mm	Final diameter mm	Final height mm	Final swelling %
HR-Iso	MX-80	23.2	1684[1]	99	89	62	100	70	43

[1] Sampled from larger block with given density.

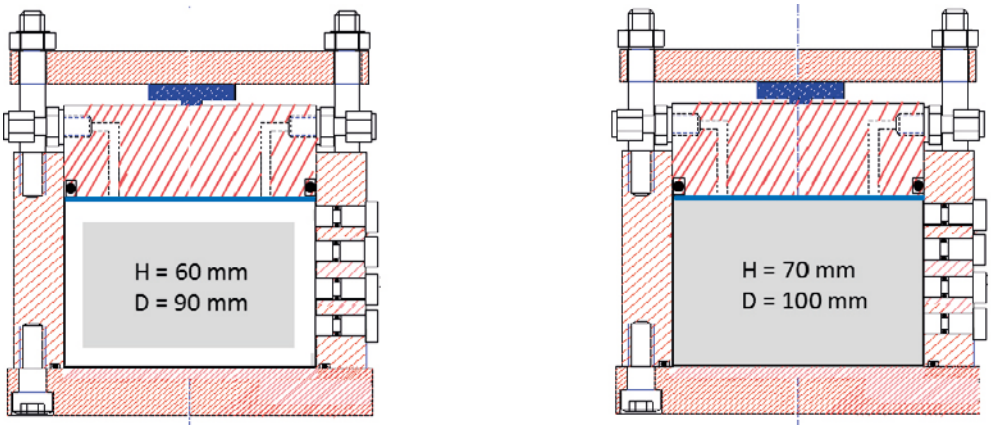

Figure 5-57. *Set-up used for the special test HR-Iso, cf. also Figure 4-5.*

Figure 5-58. *Photo of the specimen, suspended in the upper piston, before mounting into the test device.*

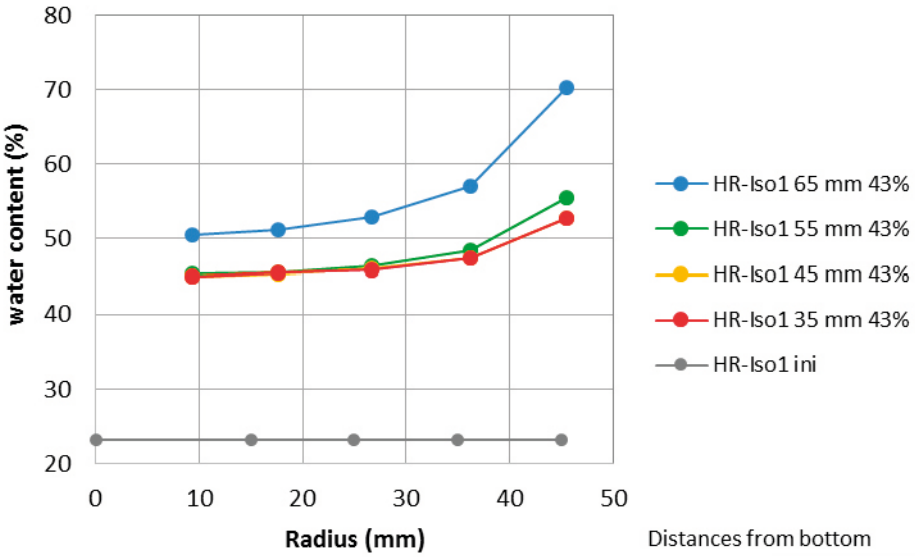

Figure 5-59. *Distribution of water content at different levels after the HR-Iso test. Each value represents an average of two measurements.*

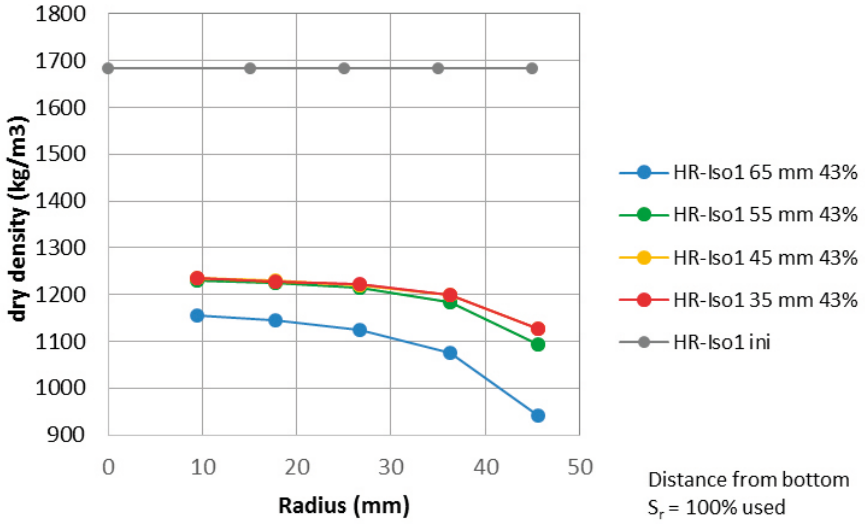

Figure 5-60. *Distribution of dry density at different levels after the HR-Iso test. Each value are calculated as an average of two measured water contents and an assumption of 100 % saturation.*

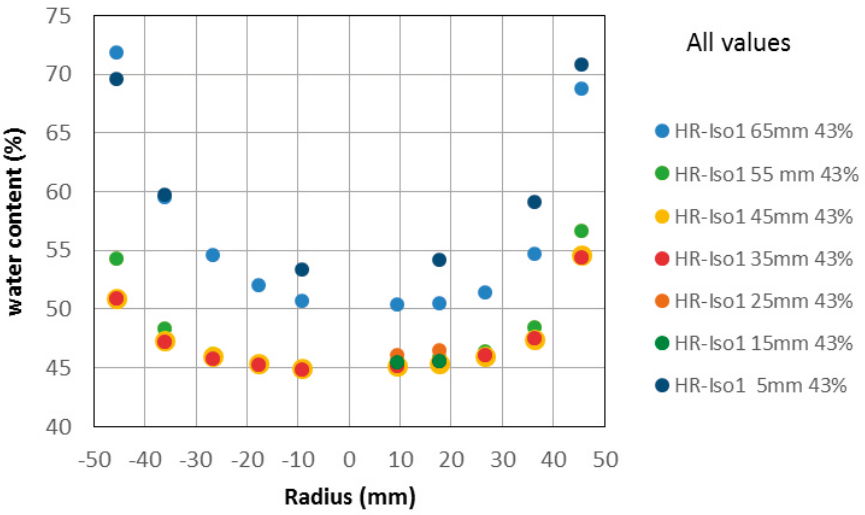

Figure 5-61. *Distribution of water content over the radius at different levels after the HR-Iso test. All measured values are shown.*

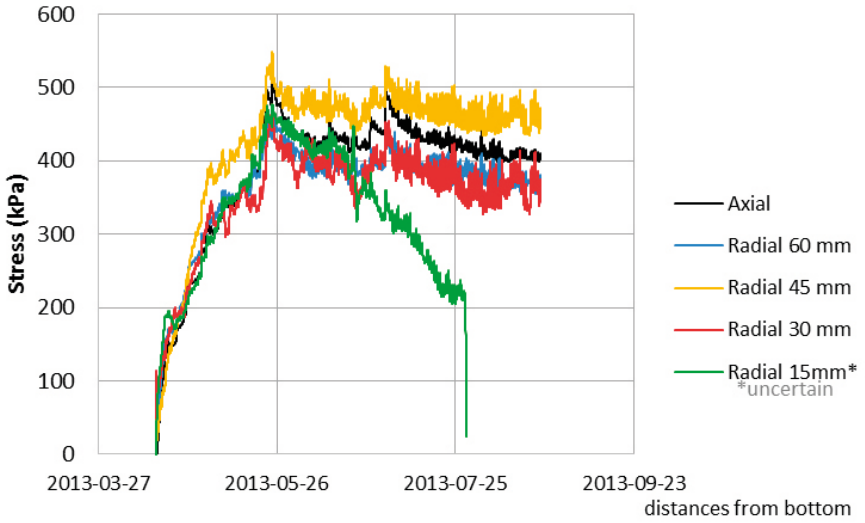

Figure 5-62. *Evolution of swelling pressure in the HR-Iso test.*

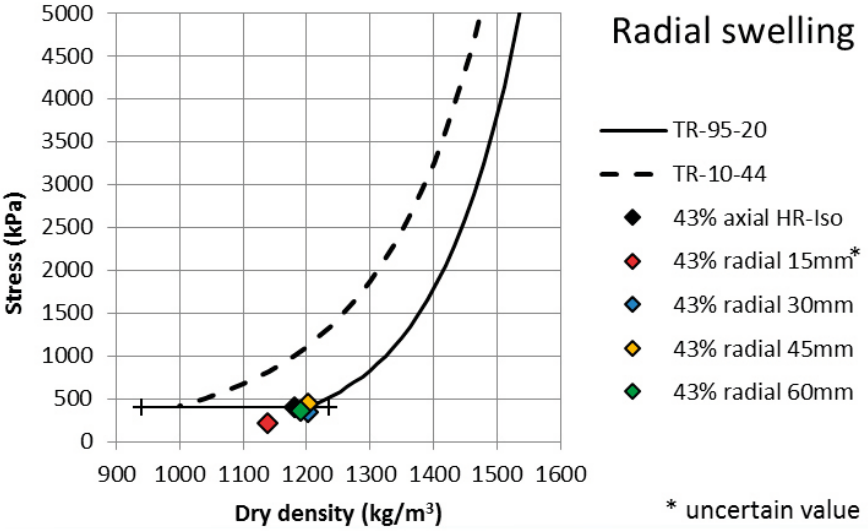

Figure 5-63. *Measured stresses as a function of dry density from HR-Iso. Models presented by Börgesson et al. (1995) and Åkesson et al. (2010) are also shown. The bars show the maximum and minimum dry densities of the specimen.*

Comments

Tests HR-A1 and HR-A2 were made to compare the homogenisation after swelling approximately 32 % into an empty space (HR-A1) with the homogenisation starting with two specimens having different initial densities and no empty space aiming at the same average density after homogenisation (HR-A2). No large difference was seen in the measured final average dry densities of HR-A1 and HR-A2 where 1 258 kg/m^3 and 1 198 kg/m^3 were measured after the testing time of 67 and 72 days, respectively. However, in the evolution of swelling pressure the stresses from HR-A2 was smoother, without the initial high peak seen in the radially measured stresses in the test results of HR-A1.

The two specimens HR-A4 (MX-80) and HR-A6 (Calcigel) swelled to approximately the same average dry density (1 197 kg/m^3 and 1 185 kg/m^3). No large difference between the test results are seen in Figure 5-45. When comparing the density distributions (Figure 5-34 and Figure 5-39) slightly different shapes can be seen. In spite of the longer time used for the homogenisation of HR-A4 (145 days) compared to HR-A6 (117 days) lower density gradient was seen in test HR-A6.

The specimen HR-Ro2 (Calcigel) swelled approximately the same as specimen HR-Ro1 (MX-80) but had a larger final dry density, due to higher initial dry density. The relatively small density gradient seen at dismantling of specimen HR-Ro2 compared to the larger density gradient seen in HR-Ro1 may be a result of the testing time. Longer testing time (122 days) was used for HR-Ro2 than for HR-Ri1 (49 days). The difference could also be an effect of the different materials. However, from the brittleness seen in specimen HR-Ro2, which has not been seen in other tests with Calcigel specimens, it cannot be excluded that the water distribution was insufficient and unevenly distributed in this test which could also have influenced the results. To further study this, a similar specimen was tested and the results will be presented in a later report.

Considering the radial inward swelling the measured stresses corresponded well to previous comparable results in other tests; with a clear peak at the first part of the swelling and an average stress located to the left of the values from the model presented by Börgesson et al. 1995 (TR-95-20) in Figure 5-55. The high values of the degree of saturation of the innermost specimens, cf. Figure 5-53, could be regarded as a measure of the uncertainties in the determinations and comparable to the scatter seen in the degree of saturation of the innermost samples after this type of swelling in the basic test series. The uncertainties of the results are probably related to the difficulty to get representative samples of both water content and density from the small innermost volume, where large gradients, of the actual variables, are expected.

From the special test with swelling in all directions the measured stresses provided logical results compared to other test results and the swelling was almost symmetric. The maximum difference

in water content between samples representing the same position was seen at the outer part of the specimen. In Figure 5-61 the maximum difference is seen when comparing water contents at the top and bottom of the specimen (light and dark blue circles) and when comparing samples at maximum radius at mid-height (red circles at the radius ±45.5 mm). The difference in water content from samples representing the same positions was everywhere less than $\Delta w < 3.8$ %.

5.3 Measurement of friction between bentonite and different surfaces

Results from new tests in the test series where friction between bentonite and different surfaces was studied are presented in Table 5-8. See section 4.3 for a test description. Previous results from the test series were presented in the status report TR-14-25. The angel of friction was calculated according to Equation 4-2. The value was evaluated both as a peak value and a residual value after some deformation. The evaluation was made for both the axial stress and the radial stress when both were measured. The evolution of the swelling pressure with time and the friction angle evaluated during the entire test evolution are for all tests shown in Appendix 5.

Table 5-8. Results from measurement of friction between bentonite and different surfaces. The evaluated angle of friction δ is given as a peak value (δ_{peak}) and as a residual value after some deformation at the deformation rate 0.1 mm/min (δ_{res}). Also given are the axially and radially measured stresses before the shearing and the water content, dry density and degree of saturation determined after the tests.

Test ID	Measured stress	Direction[1]	Friction angle		Surface	After dismantling			Type of specimen
	P kPa		δ_{peak} °	δ_{res} °		w %	ρ_d kg/m³	S_r %	
Fr1-10	4 670	radial	9.4	5.1	grooves (square)	28.0	1 544	97	Compacted MX-80
	6 157	axial	7.1	3.8					
Fr1-11	300	radial	3.6	2.1	steel	71.8	912	97	Extruded MX-80 pellet
	103	axial	10.4	6.3					
Fr1-12	4 580	radial	10.3	6.6	grooves (triangular)	47.9	1 190[2]	100	Compacted MX-80
	5 590	axial	8.5	5.4					
Fr1-13	6 000	radial	7.6	5.4	plastic (smooth side)	29.5	1 490	95	Compacted MX-80
	4 885	axial	9.5	6.6					
Fr1-14	350	radial	5.7	4.3	grooves (triangular)	65.1	991	100	Extruded MX-80 pellet
	220	axial	9	6.9					
Fr1-15	440	radial	17.6	10.4	grooves (triangular)	50.4	1 159	100	MX-80 powder
	440	axial	17.6	10.4					
Fr1-16	440	radial	10.5	7.4	grooves (triangular)	58.2	1 044	97	MX-80 powder
	240	axial	18.9	13.4					
Fr1-17	537	axial corr[3]		8	acrylic plastic	48.8	1 179	100	Compacted MX-80
Fr1-19	454	axial corr[3]		9	acrylic plastic	50.1	1 169	101	Compacted MX-80
Fr1-20	2 302	radial	9.2	7.2	plastic (friction side)	36.0	1 397	101	Compacted MX-80
	2 270	axial	9.4	7.3					
Fr2-1	520	radial	10.1	6.9	steel	47.8	1 191	100	Compacted Calcigel
	569	axial	9.3	6.3					

[1] Direction in which the swelling pressure was measured which was used for the interpretation of friction angle.

[2] The measured density and water content deviate largely from the values expected from the measured stresses.

[3] A correction of 0.06 kN was used to account for the influence of the used o-ring.

The normal stress acting on the slipping wall during the movement is used for evaluating the angle of friction. The radially measured stress will therefore be used for the interpretation as well as for the presentations, Figure 5-64. For the completeness the results are also interpreted and plotted with the axially measured stress, Figure 5-65.

Most of the tests were made with a confining ring of steel (cf. Figure 4-8 and Figure 4-9) having different inner surfaces towards the bentonite specimens; e.g. grooves or a plastic inner-surface. However, in two of the tests the confining ring was made of acrylic plastic (Fr1-17, Fr1-19). In these tests only the axial stress was measured why the test results are only plotted in Figure 5-65. With this special test set up the influence of the used o-ring was not negligible but necessary to take into account why a separate test was made for this.

All test results are plotted with the results from a model used by Åkesson et al. (2010) where the bentonite friction angle was related to the shear strength determined from triaxial tests.

Comments

In Figure 5-66 the left part of Figure 5-65, with swelling pressure below 1 000 kPa, is shown. Included in the diagram are also corresponding results from the previous report TR-14-25. If the encircled results are excluded the other results are logical with peak values corresponding to the bentonite friction angel in the tests with grooves and lower friction angles when other surfaces were used and at higher swelling pressure. It is also seen that the difference between the peak value and the residual value is largest in the tests with grooves which is logical. The only test with Calcigel is also shown in this plot (light blue circles).

The deviating encircled test results come from tests on pellet samples. The deviation is seen although the results are plotted as a function of the axial stress which is measured over a large area reducing the possible effect of a single pellet. Why these results are deviating is not clear.

The specimen in test Fr1-16 was used for other tests after the dismantling. Two cone tests and two unconfined compression tests were made on this specimen. The tests and results are further described in the final part of Appendix 5. These test results can be compared to the results shown in Figure 5-66. The bentonite friction angle evaluated from the unconfined compression tests were $\phi = 14.9°$ and $\phi = 17.5°$ while the two cone tests gave $\phi = 13.6°$ which corresponds to the residual strength using the axially measured swelling pressure of Fr1-16 (P_{axial} = 240 kPa).

In Figure 5-67 all results from the tests on friction between MX-80 and steel, lubricated steel and steel grooves from this project are shown. The results from tests on steel and lubricated steel show friction angles below the line representing the shear strength of MX-80. At low swelling pressure the results are ambiguous.

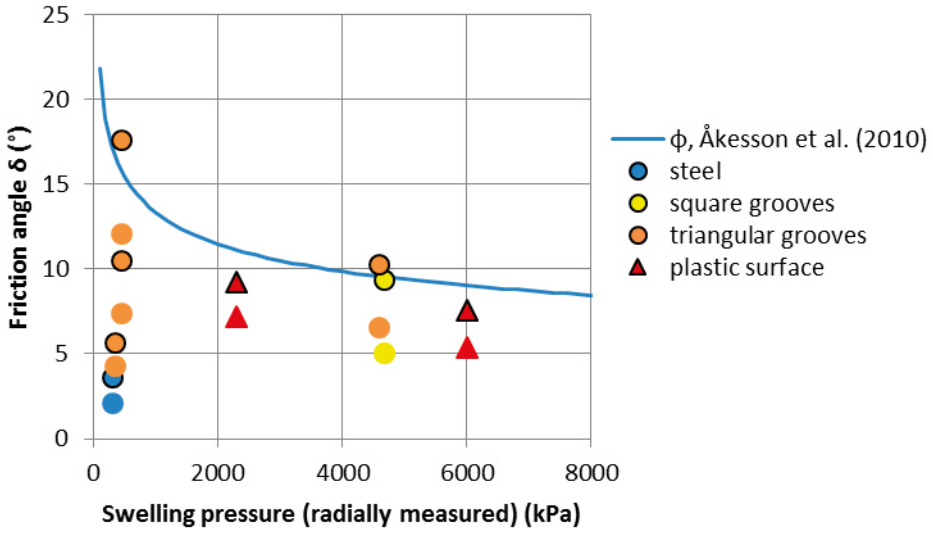

Figure 5-64. *Friction angle evaluated and plotted with the radially measured stress for the tests on MX-80 shown in Table 5-8. From each test both the peak value (with marker line) and the residual value (without marker line) are shown.*

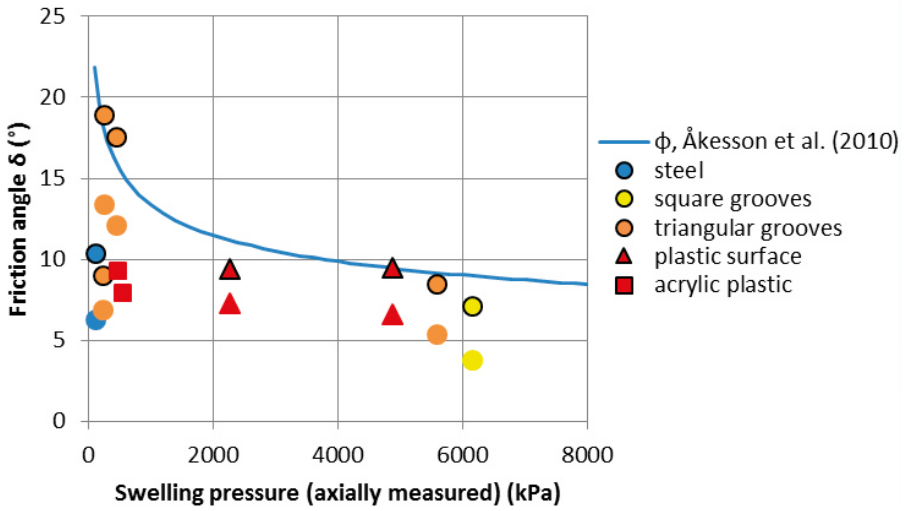

Figure 5-65. *Friction angle evaluated and plotted with the axially measured stress for all tests on MX-80 shown in Table 5-8. From each test both the peak value (with marker line) and the residual value (without marker line) are shown.*

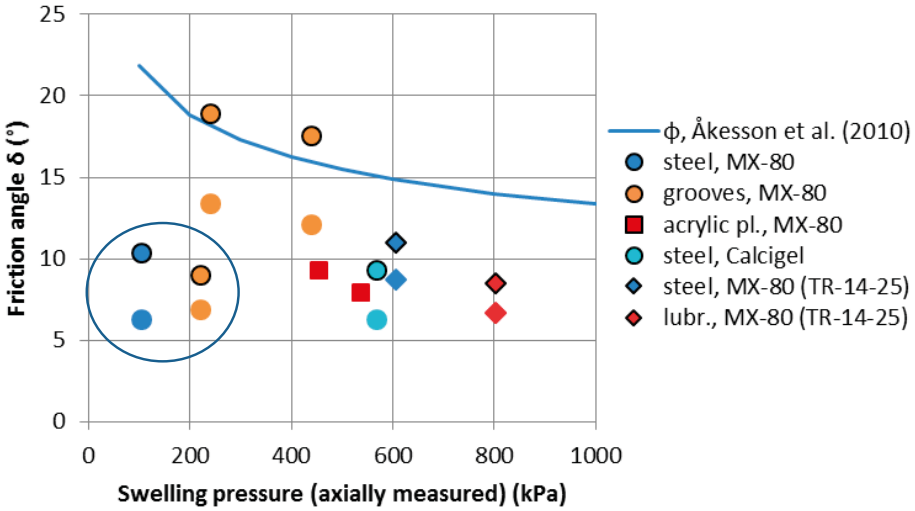

Figure 5-66. *Part of Figure 5-65 including one test on Calcigel. In addition, corresponding results from the report TR-14-25 are shown with diamonds.*

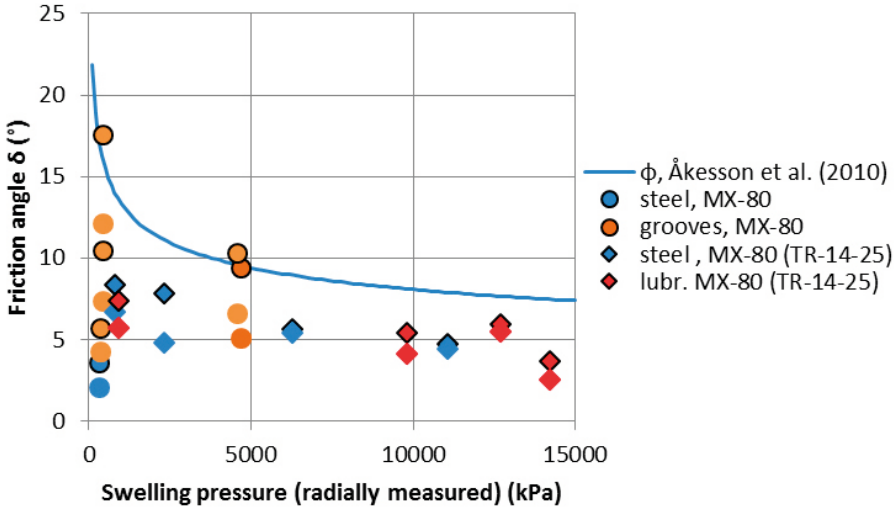

Figure 5-67. *All results from tests on friction between MX-80 and steel, lubricated steel and grooves are shown. Results from the report TR-14-25 are shown with diamonds. From each test both the peak value (with marker line) and the residual value (without marker line) are shown.*

6 Homogenisation after loss of bentonite – medium scale laboratory test

6.1 General

Buffer homogenisation involving loss of bentonite has been studied by two medium scale laboratory tests. The two tests, SH1 and SH2, having the same boundary conditions, were started in December 2012. The non-instrumented SH2 was finished and dismantled in May 2014. The instrumented SH1 is still ongoing.

The test SH1 should be regarded as the main test while SH2 was carried through mainly as a trial test where the methods for adding water and for dismantling were tested. The focus of this chapter is the detailed description of the preparation and start conditions of both tests SH1 and SH2 and the dismantling and the results from the sampling of SH2.

6.2 Experiment description

The self-sealing ability of large and irregular cavities was studied in this part of the project. Since the main results are the final density distribution, the combination of the block size and the size of the cavities at start are important parameters. The size of the blocks, i.e. cylinder rings, was chosen to be as large as possible, still having a reasonable estimated time to saturation and homogenisation while the size of the cavities was chosen large enough to get good resolution of the sampling after termination of the tests. In addition, the evolution of swelling pressure was measured at strategic points in SH1 in order to follow the evolution of the homogenisation.

Test set-up

The geometry of the set-ups used for the tests SH1 and SH2 is shown with photos in Figure 6-1 and a sketch in Figure 6-2. The device is a very stiff cylinder with the inner diameter 300 mm and the height 100 mm. A simulated canister with the outer diameter 100 mm is included in the center. A stiff filter is mounted to the inside of the ring with the purpose to provide water to the bentonite from the radial surface. In each bentonite block two cavities were cut out, in two diametrical positions, to simulate loss of material. In the set ups of SH1 nine transducers for measuring swelling pressure and two for measuring suction were included.

Figure 6-1. *Photos of one of the devices used (for SH1) in this study.*

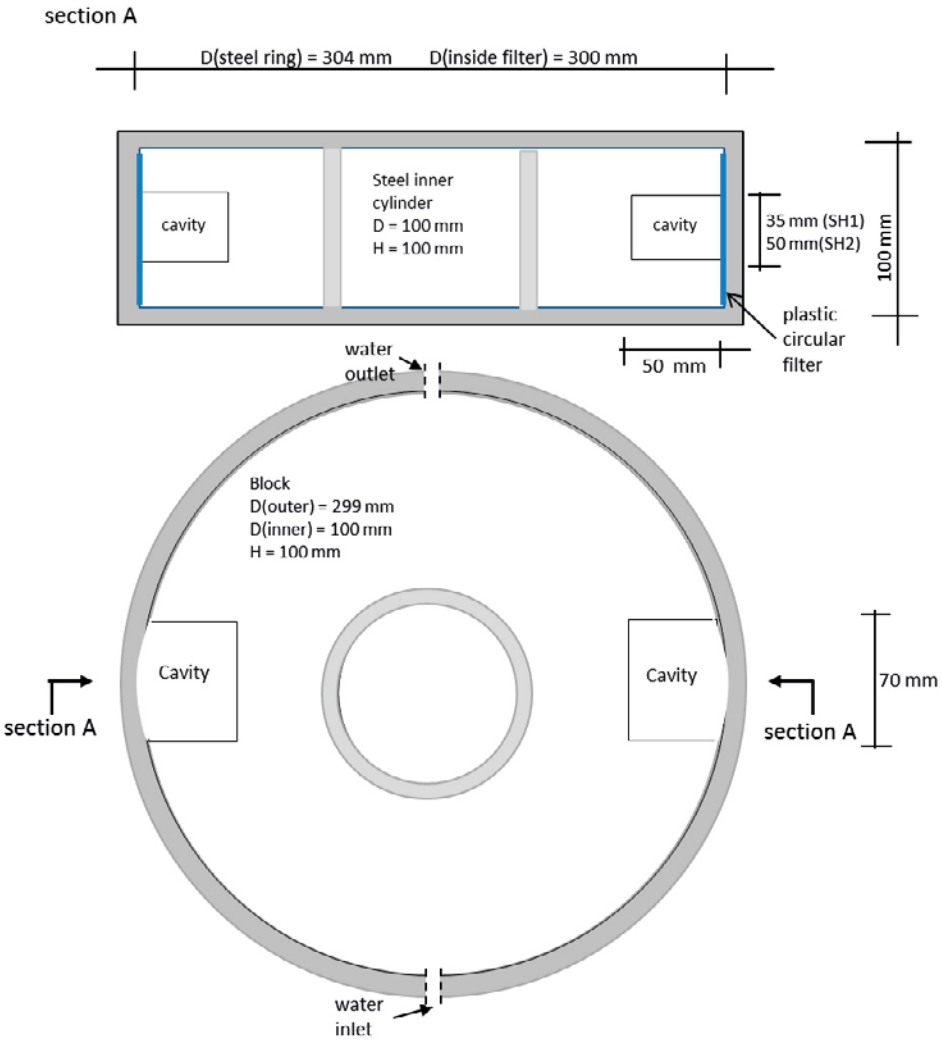

Figure 6-2. *A sketch of the set up used for the tests SH1 and SH2. The dimensions of the outer and inner steel cylinders and the bentonite block with the cavities are given. In addition, the plastic filters and the locations of the water inlet and outlet are shown.*

Test procedure

De-ionised water was supplied to the filters, attached to the inside of the cylinder rings. Circulation of water through the filters was possible by use of the water inlet and outlet, located in two diametrical positions of the steel ring, see Figure 6-2.

After mounting of transducers, bentonite rings and lids each test was started by filling the filter and the cavities with water and applying a low water pressure (10 kPa). During the test period the filters were flushed regularly in order to eliminate air bubbles that may be collected in the filters. After about one month a steady water pressure of 100 kPa was applied to SH1 and after approximately 11 months 100 kPa was also applied to SH2. SH2 was finished after 17 months and SH1 will be finished after more than 30 months.

6.3 Results

The manufacturing of the blocks for SH1 and SH2 were made during November and December 2012. After mounting of transducers, blocks and lids the test SH1 started on 2012-12-18 and the test SH2 started on 2012-12-17. Both tests were started by opening the water supplies to the filters. The test SH2 was finished and dismantled on 2014-05-13 while the test SH1 is still ongoing.

Preparation and installation of SH1 and SH2

The geometry of the set-up was shown in Figure 6-2. Powder of MX-80 was mixed with de-ionised water to get a water content of 24 % to reach a high initial degree of saturation after compaction. Aiming at a dry density of approximately 1 660 kg/m^3 a compaction pressure of 40–60 MPa was used for the two uniaxial compacted cylinder blocks, Table 6-1.

Each block was machined with a rotating lathe aiming at the following dimensions: height = 100 mm, outer diameter = 298.7 mm and inner diameter = 100.0 mm. There was thus a small gap of 0.65 mm between the block and the outer ring and virtually no gap at the inner ring and at the lid. The height of the block after compaction of SH2 was kept to 100.5 mm (Table 6-1) while the height of SH1 was machined to 100.0 mm. The water content, dry density and degree of saturation were determined on samples of the removed inner cylinders. The distribution of the initial dry density over the block height is shown in Figure 6-3.

Table 6-1. Data for the uniaxial compacted blocks used for the tests SH1 and SH2 directly after compaction in terms of water content *w*, mass *m* and dimensions of the blocks *H* and *D* and the required compaction pressure P_c.

Block	SH1	SH2
w (%)	24.2	24.2
m (kg)	15.18	14.90
H (mm)	103.05	100.51
D (mm)	305.3	305.3
Pc (MPa)	44	51

Cavities were cut in two diametrical positions of each block, Figure 6-4. The dimensions (height × length × depth) of the cavities in SH1 and SH2 were (35 × 70 × 50) mm^3 and (50 × 70 × 50) mm^3, respectively, see also Figure 6-2.

In Table 6-2 and Table 6-3 the initial conditions of the installed bentonite blocks are presented in terms of bulk density ρ, water content w, dry density ρ_d and degree of saturation S_r derived in four different ways (case 1-4);

1. Initial block density calculated from the initial mass and the initial volume of the blocks.
2. Initial block density measured on the center cylinder, sampled at the preparation.
3. Final average density calculated from the initial mass and the final dimensions inside the device without including the cavities.
4. Final average density calculated in the same way as 3 with the filter deformation taken into account without including the cavities.

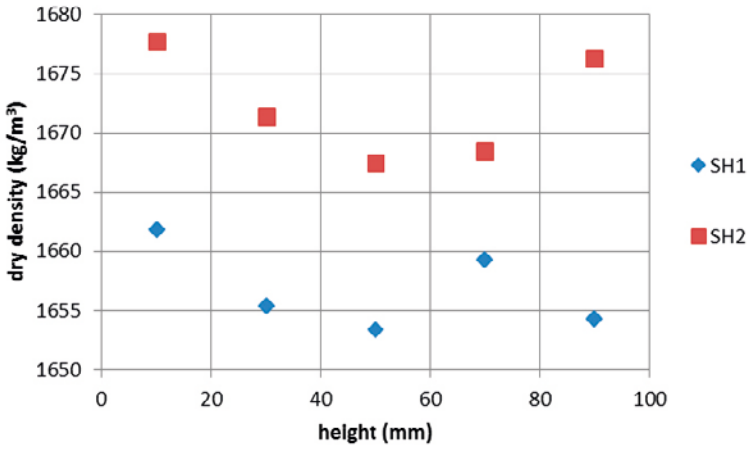

Figure 6-3. *Initial distribution of dry density versus block height of SH1 and SH2 from samples taken of the inner cylinder of the blocks.*

Figure 6-4. The cylindrical bentonite block used in the tests SH1 (to the left) and SH2 (to the right) with cut cavities. In the diametrical position of each block a second cavity was cut. The dimensions of the cavities in SH1 and SH2 were (height × length × depth) (35 × 70 × 50) mm³ and (50 × 70 × 50) mm³, respectively.

Table 6-2. Initial conditions of the installed bentonite block in SH1. The base variables ρ, w, ρ_d, e and S_r are shown for the initial conditions 1-4.

Case	Bulk density ρ	Water content w	Dry density ρ_d	Void ratio e	Degree of saturation S_r	Remarks
	kg/m³	%	kg/m³	–	%	
1	2029	23.6	1642	0.69	95	Calculated from the initial mass and the initial volume of the block.
2	2047	23.6	1657	0.68	97	Measured on the center of the block, sampled at preparation.
3	2009	24.2	1618	0.72	94	Calculated from the initial mass and the final dimensions with water in the gap.
4	2006	24.2	1616	0.72		Calculated according to Initial Conditions 3, above, with the filter deformation taken into account.

Table 6-3. Initial conditions of the installed bentonite block in SH2. The base variables; ρ, w, ρ_d, e and S_r are shown for the initial conditions 1-4.

Case	Bulk density ρ	Water content w	Dry density ρ_d	Void ratio e	Degree of saturation S_r	Remarks
	kg/m³	%	kg/m³	–	%	
1	2049	23.5	1659	0.68	97	Calculated from the initial mass and the initial volume of the block.
2	2066	23.5	1672	0.66	99	Measured on the center of the block, sampled at preparation.
3	2037	24.1	1641	0.69	97	Calculated from the initial mass and the final dimensions with water in the gap.
4	2034	24.1	1639	0.70		Calculated according to Initial Conditions 3, above, with the filter deformation taken into account.

Water saturation and water supply of SH2

After one hour the filter and approximately 90 % of the available empty space, mainly consisting of gaps and cavities, was filled with water. 24 hours after the start approximately 95 % of the available volume was filled. The water supply was open during the entire test period but the applied water pressure varied from the initial value of 10 kPa to 40 kPa during the main part of the test period (2013-01-07 to 2013-11-20) and 100 kPa during the last part of the test (2013-11-20 to termination).

Termination and dismantling of SH2

The test was terminated on 2014-05-13 and four days before the termination the applied water pressure 100 kPa was lowered to zero. Before the opening of the device an attempt was made to evacuate the filter from water but only a small volume of water was possible to remove. The dismantling started with lifting the lid and removing the bottom from the cylinder ring and marking the planned sampling locations on the uncovered bentonite surfaces. The dismantling continued by free-drilling and removing of the inner steel cylinder and then dividing the bentonite cylinder into two half circles by sawing radially. Figure 6-5 shows two photos taken during the dismantling.

Sampling of SH2 and denomination of the samples

The bentonite cylinder ring was divided into two half-cylinders during the dismantling. One of the half-cylinders was directly used for the sampling and determination of the distributions of water content and of density while the other one was sealed and stored for later analyses.

The half-cylinder for sampling was further divided axially at mid-height and the determinations of density were made on the upper part while the determinations of water content were made on the lower part, see Figure 6-6 (to the right). Both the water content and the density were determined at three different levels axially; 1 – outermost, 2 – second outermost and 3 – innermost.

Figure 6-5. *Photos from the dismantling of SH2***.**

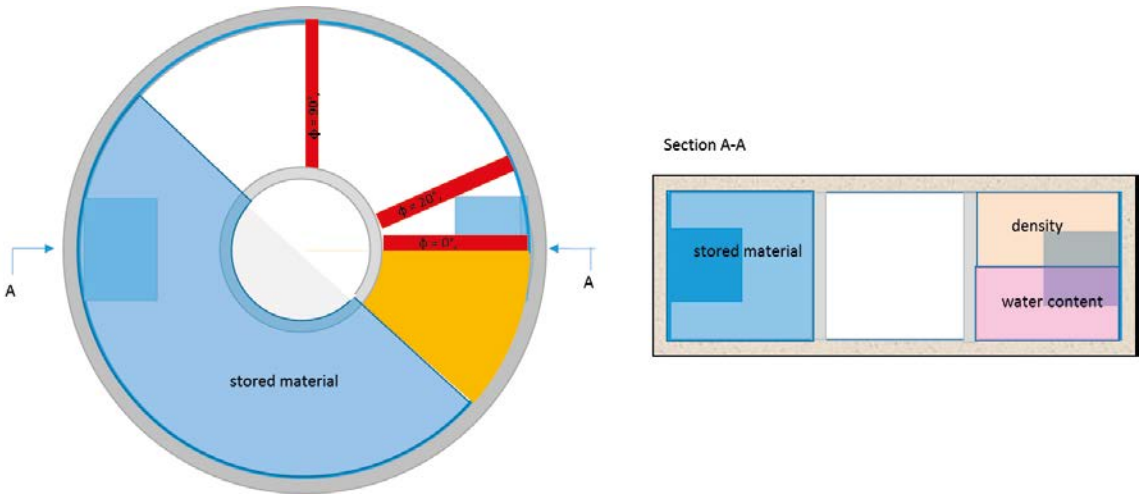

Figure 6-6. *Plan view (to the left) and section (to the right) of the bentonite block at dismantling. The plan view shows the bentonite cylinder ring with the stored material (blue area), the lines of sampling (red lines) and the sector for continuous sampling (yellow area) marked. The section shows the stored part and the parts used for determinations of density and water content.*

Extensive sampling was made with two different strategies as shown in Figure 6-6 (to the left) and Figure 6-7; along three lines and continuously within a sector. The lines were located at the angles 0°, 20° and 90° from the middle of the initial cavity and the sector, with a center angle of 45°, included parts both inside and outside of the initial cavity. The lines and sector are marked red and yellow, respectively, in Figure 6-6 (to the left). The samples taken along the lines were denominated L0, L20 and L90. The sector, with continuous sampling, was divided into the subsectors A, B, C and D at the angles 6°, 17°, 28° and 39° from the center of the cavity. The sampling and denominations are shown in Figure 6-7 to Figure 6-9. The subsectors A, B, C and D were further divided into two sectors each, along which the samples were taken. The denominations of all subsectors were A(2), A, B(2), B, C(2), C, D(2), D starting from the center of the cavity.

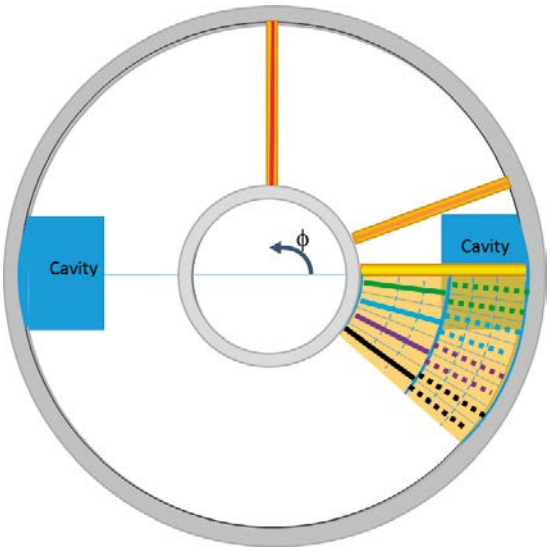

Figure 6-7. *Plan view which shows the sampling along lines at different angles from the middle of the cavity; 0° (yellow), 20° (orange) and 90° (red) and the sampling continuously within a sector along the dotted and solid lines (green, blue, purple and black).*

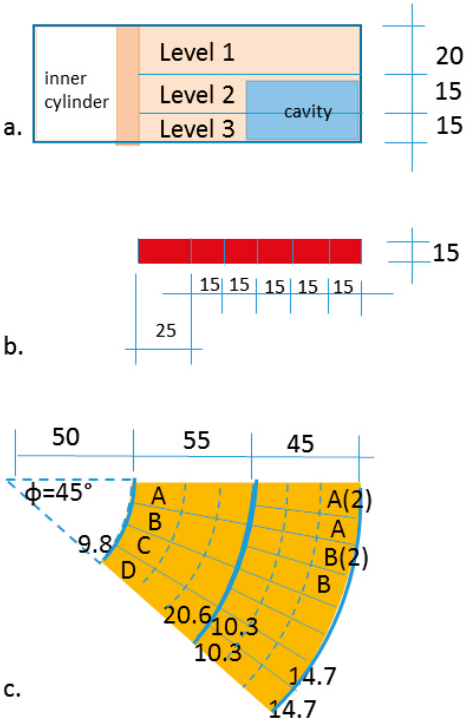

Figure 6-8. *Positions of the sampling shown as: a. section with different sampling levels, b. plan view of a sampling line and c. plan view of the sampled sector with subsectors. The numbers show the length, width and height of the samples in the unit mm. Also shown is the center angle of the sampled sector, i.e. 45°.*

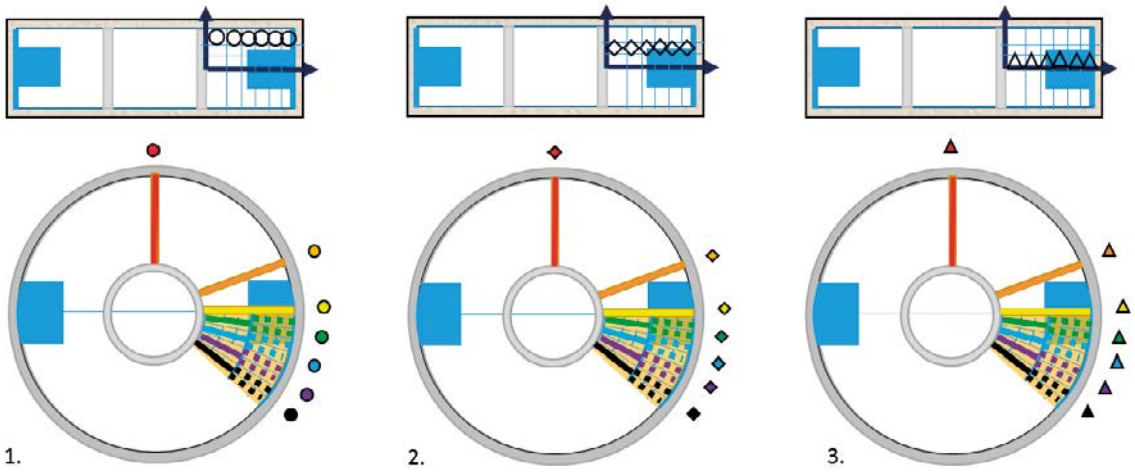

Figure 6-9. *Markers and colours used in the presentation of results showing the sample positions. The positions are shown both in sectors (upper squares) and plan views (lower circles). The markers (circle, diamond, triangle) show the horizontal levels of the samples (1 – outermost, 2 – second outermost, 3 – innermost). The colours (red, orange, yellow, green, blue, purple, black) show the sampling lines at different angles from the center of the initial cavity (90°, 20°, 0°, −6°, −17°, −28°, −39°) denoted (L90, L20, L0, A, B, C, D). Within the sector with continuous sampling the subsectors were further divided into two parts, marked with dotted and solid lines of each of the colours (green, blue, purple, black). From the center of the cavity the denomination of all sub-sub-sectors are A(2), A, B(2), B, C(2), C, D(2), D.*

Measured distribution of water content and density of SH2

The distributions of density determined after dismantling of the non-instrumented test SH2 at the levels 1, 2, and 3 (outermost, second outermost and innermost) are shown in Figure 6-10, Figure 6-11 and Figure 6-12, respectively. The initial dry density of the block was approximately 1 650 kg/m^3, cf. Table 6-3. The average final density based on the initial mass and the final volume of the device, i.e. with the cavities taken into account, was calculated to 1 551 kg/m^3. The results show the difference in density as a function of the radial distance in different directions. The lowest values (yellow points) and the highest values (red points) were seen in the directions coinciding with and perpendicular to the direction of the cavity, respectively. Tables presenting the water contents and densities of all samples are shown in Appendix 6.

After the first sampling the results from the samples taken along line L0, i.e. in the center of the cavity, were found uncertain (marked in Figure 6-11) since they were not quite logical and additional samples along a line between L0 and L20 were taken. The new sampling line, denoted L6, was located at an approximate angle of 6° from the center of the cavity and the results from the samples taken along this line are shown with black marker lines, yellow markers and yellow lines in Figure 6-10 to Figure 6-12.

Comments

The diagrams show that the dry density increases logically from the lines through the center of the cavity L0 (yellow lines) to the lines perpendicular to the center of the cavity L90 (red lines) further away from the cavity. However, the relatively low density at the radial distance 92 mm along the sampling line L90 (red lines) was not expected.

The lowest densities were found within a volume with its center deviating from the center of the initial cavity. The low density volume seems to have its center deviating between 0–6° in the horizontal plane and 0–20 mm in the vertical plane from the vertical and horizontal symmetry planes, respectively. In the radial direction the lowest density was, as expected, found close to the outer surface of the block. The degree of saturation for all samples taken are summarised in Table 6-4 and also shown in Appendix 5.

In addition, to the results presented above samples were taken in order to study the horizontal symmetry in the results, i.e. the correspondence between the results from samples taken in the upper and in the lower parts of the bentonite block. Water contents were determined on samples taken in the same positions in the upper and lower parts of the block. The results are presented in Figure 6-13 where it is seen that the water contents determined on samples from the lower part (blue) are in general higher than the water contents determined on samples from the upper part (red).

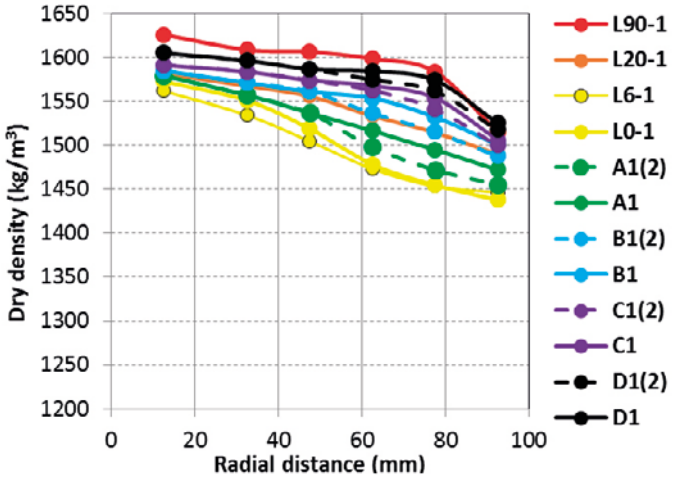

Figure 6-10. *Distribution of dry density at the outermost level 1 in different directions. The colours (red, orange, yellow, green, blue, purple, black) show the angles (90°, 20°, 0°, −6°, −17°, −28°, −39°) to the center of the cavity. In addition, the results from the sampling along line L6 are shown.*

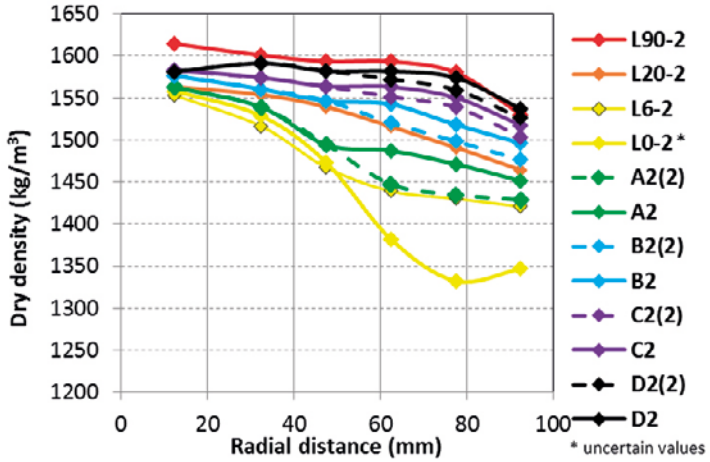

Figure 6-11. *Distribution of dry density at the second outermost level 2 in different directions. The colours (red, orange, yellow, green, blue, purple, black) show the angles (90°, 20°, 0°, −6°, −17°, −28°, −39°) to the center of the cavity. In addition, the results from the sampling along line L6 are shown.*

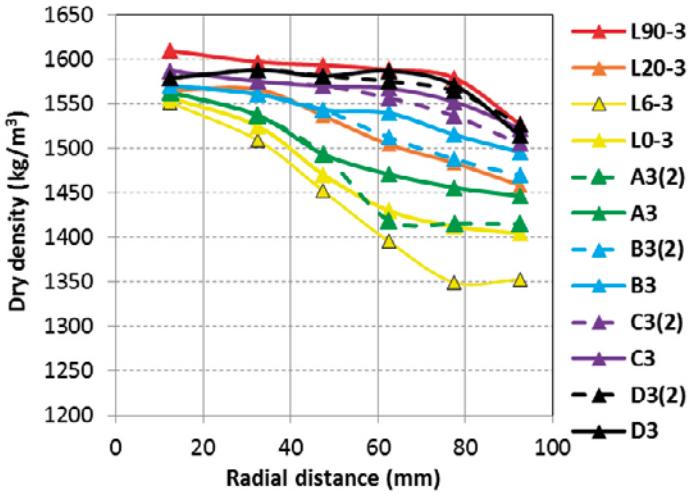

Figure 6-12. *Distribution of dry density at the innermost level 3 in different directions. The colours (red, orange, yellow, green, blue, purple, black) show the angles (90°, 20°, 0°, −6°, −17°, −28°, −39°) to the center of the cavity. In addition, the results from the sampling along line L6 are shown.*

The different levels (1, 2 and 3) refer to the outermost, second outermost and innermost levels shown in Figure 6-8a. The difference between samples taken from the upper and lower parts of the block is at least valid for the actual samples which were all taken along a line 26° from the center of the cavity, i.e. the denomination should be L26 for these samples. The largest discrepancy between the upper and lower parts, 2 %, is seen in the outermost part.

Table 6-4. Degree of saturation from all samples taken from SH2.

	Degree of saturation %	Number of samples
	99	1
	100	8
	101	33
	102	87
	103	28
	104	3
	105	0
	106	2
Average	**102**	
Total number		**162**

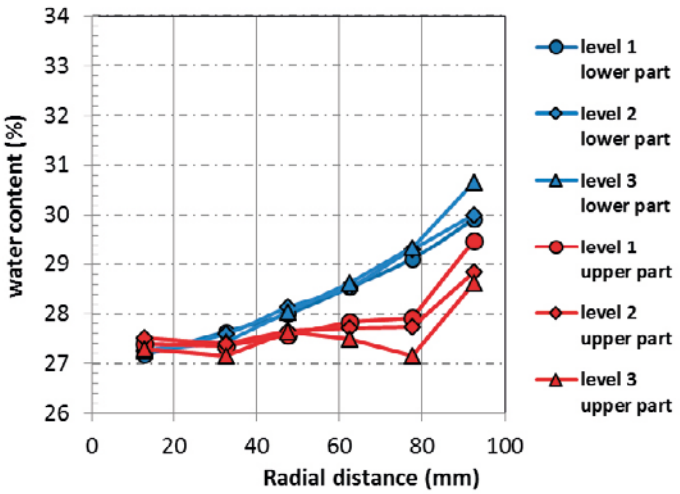

Figure 6-13. *Measured water contents in coinciding positions of the upper and lower parts of the bentonite ring. The original determinations of water contents were made on samples from the lower part.*

7 Final comments

The present status report is a compilation of laboratory test results from a project on homogenisation tests of bentonite. The main purpose of this status report is to account for results derived up to July 2014 and to provide results that can be used for modelling some well-defined benchmark tests in order to improve the models or determine mechanical parameters for thermo-hydro-mechanical modelling of the behaviour of the buffer. Further analysis of the tests, test conditions, test results and limitations of the results will be made later in the project.

The objectives of the tests and the report have been well fulfilled:

- The tests and the results derived up to July 2014 have been presented in detail.
- The knowledge of the homogenisation process has been further increased.
- The results of many of the tests have been used as modelling tasks in the TF EBF (Task Force on Engineered Barrier systems)
  - the fundamental swelling tests (both the basic and the high resolution tests) have been used for checking and improving material models and evaluate the modelling results,
  - the friction tests have been used for the contact parameters.

The results and analyses of these modelling efforts and comparisons with measuring results will be treated in a coming report.

References

SKB's (Svensk Kärnbränslehantering AB) publications can be found at www.skb.com/publications.

Börgesson L, Johannesson L-E, Sandén T, Hernelind J, 1995. Modelling of the physical behaviour of water saturated clay barriers. Laboratory tests, material models and finite element application. SKB TR 95-20. Svensk Kärnbränslehantering AB.

Dueck A, Goudarzi R, Börgesson L, 2011. Buffer homogenisation, status report. SKB TR-12-02, Svensk Kärnbränslehantering AB.

Dueck A, Goudarzi R, Börgesson L, 2014. Buffer homogenisation, status report 2. SKB TR-14-25, Svensk Kärnbränslehantering AB.

Karnland O, Olsson S, Nilsson U, 2006. Mineralogy and sealing properties of various bentonites and smectite-rich clay materials. SKB TR-06-30, Svensk Kärnbränslehantering AB.

Svensson D, Dueck A, Nilsson U, Olsson S, Sandén T, Lydmark S, Jägerwall S, Pedersen K, Hansen S, 2011. Alternative buffer material. Status of the ongoing laboratory investigation of reference materials and test package 1. SKB TR-11-06, Svensk Kärnbränslehantering AB.

Åkesson M, Börgesson L, Kristensson O, 2010. SR-site Data report. THM modelling of buffer, backfill and other system components. SKB TR-10-44, Svensk Kärnbränslehantering AB.

Appendix 1

Evolution of stresses (basic series)

Evolution of swelling pressure, axially and radially measured stresses, with time is given in diagrams for all tests of the actual types (shown in Figure 4-2, Figure 4-3 and Figure 4-4) and presented in this report. Tabulated values of stresses, dry densities and swelling are also given. Each series is presented in separate sections. Additional test results were presented in section 5.1.

A1.1 Axial swelling

A01-14	Test description		Axial swelling of drilled specimen with initial water content w_i = 23.8%. MX-80				Final H (mm)	27.5
							Final D (mm)	50
Date	Diameter of cavity mm	Dry density kg/m^3	Axial stress kPa	Radial stress kPa	Mean stress kPa	Swelling ρ_{di}/ρ_{df}-1 %	Remarks	
	20.0	1618					compaction	
2012-08-06	20.0	1618	49	247	181		start	
2012-09-06	27.5	1187	480	573	542	36.4	final swelling (f)	

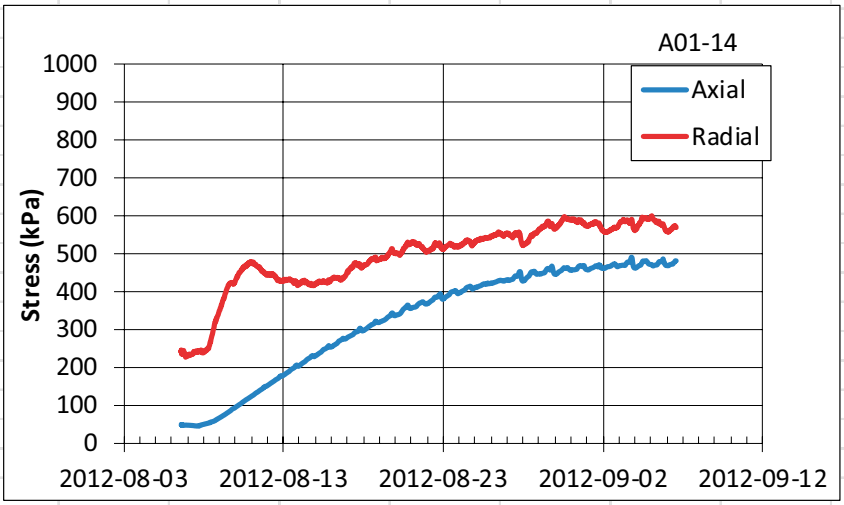

A01-15	Test description		Test with doubled time compared to A01-9				Final H (mm)	25.0
			MX-80				Final D (mm)	50
Date	Diameter of cavity mm	Dry density kg/m^3	Axial stress kPa	Radial stress kPa	Mean stress kPa	Swelling ρ_{di}/ρ_{df}-1 %	Remarks	
	20.0	1656					compaction	
2012-11-22	20.0	1656	100	196	164		start	
2012-12-11	20.0	1656	8832	6533	7299		saturation (i)	
2012-12-11	25.0		43	179	133		start swelling	
2013-01-08	25.0	1300	1024	1203	1143	27.4	final swelling (f)	

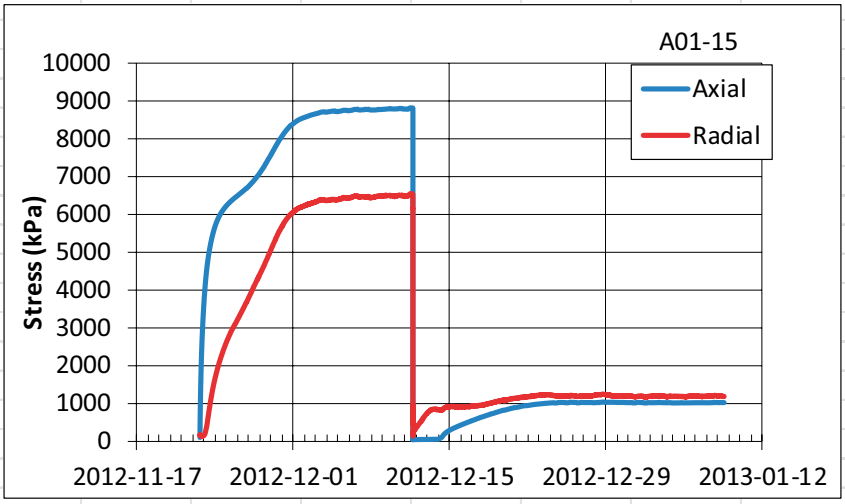

A01-16	Test description		MX-80, water pressure applied				Final H (mm)	21.0
							Final D (mm)	50
Date	Diameter of cavity mm	Dry density kg/m^3	Axial stress kPa	Radial stress kPa	Mean stress kPa	Swelling ρ_{di}/ρ_{df}-1 %	Remarks	
	20.0	1671					compaction	
2013-01-23	20.0	1671	572	1302	1058		start	
2013-02-08	20.0	1658	9261	6733	7576		saturation (i)	
2013-02-08	21.0		277	106	163		start swelling	
2013-03-12	21.0	1539	6089	5227	5514	7.7	final swelling, end of test (f)	

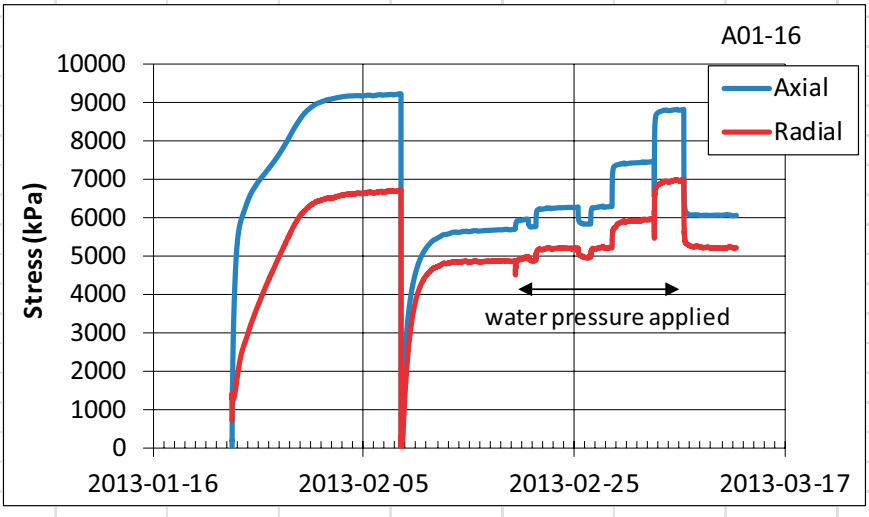

A04-01	Test description		Calcigel				Final H (mm)	25.0
							Final D (mm)	50
Date	Diameter of cavity mm	Dry density kg/m^3	Axial stress kPa	Radial stress kPa	Mean stress kPa	Swelling ρ_{di}/ρ_{df}-1 %	Remarks	
	20.0	1738					compaction	
2014-04-04	20.0	1738	1465	1109	1228		start	
2014-04-25	20.0	1661	12670	13369	13136		saturation (i)	
2014-04-25	25.0		43	3838	2573		start swelling	
2014-05-26	25.0	1301	953	1851	1552	27.7	final swelling (f)	

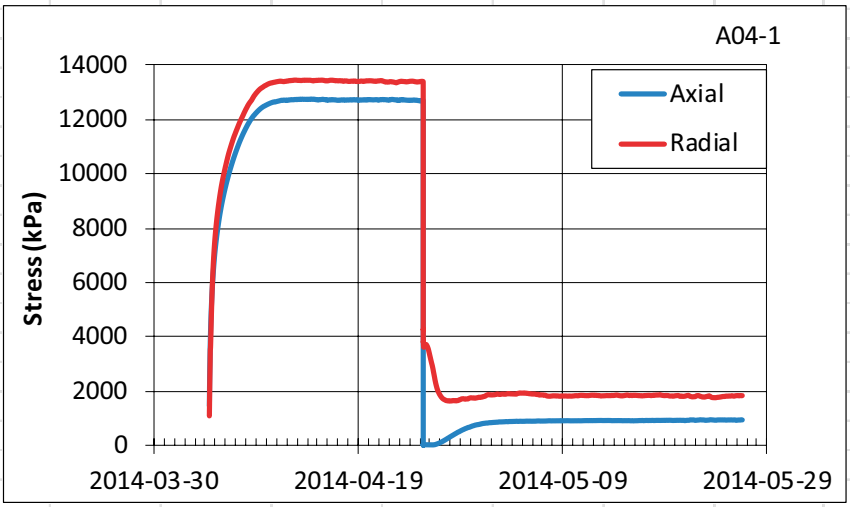

A04-02	Test description		Calcigel				Final H (mm)	27.5
							Final D (mm)	50
Date	Diameter of cavity mm	Dry density kg/m^3	Axial stress kPa	Radial stress kPa	Mean stress kPa	Swelling ρ_{di}/ρ_{df}-1 %	Remarks	
	20.0	1720					compaction	
2014-05-28	20.0	1720	91	99	96		start	
2014-06-11	20.0	1661	12637	13190	13006		saturation (i)	
2014-06-11	27.5		68	4038	2715		start swelling	
2014-07-21	27.5	1230	299	894	696	35.0	final swelling (f)	

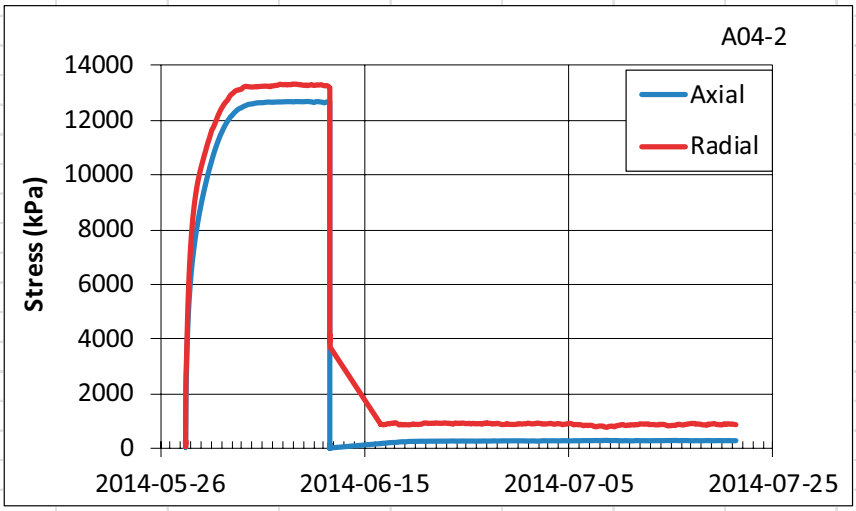

A1.2 Radial outward swelling

R11-22	Test description:	Radial sampling					Final H (mm)	40
							Final D (mm)	46.8
Date	Diameter	Dry density	Axial stress	Radial stress	Mean stress	Swell ρ_{di}/ρ_{df}-1	Remarks	
	mm	kg/m^3	kPa	kPa	kPa	%		
		1655					drilled	
2012-08-10		1599	220	23	89	0.0	start	
2012-09-18	46.8	1599	6184	6300	6261		saturation (i)	
2012-09-18	40.8	1599	21	61	48		start swelling	
2012-10-08	46.8	1197	643	591	608	33.6	final swelling (f)	

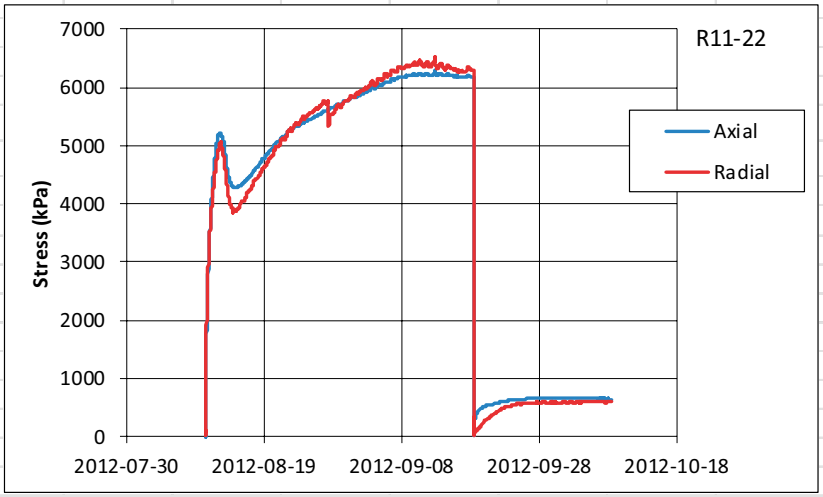

R11-23	Test description:	Starting with 2 compacted specimens					Final H (mm)	40
		MX-80					Final D (mm)	46.8
Date	Diameter	Dry density	Axial stress	Radial stress	Mean stress	Swell ρ_{di}/ρ_{df}-1	Remarks	
	mm	kg/m^3	kPa	kPa	kPa	%		
		1736					compaction	
2012-10-15		1655	169	45	86	0.0	start	
2012-11-30	46.8	1655	11698	10075	10616		saturation (i)	
2012-11-30	40.8	1655	72	101	92		start swelling	
2013-01-21	46.8	1336	1494	1147	1263	23.9	final swelling (f)	

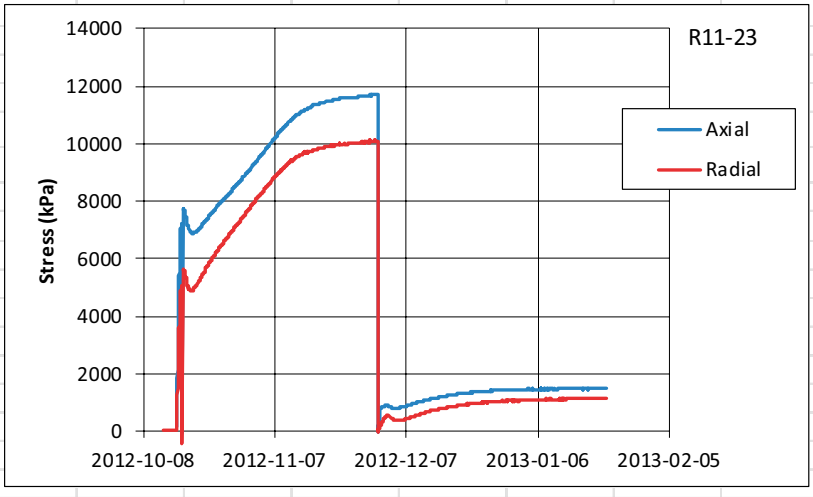

R11-24	Test description:	MX-80, water pressure applied					Final H (mm)	40
							Final D (mm)	46.8
Date	Diameter	Dry density	Axial stress	Radial stress	Mean stress	Swell ρ_{di}/ρ_{df}-1	Remarks	
	mm	kg/m^3	kPa	kPa	kPa	%		
		1760					compaction	
2014-05-06		1648	159	48	85	0.0	start	
2014-07-18	46.8	1648	8810	9152	9038		saturation (i)	
2014-07-18	40.8	1648	139	83	102		start swelling	
2014-12-02	46.8	1207	565	458	493	36.5	final swelling (f)	

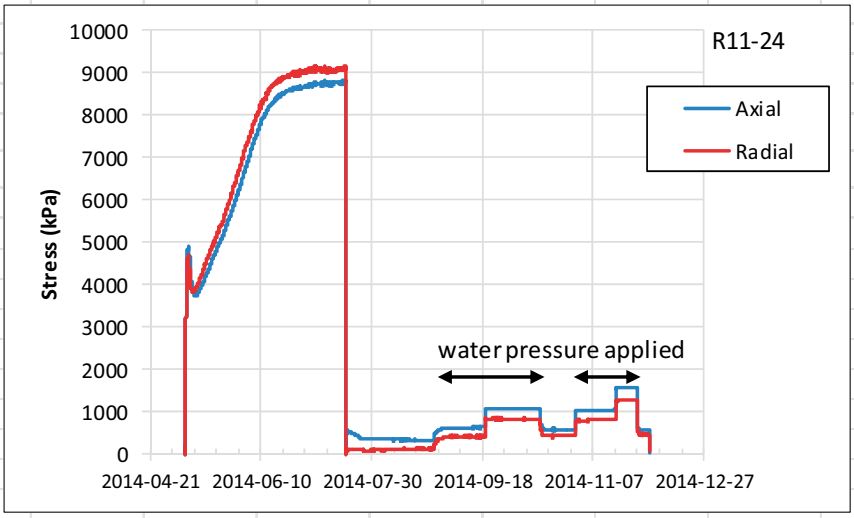

R14-1	Test description:	Starting with 2 compacted specimens CALCIGEL					Final H (mm)	40
							Final D (mm)	46.8
Date	Diameter	Dry density	Axial stress	Radial stress	Mean stress	Swell ρ_{di}/ρ_{df}-1	Remarks	
	mm	kg/m^3	kPa	kPa	kPa	%		
		1707					compaction	
2013-01-28		1649	346	114	191	0.0	start	
2013-02-13	46.8	1649	13113	11111	11778		saturation (i)	
2013-02-13	40.8	1649	386	27	147		start swelling	
2013-03-06	46.8	1227	835	506	616	34.4	final swelling (f)	

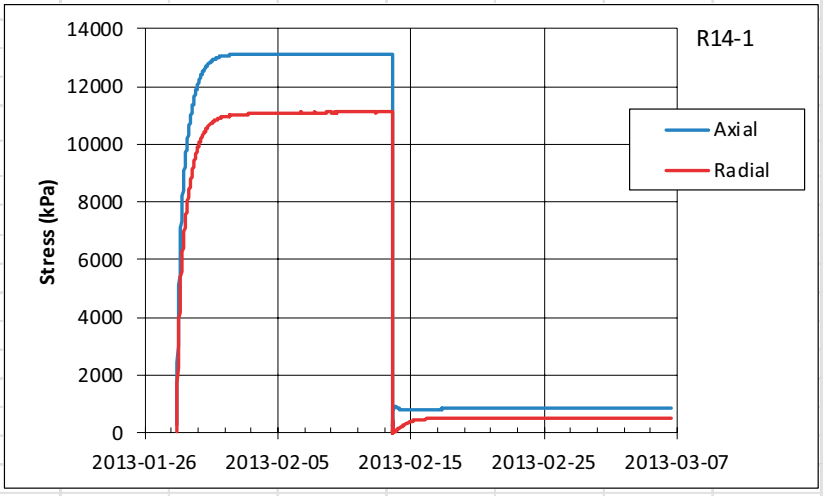

R14-2	Test description:		Starting with 2 compacted specimens				Final H (mm)	40
			CALCIGEL				Final D (mm)	46.8
Date	Diameter	Dry density	Axial stress	Radial stress	Mean stress	Swell ρ_{di}/ρ_{df}-1	Remarks	
	mm	kg/m^3	kPa	kPa	kPa	%		
		1708					compaction	
2013-08-16		1650	77	171	139	0.0	start	
2013-09-02	46.8	1650	11977	10317	10870		saturation (i)	
2013-09-02	43.8	1650	143	174	163		start swelling	
2013-09-17	46.8	1419	2583	1961	2168	16.2	final swelling (f)	

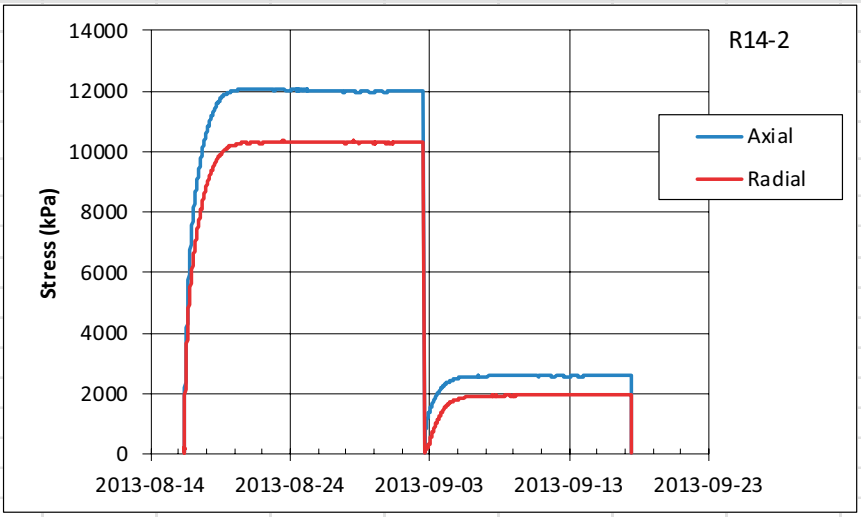

A1.3 Radial inward swelling

R21-13	Test description:		Saturation and radial inward swelling				Final H (mm)	40
			Initially 2 spec. with almost perfect fit into device.				Final D (mm)	46.7
Date	Diameter of cavity	Dry density	Axial stress	Radial stress	Mean stress	Swelling ρ_{di}/ρ_{df}-1	Remarks	
	mm	kg/m^3	kPa	kPa	kPa	%		
	0.0	1714	0	0			compaction	
2012-03-05 11:24	0.0	1656	86	142	123		start	
2012-04-10 12:30	0.0	1656	12178	11126	11476	0.0	saturation (i)	
2012-04-10 14:07	33.0	1656	754	316	462			
2012-04-24 12:30	0.0	790	147	129	135	109.5	final swelling (f)	

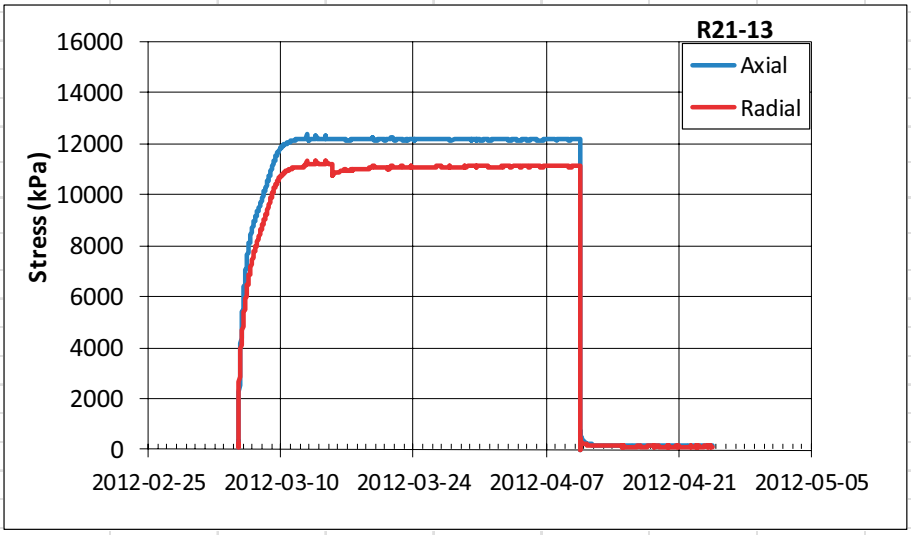

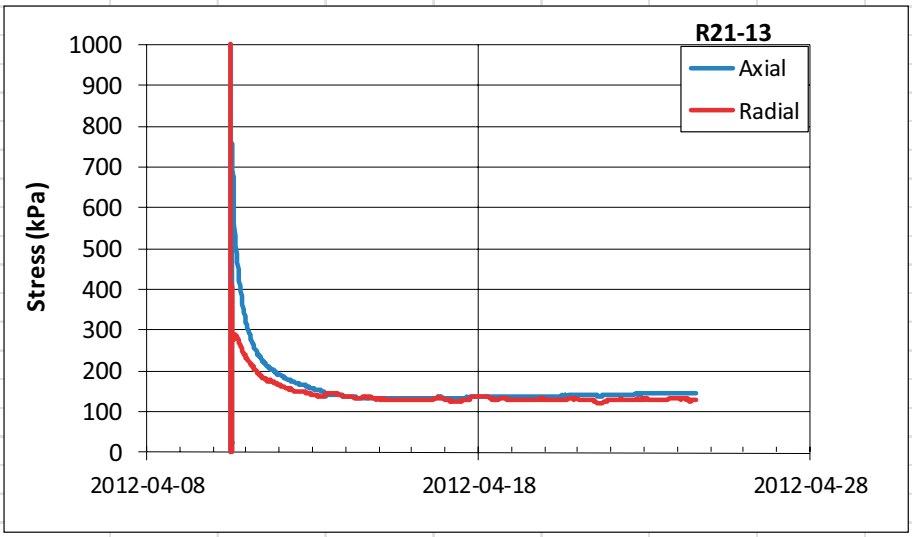

R21-14	Test description:		Saturation and radial inward swelling Long time for homogenisation				Final H (mm) Final D (mm)	40 46.7
Date	Diameter of cavity mm	Dry density kg/m^3	Axial stress kPa	Radial stress kPa	Mean stress kPa	Swelling ρ_{di}/ρ_{df}-1 %	Remarks	
	0.0	1662					compaction	
2012-06-08 14:31	0.0	1606	195	121	146		start	
2012-06-26 09:30	0.0	1606	7959	7473	7635	0.0	saturation (i)	
2012-06-26 11:09	33.0	1606	834	25	295			
2012-07-31 15:00	0.0	826	235	134	168	94.4	final sw elling (f)	

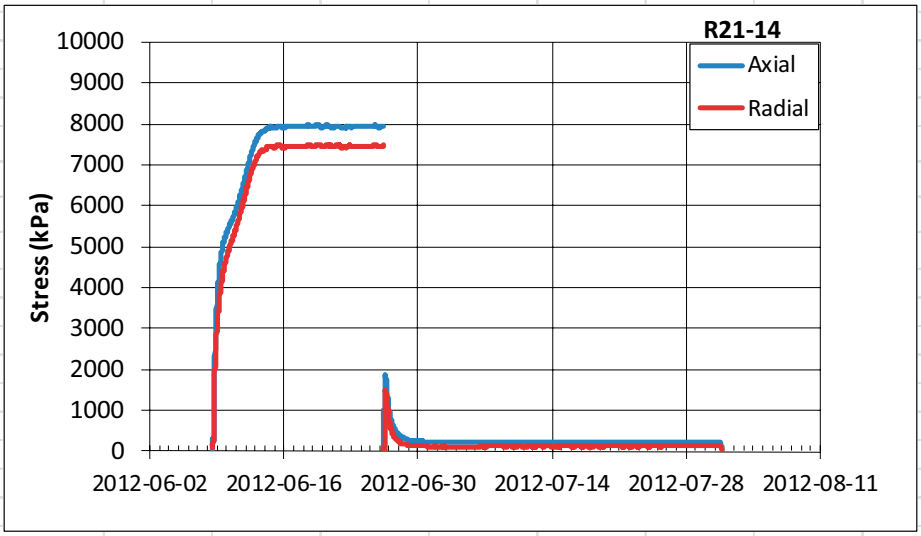

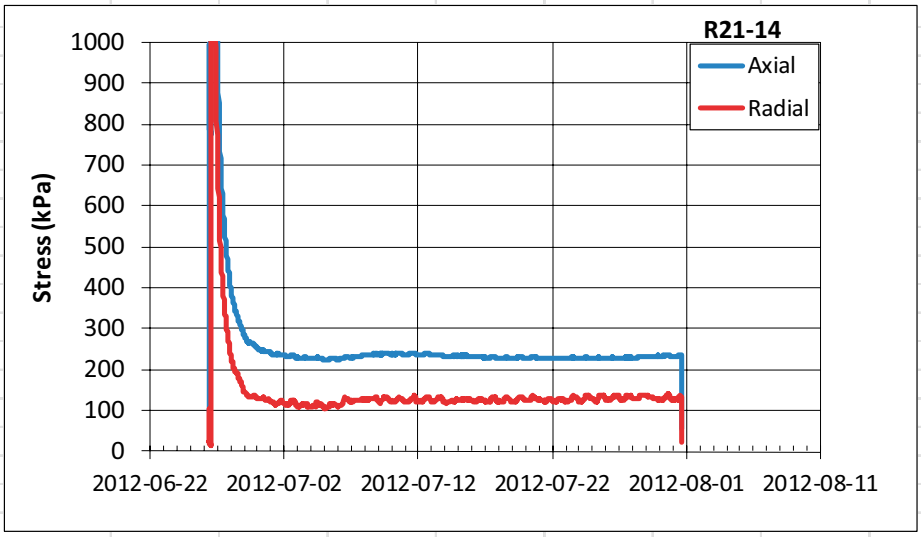

R24-1	Test description:		Saturation and radial inward swelling				Final H (mm)	40
			Calcigel (compacted in two parts)				Final D (mm)	46.7
Date	Diameter of cavity	Dry density	Axial stress	Radial stress	Mean stress	Swelling ρ_{di}/ρ_{df}-1	Remarks	
	mm	kg/m^3	kPa	kPa	kPa	%		
	0.0	1731					compaction	
2013-11-29 14:32	0.0	1658	144	91	109		start	
2013-12-17 13:00	0.0	1658	12927	10300	11175	0.0	saturation (i)	
2013-12-17 14:12	33.0	1658	4220	3227	3558			
2014-02-07 13:00	0.0	815	107	1110	776	103.5	final swelling (f)	

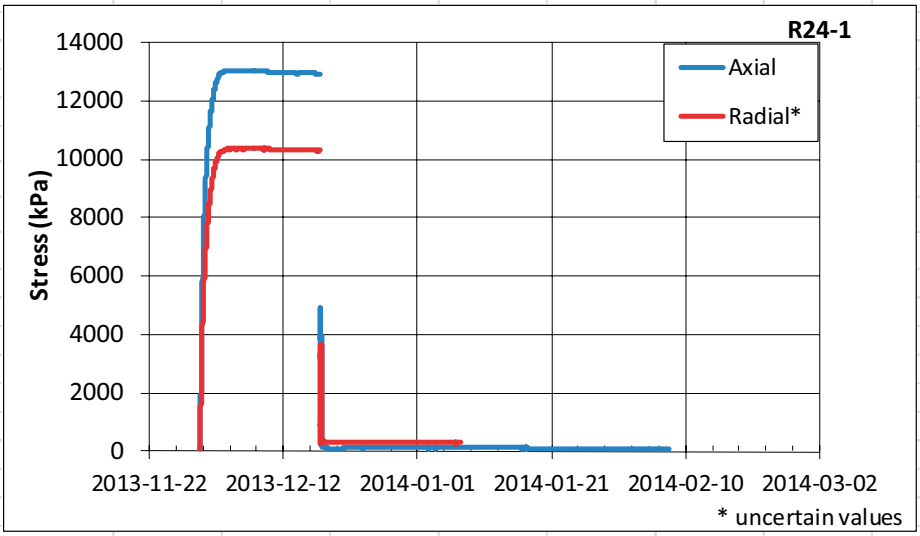

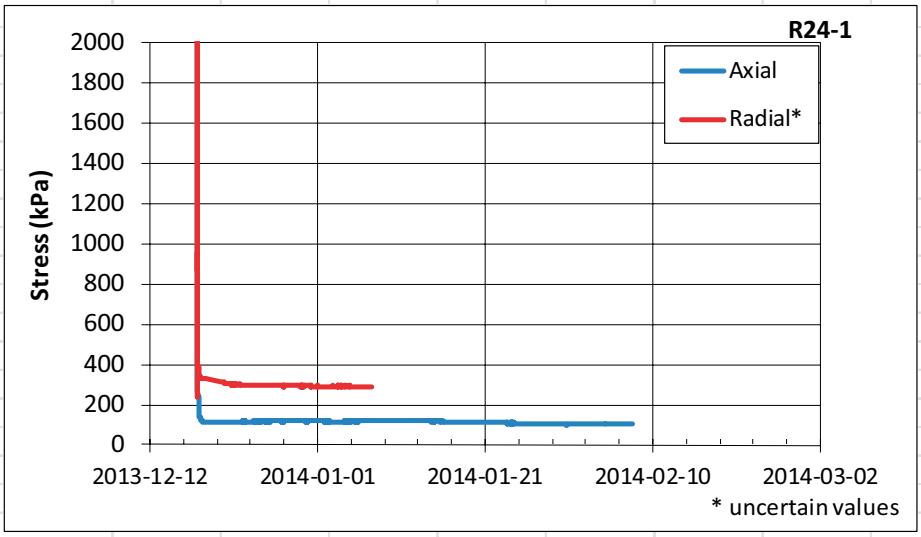

R24-2	Test description:		Saturation and radial inward swelling				Final H (mm)	40
			Calcigel (compacted in two parts)				Final D (mm)	46.7
Date	Diameter of cavity	Dry density	Axial stress	Radial stress	Mean stress	Swelling ρ_{di}/ρ_{df}-1	Remarks	
	mm	kg/m^3	kPa	kPa	kPa	%		
	0.0	1731					compaction	
2014-03-14 14:43	0.0	1658	281	66	137		start	
2014-03-28 07:00	0.0	1658	12026	9073	10057	0.0	saturation (i)	
2014-03-28 09:16	10.5	1658	266	789	615			
2014-04-28 10:30	0.0	1536	6800	5940	6227	7.9	final swelling (f)	

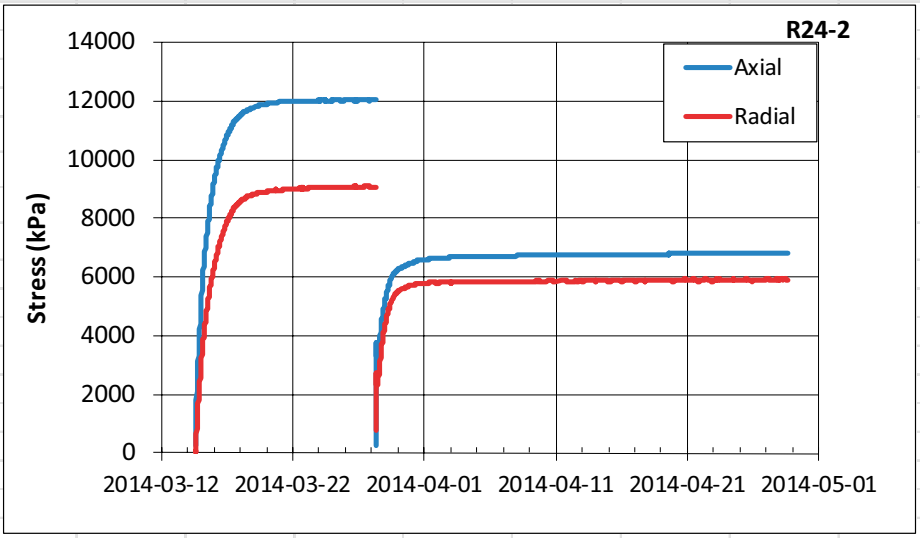

Appendix 2

Distribution of basic variables in the direction of swelling (basic series)

Distribution of the basic variables water content w, bulk density ρ, void ratio e, dry density ρ_d and degree of saturation S_r, over the specimens in the swelling direction for all tests of the actual types (shown in Figure 4-2, Figure 4-3 and Figure 4-4) and presented in this report. Results were also given in section 5.1 and in Appendix 1.

Table A2-1. Axial swelling. Distribution of basic variables over the specimen height.

A01-14								
from bottom mm	**thickness mm**	**ρ_s kg/m³**	**ρ_w kg/m³**	**w %**	**ρ kg/m³**	**ρ_d kg/m³**	**e**	**S_r %**
3	6	2780	1000	43.2	1812	1265	1.20	100
8.75	5.5	2780	1000	45.4	1802	1239	1.24	101
14.25	5.5	2780	1000	44.6	1799	1244	1.24	100
19.5	5	2780	1000	49.7	1758	1174	1.37	101
24.5	5	2780	1000	66.1	1639	986	1.82	101
average				**49.4**	**1765**	**1187**	**1.36**	**101**
A01-15								
from bottom mm	**thickness mm**	**ρ_s kg/m³**	**ρ_w kg/m³**	**w %**	**ρ kg/m³**	**ρ_d kg/m³**	**e**	**S_r %**
2.5	5	2780	1000	36.8	1856	1356	1.05	98
7.5	5	2780	1000	38.2	1862	1347	1.06	100
13.75	7.5	2780	1000	40.4	1839	1310	1.12	100
21.25	7.5	2780	1000	45.7	1779	1221	1.28	100
average				**40.8**	**1829**	**1300**	**1.14**	**99**
A01-16								
from bottom mm	**thickness mm**	**ρ_s kg/m³**	**ρ_w kg/m³**	**w %**	**ρ kg/m³**	**ρ_d kg/m³**	**e**	**S_r %**
2.75	5.5	2780	1000	27.3	1988	1561	0.78	97
8.25	5.5	2780	1000	26.8	1999	1577	0.76	98
13.5	5	2780	1000	27.5	1946	1527	0.82	93
18.5	5	2780	1000	31.5	1951	1484	0.87	100
average				**28.2**	**1972**	**1539**	**0.81**	**97**
A04-1								
from bottom mm	**thickness mm**	**ρ_s kg/m³**	**ρ_w kg/m³**	**w %**	**ρ kg/m³**	**ρ_d kg/m³**	**e**	**S_r %**
2.5	5	2695	1000	36.2	1889	1387	0.94	103
7.5	5	2695	1000	37.2	1823	1328	1.03	98
12.5	5	2695	1000	38.0	1786	1294	1.08	95
17.5	5	2695	1000	40.9	1804	1281	1.10	100
22.5	5	2695	1000	45.5	1766	1214	1.22	100
average				**39.6**	**1814**	**1301**	**1.08**	**99**
A04-2								
from bottom mm	**thickness mm**	**ρ_s kg/m³**	**ρ_w kg/m³**	**w %**	**ρ kg/m³**	**ρ_d kg/m³**	**e**	**S_r %**
2.5	5	2695	1000	39.5	1829	1312	1.05	101
7.5	5	2695	1000	40.8	1819	1292	1.09	101
12.5	5	2695	1000	41.6	1807	1276	1.11	101
17.5	5	2695	1000	49.3	1733	1161	1.32	101
22.5	5	2695	1000	53.4	1701	1109	1.43	101
average				**44.9**	**1778**	**1230**	**1.20**	**101**

Table A2-2. Radial outward swelling. Distribution of basic variables over the specimen height.

R11-22								
radius mm	**thickness mm**	**ρ_s kg/m³**	**ρ_w kg/m³**	**w %**	**ρ kg/m³**	**ρ_d kg/m³**	**e**	**S_r %**
4	8	2780	1000	41.4	1820	1287	1.16	99
12	8	2780	1000	38.5	1808	1305	1.13	95
20	8	2780	1000	56.1	1739	1114	1.50	104
	average			**48.6**	**1771**	**1197**	**1.34**	**101**
R11-23								
radius mm	**thickness mm**	**ρ_s kg/m³**	**ρ_w kg/m³**	**w %**	**ρ kg/m³**	**ρ_d kg/m³**	**e**	**S_r %**
4	8	2780	1000	37.0	1883	1375	1.02	101
12	8	2780	1000	36.9	1869	1365	1.04	99
20	8	2780	1000	39.4	1827	1311	1.12	98
	average			**38.3**	**1847**	**1336**	**1.08**	**98**
R11-24								
radius mm	**thickness mm**	**ρ_s kg/m³**	**ρ_w kg/m³**	**w %**	**ρ kg/m³**	**ρ_d kg/m³**	**e**	**S_r %**
4	8	2780	1000	43.2	1815	1268	1.19	101
12	8	2780	1000	44.0	1805	1254	1.22	100
20	8	2780	1000	50.1	1752	1167	1.38	101
	average			**47.3**	**1777**	**1207**	**1.31**	**101**
R14-1								
radius mm	**thickness mm**	**ρ_s kg/m³**	**ρ_w kg/m³**	**w %**	**ρ kg/m³**	**ρ_d kg/m³**	**e**	**S_r %**
4	8	2695	1000	38.5	1863	1345	1.00	103
12	8	2695	1000	41.1	1834	1300	1.07	103
20	8	2695	1000	51.2	1753	1160	1.32	104
	average			**46.4**	**1793**	**1227**	**1.20**	**104**
R14-2								
radius mm	**thickness mm**	**ρ_s kg/m³**	**ρ_w kg/m³**	**w %**	**ρ kg/m³**	**ρ_d kg/m³**	**e**	**S_r %**
4	8	2695	1000	31.6	1936	1471	0.83	102
12	8	2695	1000	32.0	1927	1460	0.85	102
20	8	2695	1000	36.0	1883	1385	0.95	102
	average			**34.2**	**1904**	**1419**	**0.90**	**102**

Table A2-3. Radial outward swelling. Distribution of basic variables over the specimen height.

R21-13								
radius mm	**thickness mm**	ρ_s **kg/m³**	ρ_w **kg/m³**	**w %**	ρ **kg/m³**	ρ_d **kg/m³**	**e**	S_r **%**
4	8	2780	1000	289.2	1327	341	7.15	112
12	8	2780	1000	89.5	1494	789	2.52	99
20	8	2780	1000	75.1	1543	881	2.16	97
	average			**103.7**	**1502.6**	**790.3**	**2.8**	**99.1**
R21-14								
radius mm	**thickness mm**	ρ_s **kg/m³**	ρ_w **kg/m³**	**w %**	ρ **kg/m³**	ρ_d **kg/m³**	**e**	S_r **%**
4	8	2780	1000	102.6	1330	657	3.23	88
12	8	2780	1000	86.7	1520	814	2.42	100
20	8	2780	1000	78.3	1546	867	2.21	99
	average			**83.8**	**1513.5**	**826.1**	**2.4**	**97.9**
R24-1								
radius mm	**thickness mm**	ρ_s **kg/m³**	ρ_w **kg/m³**	**w %**	ρ **kg/m³**	ρ_d **kg/m³**	**e**	S_r **%**
4	8	2695	1000	138.1		571	3.72	100*
12	8	2695	1000	113.8		663	3.07	100*
20	8	2695	1000	73.5	1656	955	1.82	109
	average			**94.1**	**920.0**	**814.6**	**2.4**	**104.8**
R24-2								
radius mm	**thickness mm**	ρ_s **kg/m³**	ρ_w **kg/m³**	**w %**	ρ **kg/m³**	ρ_d **kg/m³**	**e**	S_r **%**
4	8	2695	1000	32.5	1889	1425	0.89	98.4
12	8	2695	1000	29.1	1990	1542	0.75	104.8
20	8	2695	1000	28.6	2001	1555	0.73	105.3
	average			**29.2**	**1984.9**	**1536.4**	**0.8**	**104.4**

Appendix 3

Final values of basic variables and swelling pressure (basic series)

In the tables the final values of the basic variables (water content w, bulk density ρ, dry density ρ_d, degree of saturation S_r) and the swelling pressure (axial stress P_a, radial stress P_r) are given for all tests of the actual types (shown in Figure 4-2, Figure 4-3 and Figure 4-4). The last column contains the total time for each test divided into the time for saturation t_1 and the time for swelling and homogenisation t_2 ($t_1 + t_2$). Results were also given in section 5.1 and in Appendix 1 and 2.

Table A3-1. Axial swelling. Results from test series A0.

Sample ID	Swelling	Average over the specimen after dismantling				Swelling pressure		Total time
	%	w %	ρ kg/m³	ρ_d kg/m³	S_r %	Axial P_a kPa	Radial P_r kPa	$t_1 + t_2$ days
A01-14	36	49.4	1765	1187	101	480	573	0 + 31
A01-15	27	40.8	1829	1300	99	1024	1203	19 + 28
A01-16	8	28.2	1972	1539	97	6089	5227	16 + 32
A04-1	28	39.6	1814	1301	99	953	1851	21 + 31
A04-2	35	44.9	1778	1230	101	299	894	14 + 40

Table A3-2. Radial outward swelling. Results from test series R1.

Sample ID	Swelling	Average over the specimen after dismantling				Swelling pressure		Total time
	%	w %	ρ kg/m³	ρ_d kg/m³	S_r %	Axial P_a kPa	Radial P_r kPa	$t_1 + t_2$ days
R11-22	34	48.6	1771	1197	101	643	591	39 + 20
R11-23	24	38.3	1847	1336	98	1494	1147	46 + 52
R11-24	37	47.3	1777	1207	101	565	458	73 + 137
R14-1	34	46.4	1793	1227	104	835	506	16 + 21
R14-2	16	34.2	1904	1419	102	2583	1961	17 + 15

Table A3-3. Radial inward swelling. Results from test series R2.

Sample ID	Swelling	Average over the specimen after dismantling				Swelling pressure		Total time
	%	w %	ρ kg/m³	ρ_d kg/m³	S_r %	Axial P_a kPa	Radial P_r kPa	$t_1 + t_2$ days
R21-13	110	103.7	1503	790	99	147	129	36 + 14
R21-14	94	83.8	1513	826	98	235	134	18 + 35
R24-1	104	94.1	920	815	105	107	290	18 + 52
R24-2	8	29.2	1985	1536	104	6800	5940	14 + 31

Appendix 4

Final values of basic variables and swelling pressure (high resolution)

In the tables the final values of the basic variables (water content w, dry density ρ_d, degree of saturation S_r) and the swelling pressure (axial stress P_a, radial stress P_r) are given for all tests of the actual types (shown in Figure 4-5, Figure 4-6 and Figure 4-7) in this report. The last column contains the total time for the swelling and homogenisation. In the table the positions 1, 2, 3 and 4 means 15 mm, 30 mm, 45 mm and 60 mm, respectively from the bottom surface of the specimens and the abbreviation avr. means average over the specimen. Additional results were given in section 5.2.

Table A4-1. Axial swelling. Results from test series HR-A.

Sample ID	Material	Initial values		Swelling		Final average values			Swelling pressure		Total time
		w %	ρ_d kg/m^3	ρ_{d0}/ρ_{df} - 1 %	pos.	w %	ρ_{df} kg/m^3	S_r %	Axial P_a kPa	Radial P_r kPa	Days
HR-A2	MX-80	24.4	1232	0[1]	avr.	44.7	1198	93	383	642	72
					1	40.7	1253	93		838	
					2	43.8	1200	92		519	
					3	55.9	1072	97		568	
					4						
HR-A3	MX-80	23.7	1666	22	avr.	37.16	1362	99	1822	2182	70
					1	35.09	1401	99		2316	
					2	36.86	1364	99		2047	
					3						
					4						
HR-A4	MX-80	22.5	1693	41	avr.	48.2	1197	100	416	716	145
					1	42.5	1271	100		800	
					2	43.6	1247	99		791	
					3	46.8	1207	100		732	
					4	59.8	1044	100		542	
HR-A6	Calcigel	20.9	1730	46	avr.	48.2	1185	100	224	448	117
					1	40.1	1301	101		1019	
					2	45.1	1198	97		481	
					3	54.2	1095	100		169	
					4	57.8	1041	98		125	

[1] The specimen was compacted in two piece, with different dry densities, and no swelling took place.

Table A4-2. Radial outward swelling. Results from test series HR-Ro.

Sample ID	Material	Initial values		Swelling		Final average values			Swelling pressure		Total time
		w %	ρ_d kg/m^3	ρ_{d0}/ρ_{df} - 1 %	pos.	w %	ρ_{df}[1] kg/m^3	S_r[1] %	Axial P_a kPa	Radial P_r kPa	Days
HR-Ro2	Calcigel	20.9	1716	37	avr.	43.0	1249	100	214	156	122
					1	42.2	1262	100		346	
					2	42.5	1257	100		100	
					3	43.0	1248	100		112	
					4	42.2	1262	100		66[2]	

[1] Calculated from the water contents and an assumed Sr = 100 %.

[2] Uncertain value.

Table A4-3. Radial inward swelling. Results from test series HR-Ri.

Sample ID	Material	Initial values		Swelling		Final average values			Swelling pressure		Total time
		w %	ρ_d kg/m^3	ρ_{d0}/ρ_{df} - 1 %	pos.	w %	ρ_{df} kg/m^3	S_r %	Axial P_a kPa	Radial P_r kPa	Days
HR-Ri1	MX-80	23.7	1666	43		50	1166	100	584	501	125

Table A4-4. Swelling in all directions. Results from test series HR-Iso.

Sample ID	Material	Initial values		Swelling		Final average values			Swelling pressure		Total time
		w %	ρ_d kg/m^3	ρ_{d0}/ρ_{df} - 1	pos.	w %	ρ_{df}[1] kg/m^3	S_r[1] %	Axial P_a kPa	Radial P_r kPa	Days
HR-Iso	MX-80	23.2	1684	43		49.8	1181	100	400	340	129
					1	52.3	1139	100		214	
					2	47.3	1202	100		342	
					3	47.3	1203	100		440	
					4	48.2	1190	100		361	

[1] Calculated from the water contents and an assumption of Sr = 100 %.

Appendix 5

Measurements of friction between bentonite and different surfaces

The test results are presented as the evolution of swelling pressure with time (axial and radial stresses) and the evaluated friction angle as a function of deformation from tests Fr1_10 to Fr1_17, Fr1_19, Fr1_20 and Fr2-1, cf. Table 5-8 and section 5.3. The set up was shown in Figure 4-8. In tests where the swelling pressure was measured both radially and axially the friction angle has been determined from both stresses and the results are shown in separated diagrams.

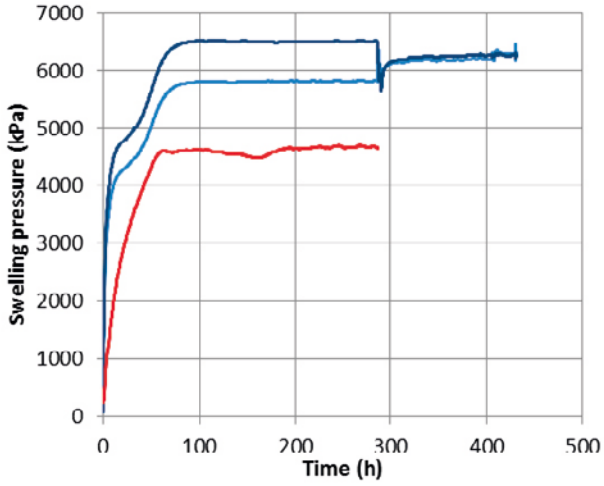

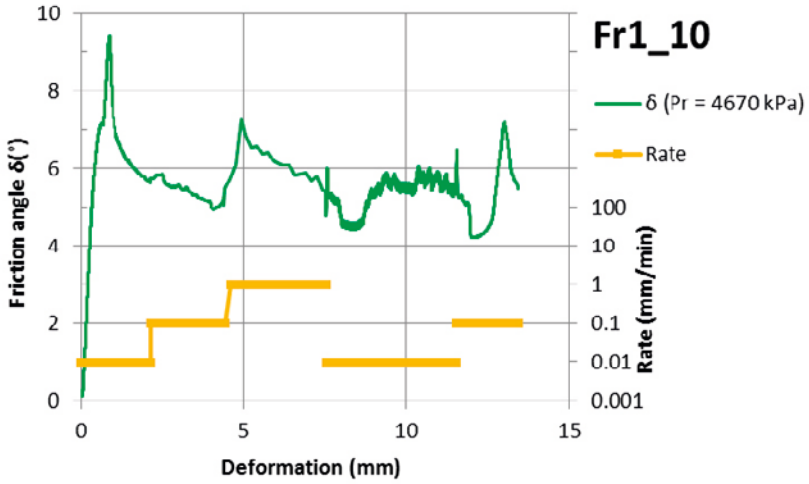

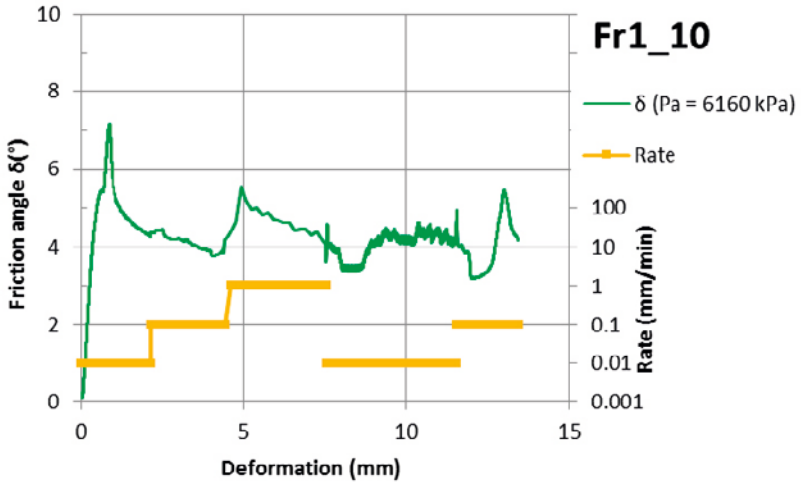

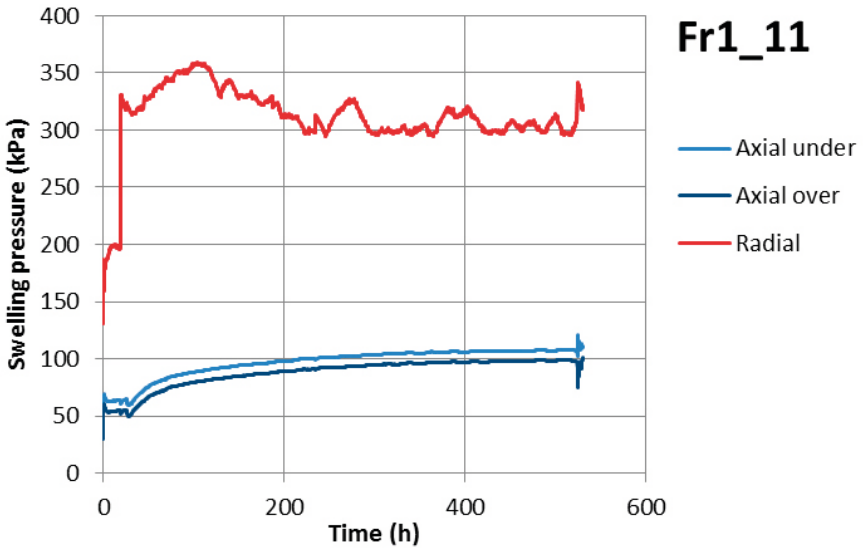
Fr1_11
Swelling pressure (kPa)
Time (h)
Axial under
Axial over
Radial

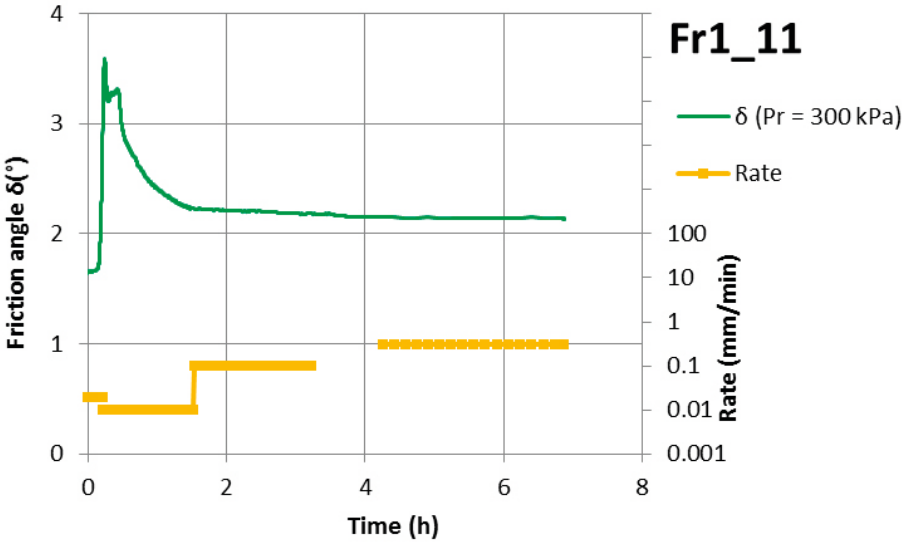
Fr1_11
Friction angle δ(°)
Rate (mm/min)
Time (h)
δ (Pr = 300 kPa)
Rate

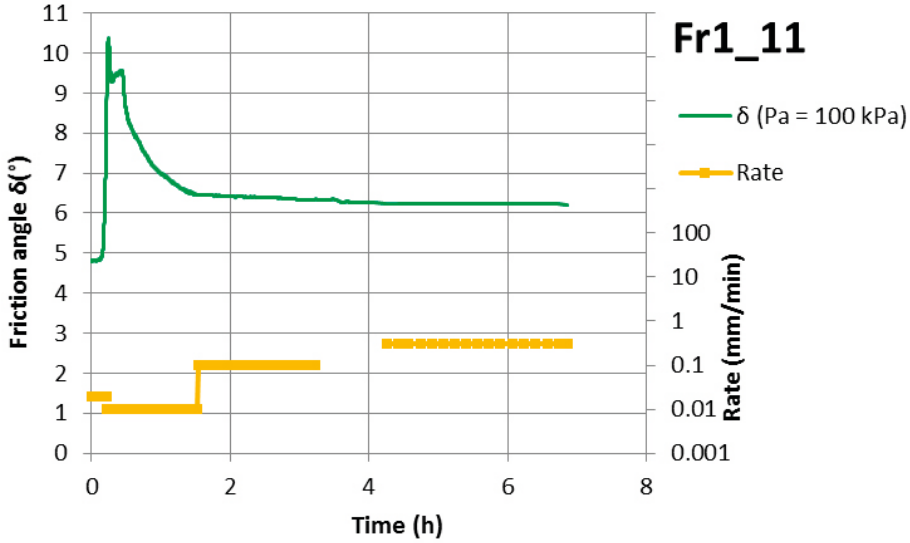
Fr1_11
Friction angle δ(°)
Rate (mm/min)
Time (h)
δ (Pa = 100 kPa)
Rate

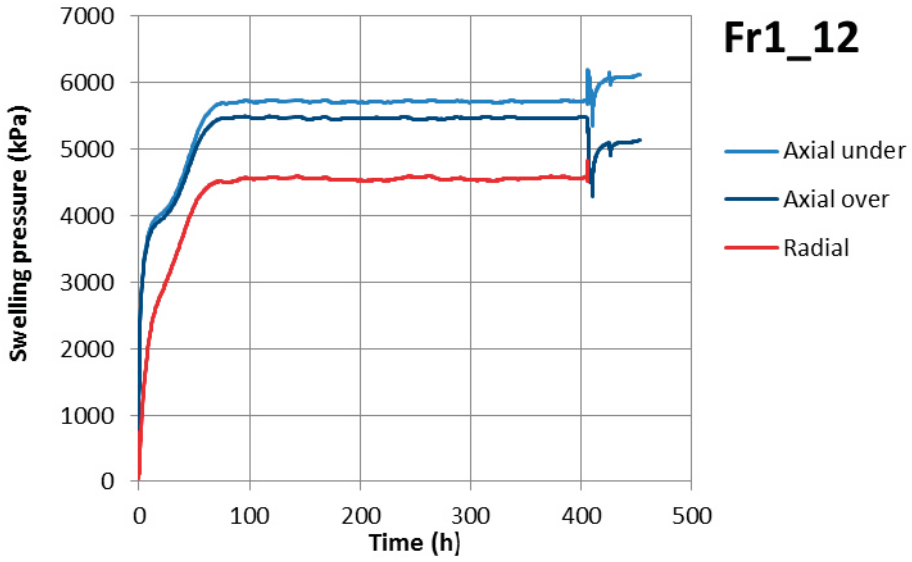
Fr1_12
Swelling pressure (kPa)
Time (h)
Axial under
Axial over
Radial
7000
6000
5000
4000
3000
2000
1000
0
0
100
200
300
400
500

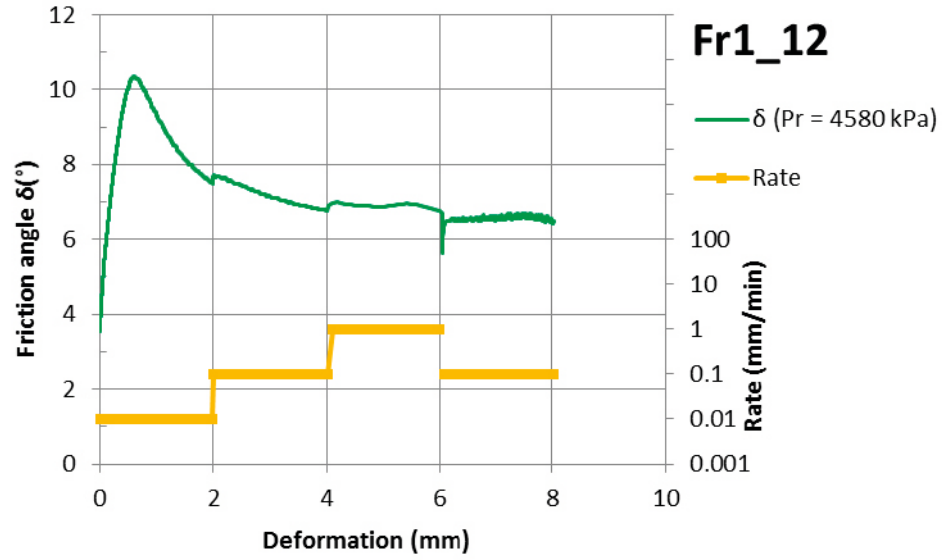
Fr1_12
Friction angle δ(°)
Deformation (mm)
Rate (mm/min)
δ (Pr = 4580 kPa)
Rate
12
10
8
6
4
2
0
0
2
4
6
8
10
100
10
1
0.1
0.01
0.001

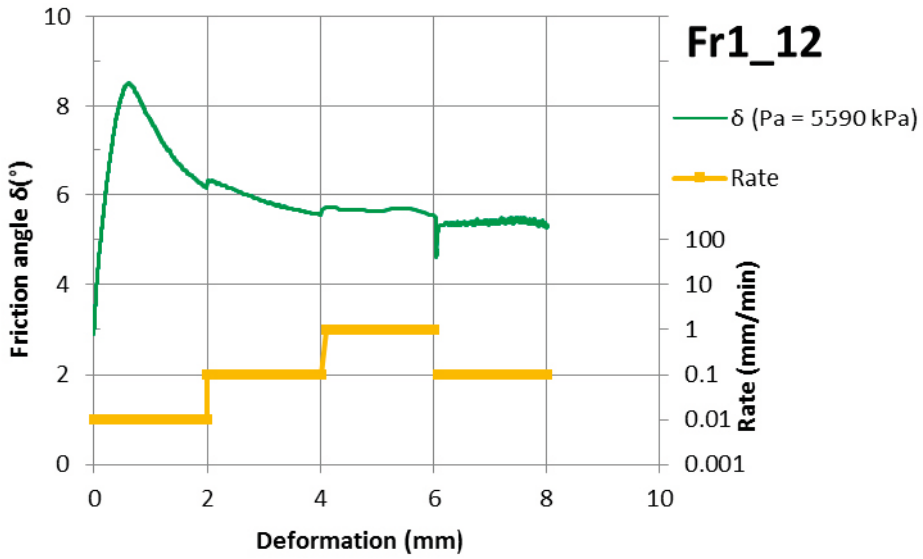
Fr1_12
Friction angle δ(°)
Deformation (mm)
Rate (mm/min)
δ (Pa = 5590 kPa)
Rate
10
8
6
4
2
0
0
2
4
6
8
10
100
10
1
0.1
0.01
0.001

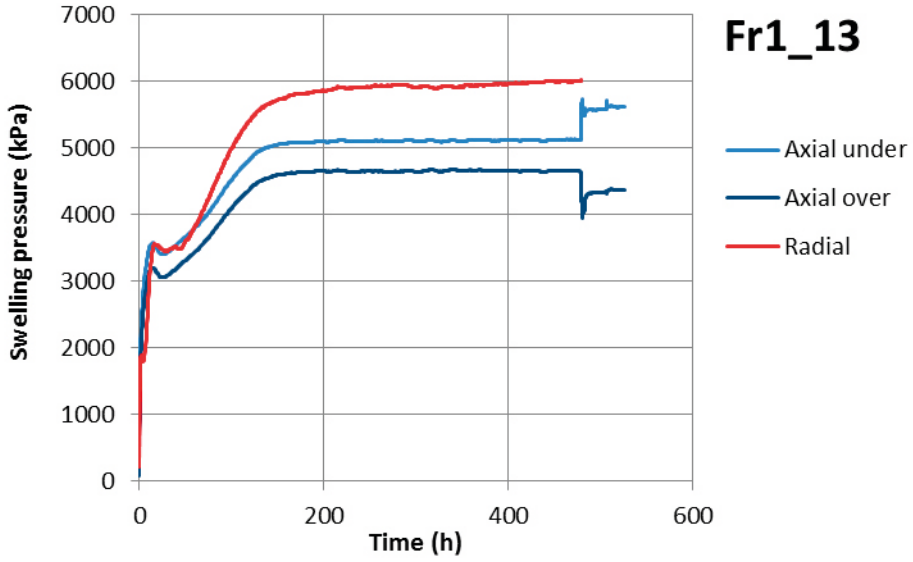
Fr1_13
Swelling pressure (kPa)
7000
6000
5000
4000
3000
2000
1000
0
0
200
400
600
Time (h)
Axial under
Axial over
Radial

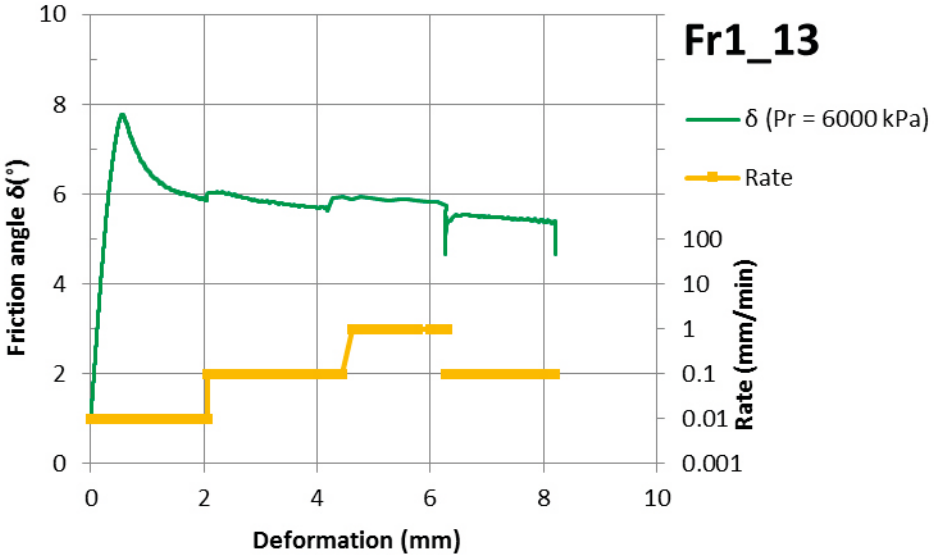
Fr1_13
Friction angle δ(°)
10
8
6
4
2
0
0
2
4
6
8
10
Deformation (mm)
δ (Pr = 6000 kPa)
Rate
100
10
1
0.1
0.01
0.001
Rate (mm/min)

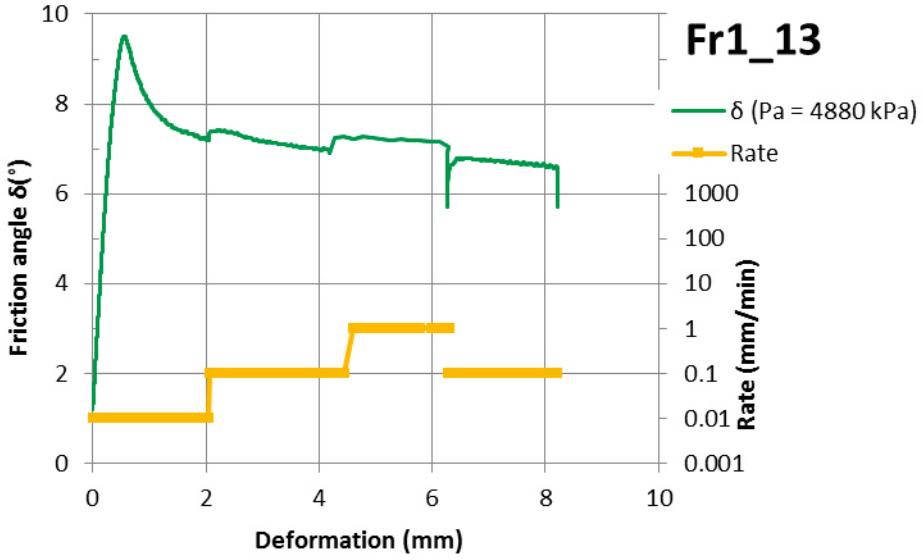
Fr1_13
Friction angle δ(°)
10
8
6
4
2
0
0
2
4
6
8
10
Deformation (mm)
δ (Pa = 4880 kPa)
Rate
1000
100
10
1
0.1
0.01
0.001
Rate (mm/min)

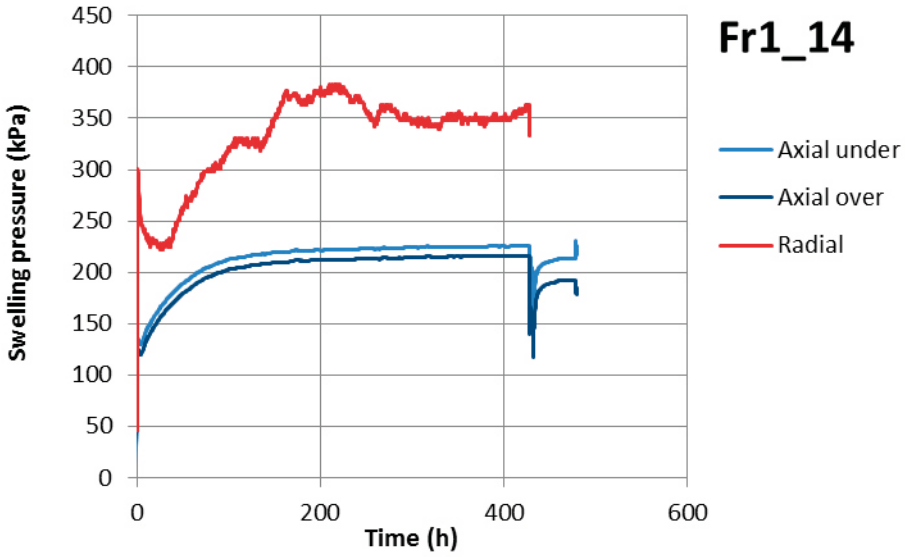
Fr1_14
Swelling pressure (kPa)
Time (h)
Axial under
Axial over
Radial

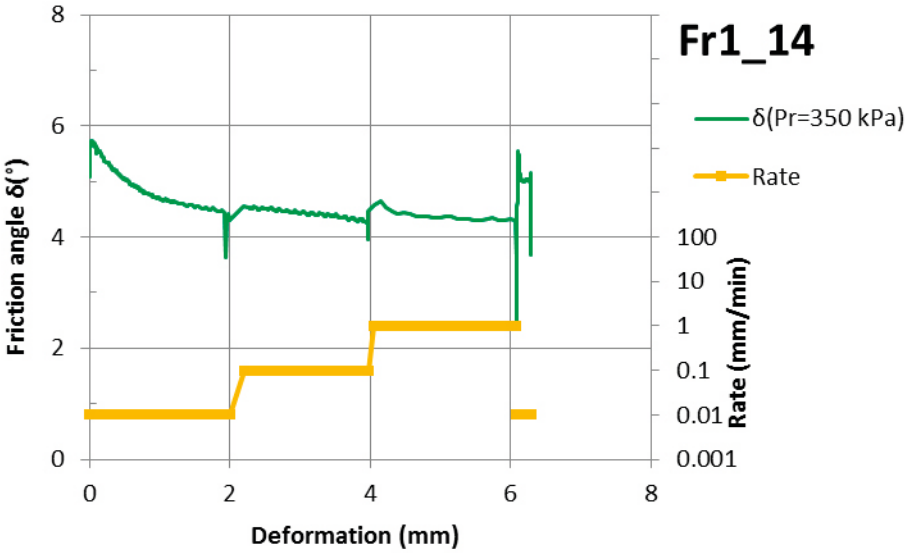
Fr1_14
Friction angle δ(°)
Deformation (mm)
Rate (mm/min)
δ(Pr=350 kPa)
Rate

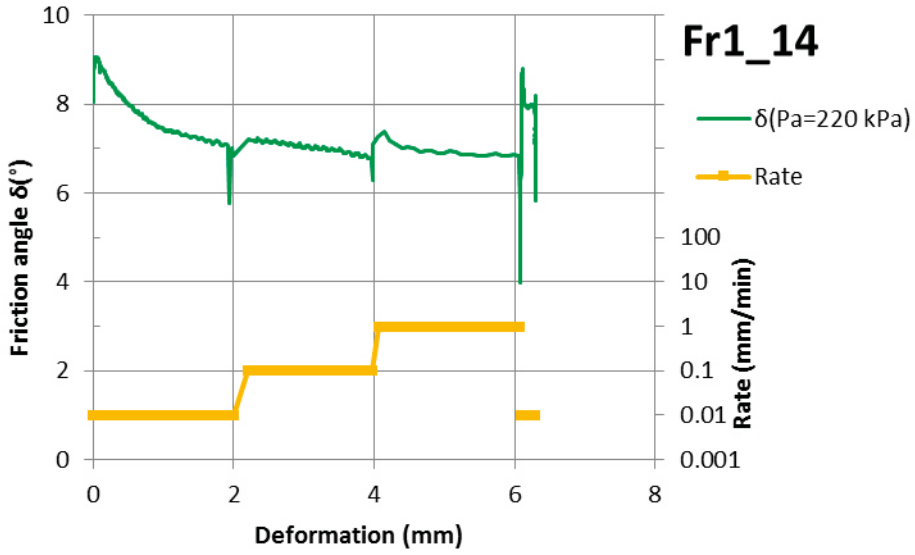
Fr1_14
Friction angle δ(°)
Deformation (mm)
Rate (mm/min)
δ(Pa=220 kPa)
Rate

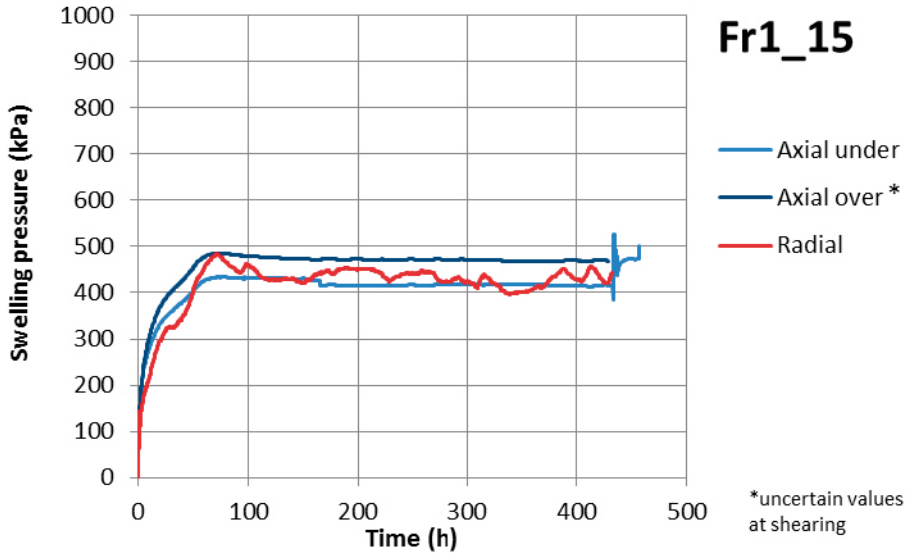
Fr1_15
Swelling pressure (kPa)
Time (h)
Axial under
Axial over *
Radial
*uncertain values at shearing

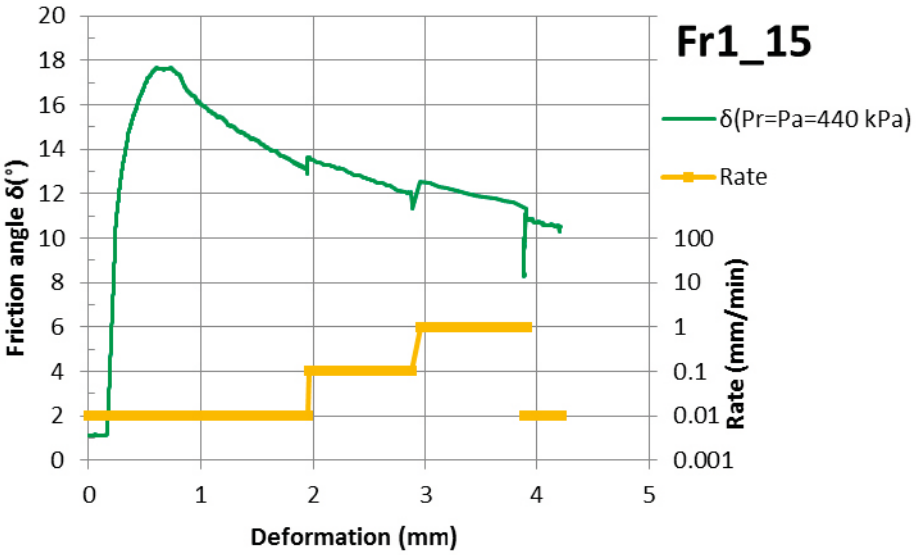
Fr1_15
Friction angle δ(°)
Deformation (mm)
Rate (mm/min)
δ(Pr=Pa=440 kPa)
Rate

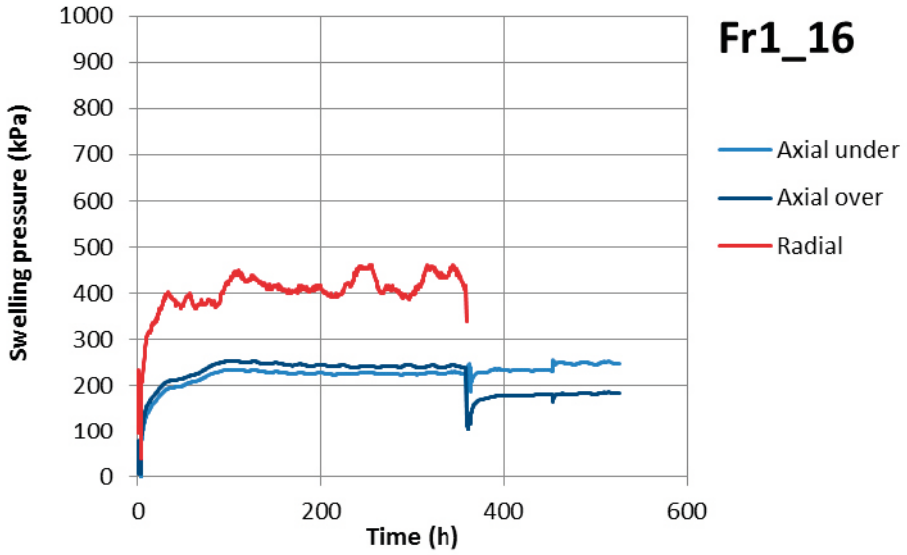
Fr1_16
Swelling pressure (kPa)
Time (h)
Axial under
Axial over
Radial

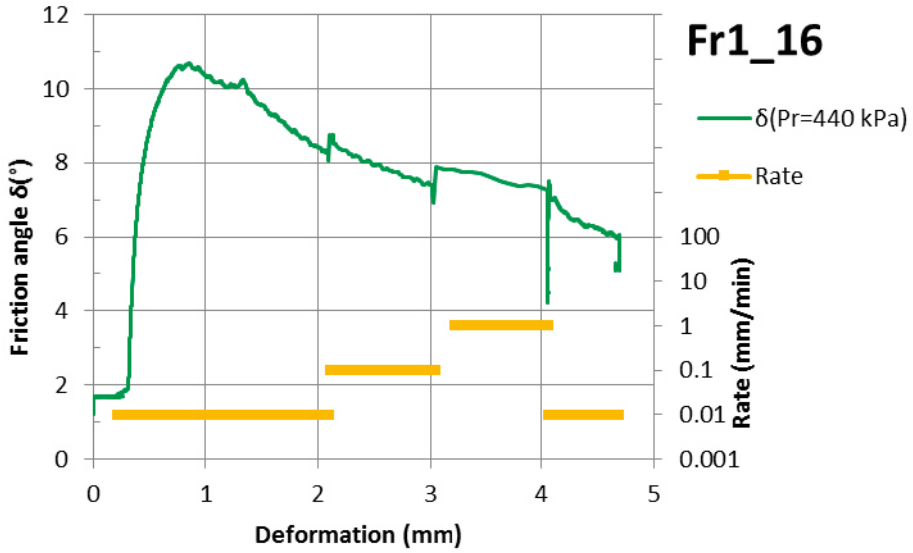
Fr1_16
Friction angle δ(°)
Deformation (mm)
Rate (mm/min)
δ(Pr=440 kPa)
Rate

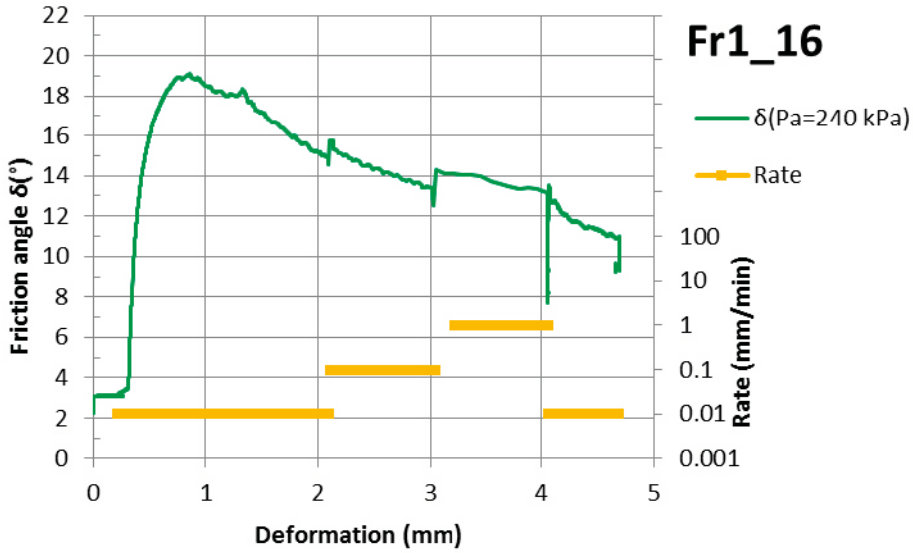
Fr1_16
Friction angle δ(°)
Deformation (mm)
Rate (mm/min)
δ(Pa=240 kPa)
Rate

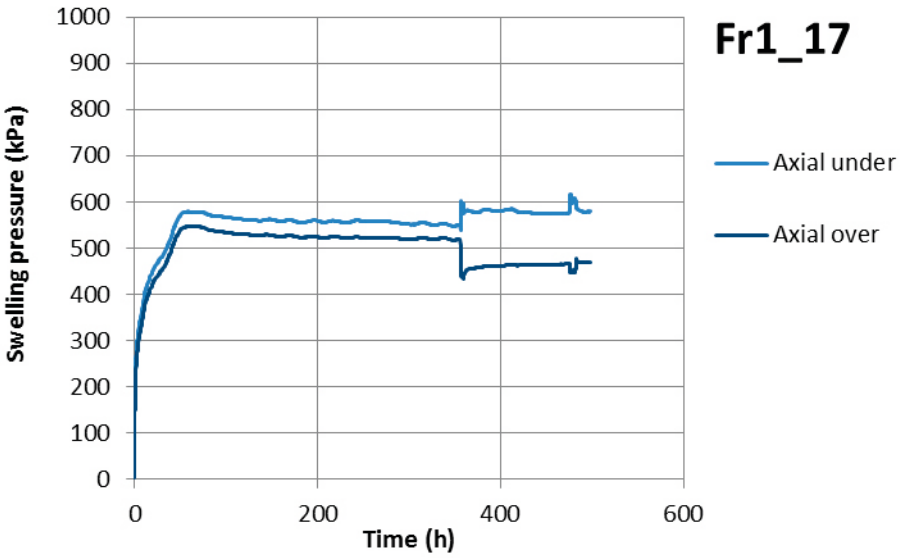
Fr1_17
Swelling pressure (kPa)
Time (h)
Axial under
Axial over
0
100
200
300
400
500
600
700
800
900
1000
0
200
400
600

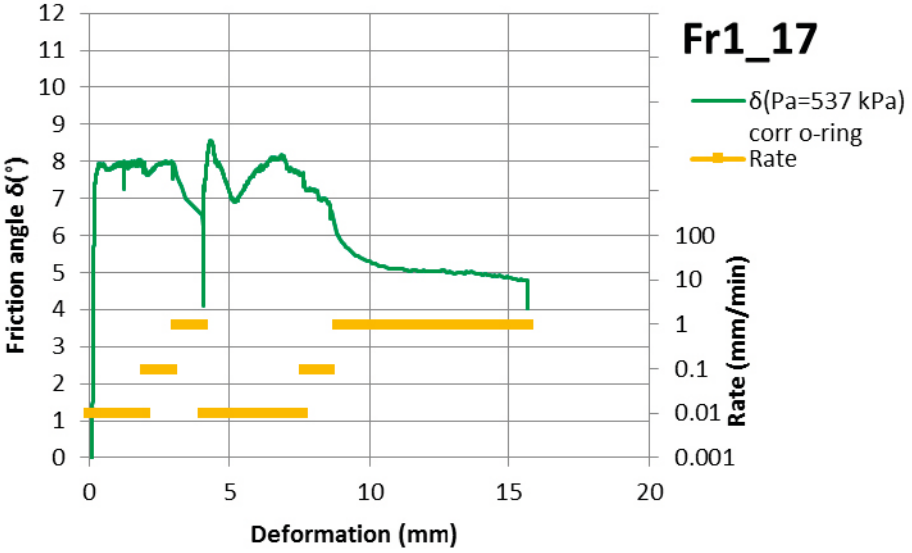
Fr1_17
Friction angle δ(°)
Deformation (mm)
Rate (mm/min)
δ(Pa=537 kPa) corr o-ring
Rate
0
1
2
3
4
5
6
7
8
9
10
11
12
0
5
10
15
20
0.001
0.01
0.1
1
10
100

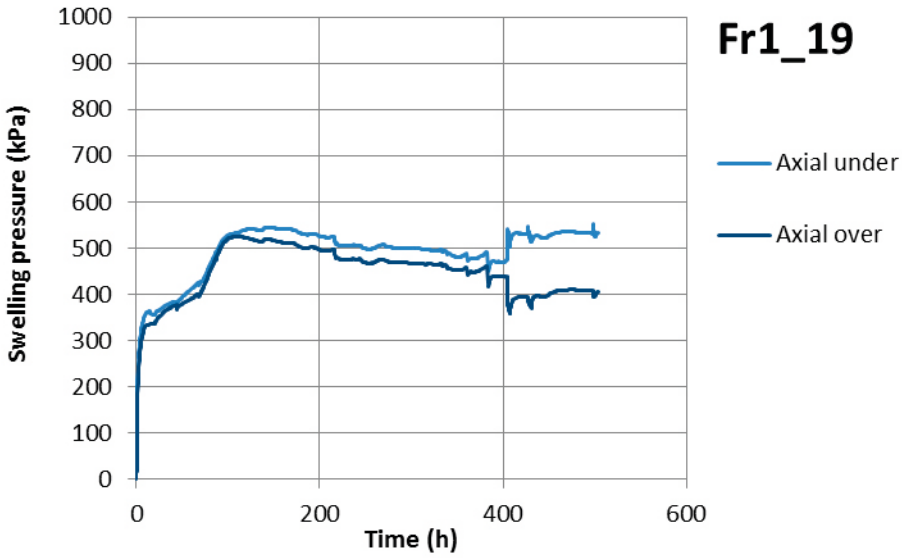
Fr1_19
Swelling pressure (kPa)
1000
900
800
700
600
500
400
300
200
100
0
0
200
400
600
Time (h)
Axial under
Axial over

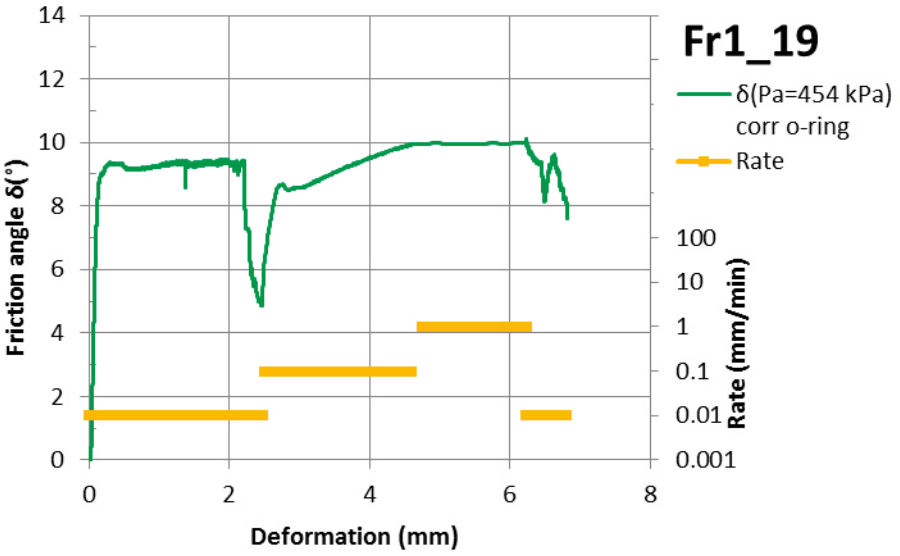
Fr1_19
Friction angle δ(°)
14
12
10
8
6
4
2
0
0
2
4
6
8
Deformation (mm)
δ(Pa=454 kPa)
corr o-ring
Rate
100
10
1
0.1
0.01
0.001
Rate (mm/min)

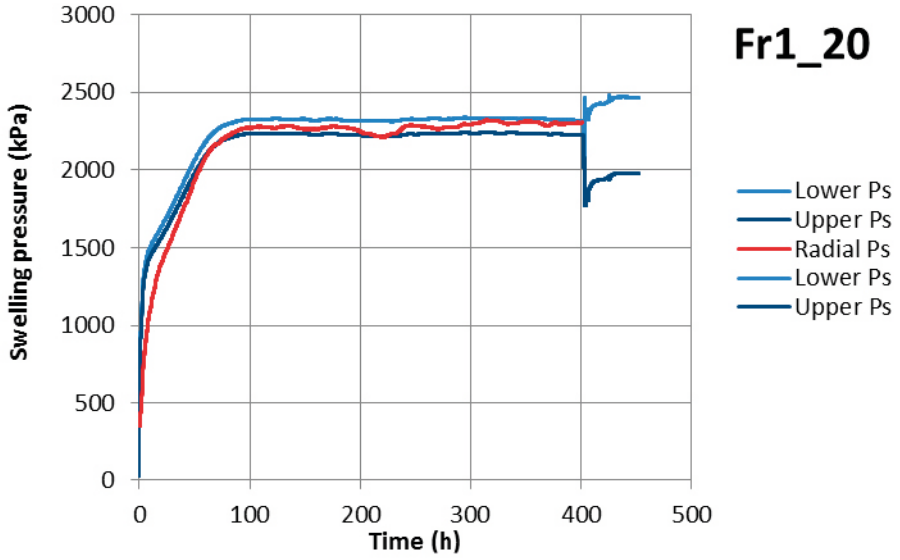
Fr1_20
Swelling pressure (kPa)
Time (h)
Lower Ps
Upper Ps
Radial Ps
Lower Ps
Upper Ps

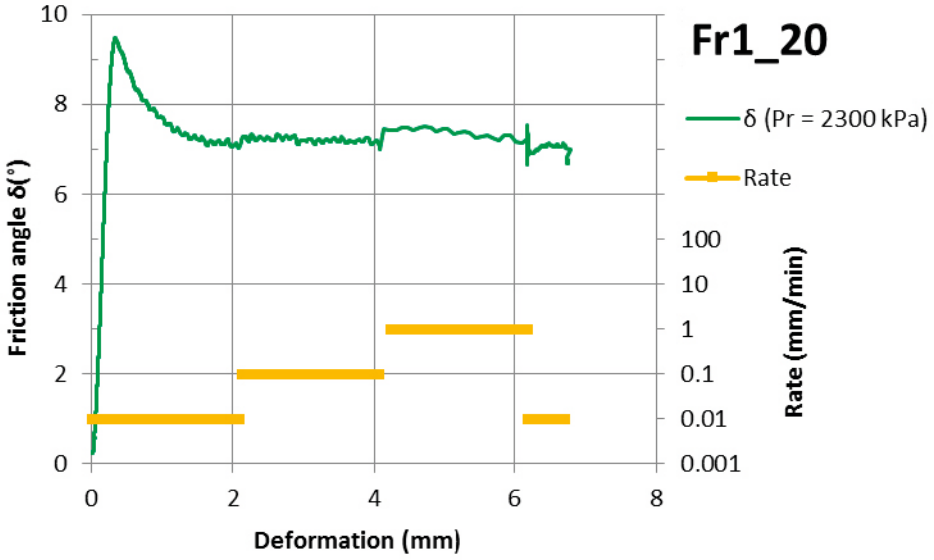
Fr1_20
Friction angle δ(°)
Deformation (mm)
Rate (mm/min)
δ (Pr = 2300 kPa)
Rate

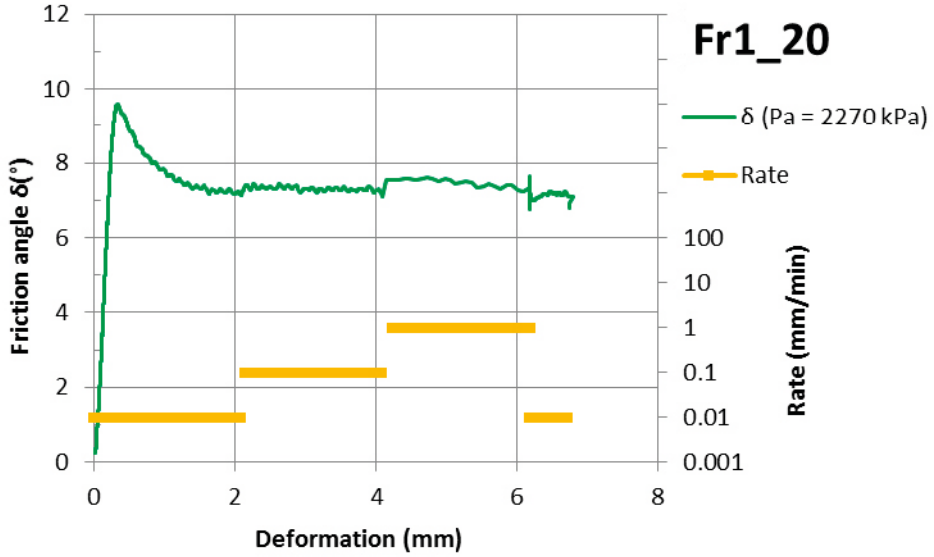
Fr1_20
Friction angle δ(°)
Deformation (mm)
Rate (mm/min)
δ (Pa = 2270 kPa)
Rate

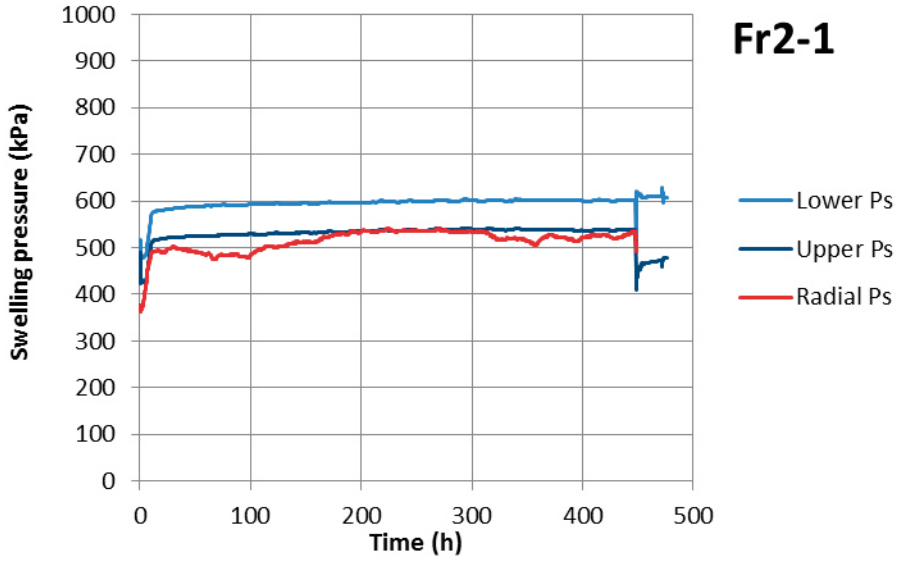
Fr2-1
Swelling pressure (kPa)
Time (h)
Lower Ps
Upper Ps
Radial Ps

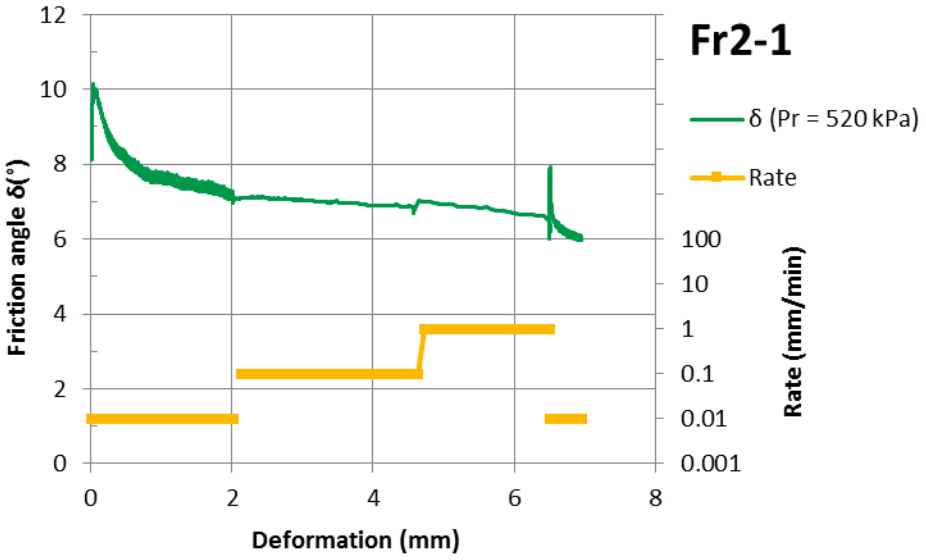
Fr2-1
Friction angle δ(°)
Deformation (mm)
Rate (mm/min)
δ (Pr = 520 kPa)
Rate

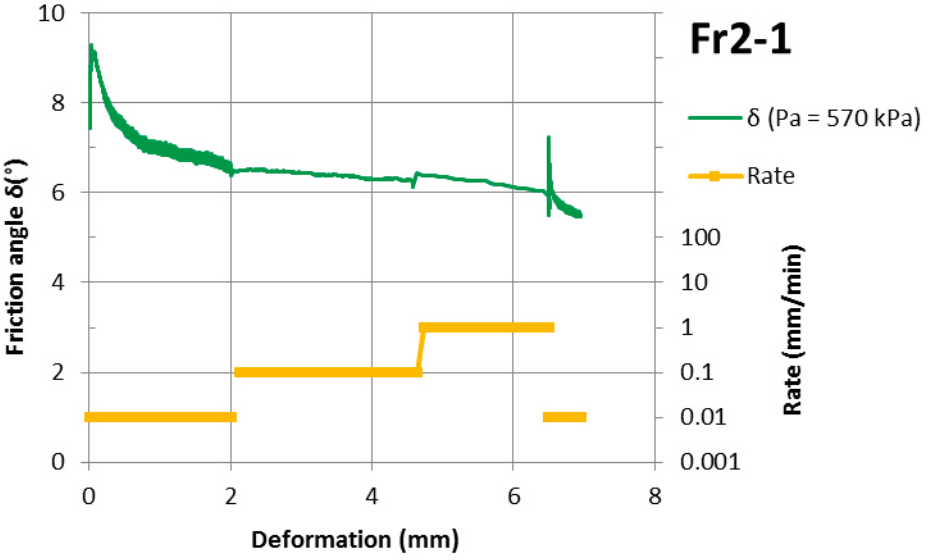
Fr2-1
Friction angle δ(°)
Deformation (mm)
Rate (mm/min)
δ (Pa = 570 kPa)
Rate

Additional tests on shear strength and friction

The specimen used for test Fr1-16 was also used for additional tests; two cone tests and two unconfined compression tests. The unconfined compression tests were made on specimens with the height and diameter 20 mm. When interpreting the strength as friction and by use of the equation used by Åkesson et al. (2010) the bentonite friction angel evaluated from the two unconfined compression tests were $\phi = 14.9°$ and $\phi = 17.5°$ while the two cone tests both gave $\phi = 13.6°$, Table A5-1. For these results the axially measured swelling pressure where used and the results can be compared to the test results marked in Figure A5-1 which is almost the same as Figure 5-66.

Table A5-1. Results from the cone tests and the unconfined compression tests on the specimens used for the friction test Fr1-16.

	Deviator stress, q kPa	Shear strength, τ_{fu} kPa	Calculated bentonite friction angle	
			p' = 240 kPa	p' = 440 kPa
UC-test	135 160		8.4 9.9	14.9 17.5
Cone test		61 61	7.7 7.7	13.6 13.6

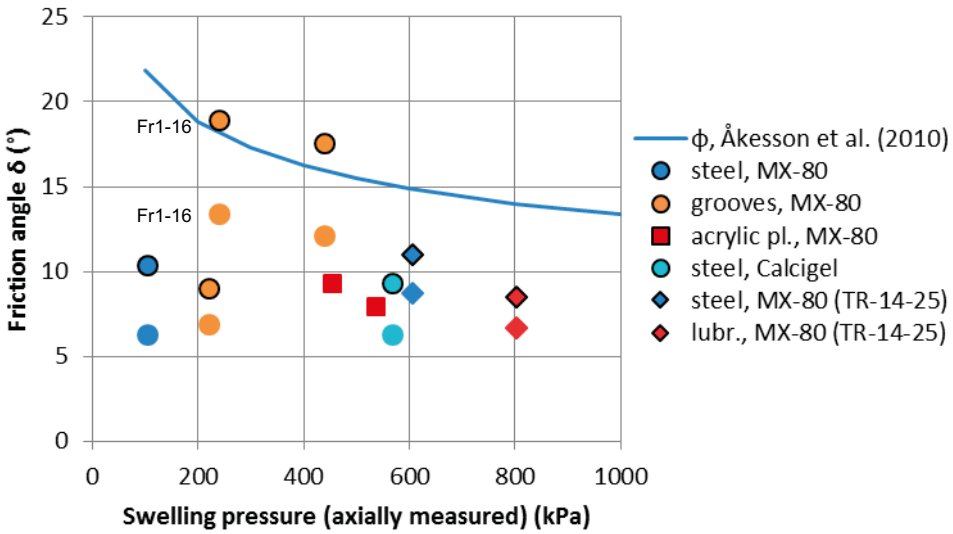

Figure A5-1. *Test results from the series with friction tests at axial stress below 1 000 kPa with the results from test Fr1-16 marked (cf. Figure 5-66).*

Appendix 6

Distribution of water content and density of the dismantled SH2

Results from sampling of the dismantled SH2 according to Figure 6-6, Figure 6-7, Figure 6-8 and Chapter 6.

Table A6-1. Distribution of water content and densities at level 1 i.e. outermost and towards the lid.

Sample ID	Level	Distance	Bulk density	Water content	Degree of saturation	Dry density	Void ratio
		mm	kg/m^3	%	%	kg/m^3	–
L0-1	1	12.5	2014	28.0	102	1573	0.77
L0-1	1	32.5	2000	29.0	102	1551	0.79
L0-1	1	47.5	1979	30.3	101	1519	0.83
L0-1	1	62.5	1953	32.1	101	1478	0.88
L0-1	1	77.5	1937	33.2	101	1455	0.91
L0-1	1	92.5	1931	34.3	102	1438	0.93
L20-1	1	12.5	2020	27.7	102	1582	0.76
L20-1	1	32.5	2012	28.3	102	1568	0.77
L20-1	1	47.5	2004	28.8	102	1556	0.79
L20-1	1	62.5	1989	29.7	102	1534	0.81
L20-1	1	77.5	1975	30.4	101	1514	0.84
L20-1	1	92.5	1955	31.3	100	1490	0.87
L90-1	1	12.5	2043	25.6	100	1626	0.71
L90-1	1	32.5	2036	26.5	101	1609	0.73
L90-1	1	47.5	2034	26.6	101	1607	0.73
L90-1	1	62.5	2029	26.9	101	1599	0.74
L90-1	1	77.5	2021	27.6	102	1584	0.76
L90-1	1	92.5	1981	30.8	102	1515	0.83
L6-1	1	12.5	2006	28.4	101	1562	0.78
L6-1	1	32.5	1989	29.6	101	1534	0.81
L6-1	1	47.5	1970	31.0	102	1505	0.85
L6-1	1	62.5	1949	32.3	101	1473	0.89
L6-1	1	77.5	1934	33.1	101	1453	0.91
L6-1	1	92.5	1932	33.6	101	1446	0.92
A1	1	12.5	2013	27.4	100	1580	0.76
A1	1	32.5	1999	28.4	101	1557	0.79
A1	1	47.5	1989	29.4	101	1537	0.81
A1	1	62.5	1975	30.3	101	1517	0.83
A1	1	77.5	1964	31.4	101	1495	0.86
A1	1	92.5	1953	32.7	102	1472	0.89
A1(2)	1	12.5	2013	27.4	100	1580	0.76
A1(2)	1	32.5	1999	28.4	101	1557	0.79
A1(2)	1	47.5	1989	29.4	101	1537	0.81
A1(2)	1	62.5	1966	31.2	101	1498	0.86
A1(2)	1	77.5	1950	32.4	102	1472	0.89
A1(2)	1	92.5	1942	33.4	102	1456	0.91
B1	1	12.5	2021	27.5	101	1585	0.75
B1	1	32.5	2014	28.2	102	1571	0.77
B1	1	47.5	2009	28.7	102	1561	0.78
B1	1	62.5	2005	29.1	102	1554	0.79
B1	1	77.5	1991	30.0	102	1532	0.81
B1	1	92.5	1978	31.8	104	1501	0.85
B1(2)	1	12.5	2021	27.5	101	1585	0.75
B1(2)	1	32.5	2014	28.2	102	1571	0.77
B1(2)	1	47.5	2009	28.7	102	1561	0.78

Sample ID	Level	Distance	Bulk density	Water content	Degree of saturation	Dry density	Void ratio
		mm	kg/m³	%	%	kg/m³	–
B1(2)	1	62.5	1993	29.7	102	1536	0.81
B1(2)	1	77.5	1979	30.6	102	1515	0.83
B1(2)	1	92.5	1968	32.3	103	1488	0.87
C1	1	12.5	2021	27.0	100	1591	0.75
C1	1	32.5	2021	27.6	102	1584	0.76
C1	1	47.5	2014	27.9	101	1574	0.77
C1	1	62.5	2008	28.0	101	1568	0.77
C1	1	77.5	1998	28.6	101	1554	0.79
C1	1	92.5	1975	31.1	102	1506	0.85
C1(2)	1	12.5	2021	27.0	100	1591	0.75
C1(2)	1	32.5	2021	27.6	102	1584	0.76
C1(2)	1	47.5	2014	27.9	101	1574	0.77
C1(2)	1	62.5	2008	28.5	102	1562	0.78
C1(2)	1	77.5	1995	29.4	102	1541	0.80
C1(2)	1	92.5	1973	31.5	103	1500	0.85
D1	1	12.5	2029	26.4	100	1605	0.73
D1	1	32.5	2031	27.2	102	1596	0.74
D1	1	47.5	2021	27.3	101	1587	0.75
D1	1	62.5	2018	27.4	101	1584	0.75
D1	1	77.5	2013	27.9	101	1574	0.77
D1	1	92.5	1984	30.1	102	1525	0.82
D1(2)	1	12.5	2029	26.4	100	1605	0.73
D1(2)	1	32.5	2031	27.2	102	1596	0.74
D1(2)	1	47.5	2021	27.3	101	1587	0.75
D1(2)	1	62.5	2012	27.8	101	1575	0.77
D1(2)	1	77.5	2005	28.4	101	1562	0.78
D1(2)	1	92.5	1981	30.5	102	1518	0.83

Table A6-2. Distribution of water content and densities at level 2 i.e. second outermost.

Sample ID	Level	Distance	Bulk density	Water content	Degree of saturation	Dry density	Void ratio
		mm	kg/m³	%	%	kg/m³	–
L0-2	2	12.5	2009	28.9	102	1558	0.78
L0-2	2	32.5	1999	30.7	104	1529	0.82
L0-2	2	47.5	1971	33.8	106	1473	0.89
L0-2	2	62.5	1916	38.6	106	1382	1.01
L0-2	2	77.5	1856	39.3	101	1332	1.09
L0-2	2	92.5	1867	38.6	101	1347	1.06
L20-2	2	12.5	2011	28.6	102	1563	0.78
L20-2	2	32.5	2006	29.1	103	1554	0.79
L20-2	2	47.5	1996	29.7	102	1539	0.81
L20-2	2	62.5	1984	30.9	103	1516	0.83
L20-2	2	77.5	1967	31.9	103	1491	0.86
L20-2	2	92.5	1947	33.0	102	1464	0.90
L90-2	2	12.5	2041	26.4	102	1614	0.72
L90-2	2	32.5	2032	26.9	102	1601	0.74
L90-2	2	47.5	2025	27.1	101	1593	0.74
L90-2	2	62.5	2027	27.2	102	1593	0.74
L90-2	2	77.5	2018	27.7	101	1580	0.76
L90-2	2	92.5	1989	29.9	102	1530	0.82
L6-2	2	12.5	2001	28.8	101	1553	0.79
L6-2	2	32.5	1980	30.6	102	1516	0.83

Sample ID	Level	Distance	Bulk density	Water content	Degree of saturation	Dry density	Void ratio
		mm	kg/m^3	%	%	kg/m^3	–
L6-2	2	47.5	1947	32.7	101	1467	0.89
L6-2	2	62.5	1929	34.0	102	1439	0.93
L6-2	2	77.5	1921	34.3	101	1430	0.94
L6-2	2	92.5	1915	34.8	101	1421	0.96
A2	2	12.5	2005	28.3	101	1563	0.78
A2	2	32.5	1993	29.5	102	1539	0.81
A2	2	47.5	1972	32.0	103	1494	0.86
A2	2	62.5	1961	31.9	103	1487	0.87
A2	2	77.5	1951	32.6	102	1471	0.89
A2	2	92.5	1938	33.6	102	1451	0.92
A2(2)	2	12.5	2005	28.3	101	1563	0.78
A2(2)	2	32.5	1993	29.5	102	1539	0.81
A2(2)	2	47.5	1972	32.0	103	1494	0.86
A2(2)	2	62.5	1933	33.6	101	1447	0.92
A2(2)	2	77.5	1928	34.4	102	1435	0.94
A2(2)	2	92.5	1926	34.9	102	1428	0.95
B2	2	12.5	2020	28.1	102	1576	0.76
B2	2	32.5	2008	28.7	102	1561	0.78
B2	2	47.5	1999	29.3	102	1546	0.80
B2	2	62.5	1998	29.5	102	1542	0.80
B2	2	77.5	1984	30.7	103	1518	0.83
B2	2	92.5	1973	31.8	103	1496	0.86
B2(2)	2	12.5	2020	28.1	102	1576	0.76
B2(2)	2	32.5	2008	28.7	102	1561	0.78
B2(2)	2	47.5	1999	29.3	102	1546	0.80
B2(2)	2	62.5	1984	30.5	102	1520	0.83
B2(2)	2	77.5	1972	31.6	103	1499	0.85
B2(2)	2	92.5	1959	32.6	103	1477	0.88
C2	2	12.5	2022	27.8	102	1583	0.76
C2	2	32.5	2019	28.2	102	1574	0.77
C2	2	47.5	2009	28.4	102	1564	0.78
C2	2	62.5	2011	28.6	102	1563	0.78
C2	2	77.5	2004	29.3	103	1550	0.79
C2	2	92.5	1983	30.6	102	1518	0.83
C2(2)	2	12.5	2022	27.8	102	1583	0.76
C2(2)	2	32.5	2019	28.2	102	1574	0.77
C2(2)	2	47.5	2009	28.4	102	1564	0.78
C2(2)	2	62.5	2007	29.3	103	1551	0.79
C2(2)	2	77.5	1999	29.9	103	1539	0.81
C2(2)	2	92.5	1974	31.3	103	1503	0.85
D2	2	12.5	2010	27.1	100	1581	0.76
D2	2	32.5	2030	27.6	103	1591	0.75
D2	2	47.5	2024	28.0	103	1582	0.76
D2	2	62.5	2022	27.9	103	1582	0.76
D2	2	77.5	2019	28.3	103	1574	0.77
D2	2	92.5	1995	29.8	102	1537	0.81
D2(2)	2	12.5	2010	27.1	100	1581	0.76
D2(2)	2	32.5	2030	27.6	103	1591	0.75
D2(2)	2	47.5	2024	28.0	103	1582	0.76
D2(2)	2	62.5	2016	28.3	102	1572	0.77
D2(2)	2	77.5	2008	28.8	102	1559	0.78
D2(2)	2	92.5	1988	30.3	102	1526	0.82

Table A6-3. Distribution of water content and densities at level 3 i.e. innermost.

Sample ID	Level	Distance	Bulk density	Water content	Degree of saturation	Dry density	Void ratio
		mm	kg/m³	%	%	kg/m³	–
L0-3	3	12.5	2004	28.7	102	1557	0.79
L0-3	3	32.5	1986	30.2	102	1525	0.82
L0-3	3	47.5	1953	32.8	102	1471	0.89
L0-3	3	62.5	1927	34.7	102	1430	0.94
L0-3	3	77.5	1915	35.6	102	1412	0.97
L0-3	3	92.5	1909	35.9	102	1405	0.98
L20-3	3	12.5	2012	28.6	102	1565	0.78
L20-3	3	32.5	2008	28.2	101	1566	0.77
L20-3	3	47.5	1996	29.9	103	1537	0.81
L20-3	3	62.5	1974	31.2	102	1504	0.85
L20-3	3	77.5	1960	32.1	102	1484	0.87
L20-3	3	92.5	1944	33.3	102	1459	0.91
L90-3	3	12.5	2038	26.6	102	1610	0.73
L90-3	3	32.5	2029	27.0	101	1597	0.74
L90-3	3	47.5	2029	27.3	102	1594	0.74
L90-3	3	62.5	2027	27.6	102	1588	0.75
L90-3	3	77.5	2021	28.0	102	1579	0.76
L90-3	3	92.5	1988	30.2	102	1527	0.82
L6-3	3	12.5	2002	29.1	102	1551	0.79
L6-3	3	32.5	1976	31.0	102	1509	0.84
L6-3	3	47.5	1937	33.4	102	1452	0.91
L6-3	3	62.5	1902	36.3	102	1396	0.99
L6-3	3	77.5	1854	37.4	98	1350	1.06
L6-3	3	92.5	1857	37.2	98	1353	1.05
A3	3	12.5	2006	28.3	101	1563	0.78
A3	3	32.5	1988	29.4	101	1537	0.81
A3	3	47.5	1958	31.1	100	1493	0.86
A3	3	62.5	1955	32.9	100	1471	0.89
A3	3	77.5	1943	33.4	102	1456	0.91
A3	3	92.5	1933	33.6	101	1447	0.92
A3(2)	3	12.5	2006	28.3	101	1563	0.78
A3(2)	3	32.5	1988	29.4	101	1537	0.81
A3(2)	3	47.5	1958	31.1	100	1493	0.86
A3(2)	3	62.5	1917	35.1	102	1419	0.96
A3(2)	3	77.5	1915	35.3	102	1416	0.96
A3(2)	3	92.5	1913	35.2	101	1415	0.96
B3	3	12.5	2014	28.2	102	1571	0.77
B3	3	32.5	2011	28.8	103	1561	0.78
B3	3	47.5	1999	29.5	102	1543	0.80
B3	3	62.5	1999	29.8	102	1540	0.81
B3	3	77.5	1981	30.7	102	1515	0.83
B3	3	92.5	1970	31.7	103	1496	0.86
B3(2)	3	12.5	2014	28.2	102	1571	0.77
B3(2)	3	32.5	2011	28.8	103	1561	0.78
B3(2)	3	47.5	1999	29.5	102	1543	0.80
B3(2)	3	62.5	1986	31.3	104	1512	0.84
B3(2)	3	77.5	1963	31.9	102	1488	0.87
B3(2)	3	92.5	1952	32.8	102	1470	0.89
C3	3	12.5	2026	27.6	102	1587	0.75
C3	3	32.5	2018	28.1	102	1575	0.76

Sample ID	Level	Distance	Bulk density	Water content	Degree of saturation	Dry density	Void ratio
		mm	kg/m^3	%	%	kg/m^3	–
C3	3	47.5	2015	28.4	102	1570	0.77
C3	3	62.5	2016	28.6	102	1568	0.77
C3	3	77.5	2003	29.1	102	1552	0.79
C3	3	92.5	1985	30.3	102	1523	0.83
C3(2)	3	12.5	2026	27.6	102	1587	0.75
C3(2)	3	32.5	2018	28.1	102	1575	0.76
C3(2)	3	47.5	2015	28.4	102	1570	0.77
C3(2)	3	62.5	2009	29.0	103	1557	0.79
C3(2)	3	77.5	1998	30.0	103	1537	0.81
C3(2)	3	92.5	1972	31.0	102	1505	0.85
D3	3	12.5	2007	27.1	99	1579	0.76
D3	3	32.5	2028	27.7	103	1588	0.75
D3	3	47.5	2022	27.9	102	1581	0.76
D3	3	62.5	2031	27.9	102	1587	0.75
D3	3	77.5	2018	28.4	103	1571	0.77
D3	3	92.5	1980	30.7	102	1515	0.84
D3(2)	3	12.5	2007	27.1	99	1579	0.76
D3(2)	3	32.5	2028	27.7	103	1588	0.75
D3(2)	3	47.5	2022	27.9	102	1581	0.76
D3(2)	3	62.5	2022	28.4	103	1575	0.76
D3(2)	3	77.5	2014	28.8	103	1564	0.78
D3(2)	3	92.5	1988	30.2	102	1527	0.82

Appendix 7

Samples and reports

The following tables show all tests mentioned in this report. Some of the tests mentioned in this report were presented in one of the previous status reports of this project; TR-02-12 (only a few tests) and TR-14-25 (all tests). The materials used, i.e. MX-80 or Calcigel, are mentioned in the tables below and for the new tests presented in this report the year of the delivery is also given; MX-80#2010[b], MX-80#2012, Calcigel#2006 or Calcigel#2014. The material MX-80#2010[b] was delivered before 2010.

Table A7-1. Tests made in the series A0 and mentioned in this report.

Sample ID	Material	Report
A01-09, A01-10	MX-80	TR-02-12
A01-12, A01-13	MX-80	TR-14-25
A01-14, A01,15, A01-16	MX-80#2010[b]	this report
A04-1, A04-2	Calcigel#2006	this report

Table A7-2. Tests made in the series R1 and mentioned in this report.

Sample ID	Material	Report
R11-10, R11-11	MX-80	TR-02-12
R11-17, R11-18, R11-19, R11-20, R11-21	MX-80	TR-14-25
R11-22, R11-23	MX-80#2010[b]	this report
R11-24	MX-80#2012	this report
R14-1, R14-2	Calcigel#2006	this report

Table A7-3. Tests made in the series R2 and mentioned in this report.

Sample ID	Material	Report
R21-09, R21-10, R21-11, R21-12	MX-80	TR-14-25
R21-13, R21-14	MX-80#2010[b]	this report
R24-1, R24-2	Calcigel#2006	this report

Table A7-4. All tests made in the series HR-A, HR-Ro, HR-Ri and HR-Iso.

Sample ID	Material	Report
HR-A1	MX-80	TR-14-25
HR-A2, HR-A3, HR-A4	MX-80#2010[b]	this report
HR-A6	Calcigel#2006	this report
HR-Ro1	MX-80	TR-14-25
HR-Ro2	Calcigel#2006	this report
HR-Ri1	MX-80#2010[b]	this report
HR-Iso	MX-80#2010[b]	this report

Table A7-5. All tests made in the series Fr.

Sample ID	Material	Report
Fr1-1 to Fr1-5, Fr1-7 to Fr1-9	MX-80	TR-14-25
Fr1-10, Fr1-12, Fr1-13	MX-80#2010[b]	this report
Fr1-11, Fr1-14	MX-80 pellet	this report
Fr1-15 to Fr1-17, Fr-19, Fr1-20	MX-80#2012	this report
Fr2-1	Calcigel#2006	this report

Table A7-6. Both tests in the series SH.

Sample ID	Material	Report
SH1, SH2	MX-80#2012	this report

Arkitektkopia AB, Bromma, 2017

SKB is tasked with managing Swedish nuclear and radioactive waste in a safe way.

skb.se